UNIVERSITY OF SOUTHAMPTON
FACULTY OF ENGINEERING AND PHYSICAL SCIENCES
SCHOOL OF ELECTRONICS AND COMPUTER SCIENCE

Performance Analysis and Impairment Mitigation of Digital Subscriber Lines in the Face of Impulsive Noise

by

Tong Bai
B. Sc., M.Sc.

A doctoral thesis report submitted in partial fulfilment of
the requirements for the award of Doctor of Philosophy
at the University of Southampton

Dec 2018

SUPERVISOR:
Professor Lajos Hanzo
FREng, FIEEE, FIEE, DSc, EIC IEEE Press
Chair of Next Generation Wireless Group
University of Southampton
Southampton SO17 1BJ
United Kingdom

Dedicated to my family and friends

UNIVERSITY OF SOUTHAMPTON

ABSTRACT

FACULTY OF ENGINEERING AND PHYSICAL SCIENCES
SCHOOL OF ELECTRONICS AND COMPUTER SCIENCE

Doctor of Philosophy

Performance Analysis and Impairment Mitigation of Digital Subscriber Lines in the Face of Impulsive Noise

by Tong Bai

Digital subscriber lines (DSL) continue to evolve in supporting home networks, whilst relying on a hybrid architecture of twisted pairs and optical fiber, as a benefit of its cost-efficiency and high quality of service. However, the preponderance of impulsive noise stifles the further improvement of the system performance. Explicitly, the throughput, reliability as well as delay, have to satisfy a range of stringent communication requirements. Against this background, in this thesis, we analyze the performance of DSL system in the face of impulsive noise. Moreover, we propose a joint impulsive noise estimation and data detection algorithm for alleviating the detriments caused by impulsive noise, which are briefly elaborated on below.

We commence by reviewing the state-of-the-art in impulsive noise mitigation, both at the transmitter as well as at the receiver. These encouraging works also consolidate our motivation of this thesis. Moreover, a range of metrics suitable for characterizing the above-mentioned deleterious is highlighted, followed by a survey of both empirical and simplified mathematical noise models.

Secondly, we analyze the bit-error ratio (BER) performance of DSL systems in the face of impulsive noise. Explicitly, we consider multi-carrier systems in the face of hidden semi-Markov model based impulsive noise. Moreover, since the overall BER performance of the system is dependent both on the occurrence probability of impulsive noise and on the specific distribution of the impulsive noise's amplitude, we analyze the statistics of impulsive noise samples both in the time- and in the frequency-domain, and then investigate the amplitude distribution of impulsive noise after multi-carrier demodulation with the aid of the Central Limit Theorem. Based on the above results, closed-form BER formulas are derived. Our extensive simulation results verify the accuracy of the analysis in quantifying the deleterious influence of impulsive noise.

Furthermore, given that hybrid automatic repeat request (HARQ) constitute a popular technique of eliminating the effects of impulsive noise, we investigate the performance of the Chase combining aided HARQ and of plain HARQ schemes in a low-density parity-check (LDPC) coded multi-carrier system inflicting impulsive noise, in terms of its outage

probability and the average number of transmission attempts as well as goodput. Specifically, a modified density evolution technique is proposed, which is then involved for characterizing the outage probability performance of the system in a finite block-length regime. The accuracy of our analysis is verified by extensive simulation results, which confirms our expectation that Chase-combining HARQ outperforms the plain HARQ.

Additionally, we conceive a joint impulsive noise estimation and data detection algorithm for LDPC-coded multi-carrier systems. More explicitly, first of all, we propose a semi-blind estimation method, which is capable of estimating the arrival of noise impulses inferred by evaluating the power of impulsive noise with an adequate accuracy. Secondly, in order to improve the accuracy of impulsive noise estimation, we propose a decision-directed (DD) method for the second stage of channel decoding and data detection with the aid of extrinsic information transfer (EXIT) charts. Our proposed two-stage scheme is capable of approaching the performance of the idealistic scenario of perfectly knowing both the arrival time and the instantaneous power of impulsive noise. Moreover, we analyze the mean square error (MSE) of the proposed schemes in order to quantify the estimation accuracy and to reduce the estimation complexity. Our simulation results demonstrate that our proposed scheme is capable of achieving a near-capacity performance in the LDPC-coded multi-carrier DSL system in the presence of impulsive noise.

Declaration of Authorship

I, **Tong Bai**, declare that the thesis entitled **Performance Analysis and Impairment Mitigation of Digital Subscriber Lines in the Face of Impulsive Noise** and the work presented in it are my own and has been generated by me as the result of my own original research. I confirm that:

- This work was done wholly or mainly while in candidature for a research degree at this University;
- Where any part of this thesis has previously been submitted for a degree or any other qualification at this University or any other institution, this has been clearly stated;
- Where I have consulted the published work of others, this is always clearly attributed;
- Where I have quoted from the work of others, the source is always given. With the exception of such quotations, this thesis is entirely my own work;
- I have acknowledged all main sources of help;
- Where the thesis is based on work done by myself jointly with others, I have made clear exactly what was done by others and what I have contributed myself;
- Parts of this work have been published.

Signed: ..... Date: .....

Acknowledgements

I would like to express my sincere appreciation to my supervisors, Prof. Lajos Hanzo and Dr. Rong Zhang, for their tremendous guidance and constructive comments. Their commitment, enthusiasm and patience have enabled me to pursue my research interests, and to accumulate diverse experience and skills that will remain beneficial for my future career.

Moreover, I wish to thank Prof. Sheng Chen, Prof. Lie-Liang Yang, Prof. Rob Maunder, Dr. Soon Xin Ng and Dr. Mohammed El-Hajjar, for their suggestions to my research work. Meanwhile, I am grateful to Dr. Hongming Zhang, Dr. Chao Xu and Jingjing Wang as well as other colleagues in the Next Generation Wireless Group for their productive collaborations and discussions. I wish to express my gratitude to Dr. Anas F. Al Rawi and Leslie Derek Humphrey in BT as well as Dr. Charalampos Tsimenidis in Newcastle University for their significant advice.

Additionally, the financial support of the joint industrial CASE studentship between University of Southampton and BT is gratefully acknowledged.

Last but not the least, I would like to thank my parents for their generous and endless love throughout my life.

List of Publications

Journals:

1. **T. Bai**, H. Zhang, R. Zhang, L.-L. Yang, A F. Al Rawi, J. Zhang and L. Hanzo, "Discrete Multi-Tone Digital Subscriber Loop Performance in the Face of Impulsive Noise", IEEE Access, vol. 5, pp. 10478 - 10495, 2017.

2. **T. Bai**, C. Xu, R. Zhang, A F. Al Rawi and L. Hanzo ,"Joint Impulsive Noise Estimation and Data Detection Conceived for LDPC-Coded DMT-Based DSL Systems", IEEE Access, vol. 5, pp. 23133 - 23145, 2017.

3. **T. Bai**, H. Zhang, J. Zhang, C. Xu, A F. Al Rawi and L. Hanzo, "Impulsive Noise Mitigation in Digital Subscriber Lines: the State-of-the-Art and Research Opportunities", submitted to IEEE Communications Magazine.

4. **T. Bai**, C. Xu, R. Zhang A F. Al Rawi and L. Hanzo, "Performance of HARQ-Assisted OFDM Systems Afflicted by Impulsive Noise: Finite-Length LDPC Code Analysis", to be submitted to IEEE Access.

5. **T. Bai**, H. Zhang, C. Xu, A F. Al Rawi and L. Hanzo, "Thirty Years of Noise Modeling and Processing in Power-Line Communications", to be submitted to IEEE Communications Surveys and Tutorials.

6. **T. Bai**, P. Pan, C. Xu, Z. Babar, R. Zhang and L. Hanzo, "Outage Probability Analysis of the Ultra-Reliable Industrial IoT", submitted to IEEE Transactions on Vehicular Technology.

7. **T. Bai**, J. Wang, Y. Ren and L. Hanzo, "Energy-Efficient Computation Offloading for Secure UAV-Edge-Computing Systems", submitted to IEEE Transactions on Vehicular Technology.

8. S. Feng, **T. Bai** and L. Hanzo, "Joint Power Allocation for the Multi-User NOMA-Downlink in a Power-Line-Fed VLC Network", Submitted to IEEE Transaction on Vehicular Technology.

9. X. Zhang, **T. Bai** and L. Hanzo, "Hybrid Visible Light and Power Line Communications for Indoor Mobile Users", under preparing.

Contents

Chapter 1

Introduction

1.1 Motivation

The future smart home is envisaged to be a theater for the orchestration compelling of various personal multimedia and of machine-to-machine communications, for supporting diverse applications of entertainment, home automation and health care as well as home security and management [1]. In other words, the devices accessing the home network will include not only communication devices (e.g. laptops, tablets and cellphones) and consumer electronics (e.g. televisions as well as radio and play stations), but also home appliances (e.g. washing machines and air-conditioners). Many equipment in the smart home are well endowed with various sensors and controllers. This real-time information aggregation paradigm imposes stringent requirements on our indoor communication systems in terms of their throughput, reliability, delay and energy consumption.

As a backbone of supporting indoor communcations, the existing wired broadband networks are pushed to their limits. The fiber-to-the-home (FTTH) concept, which is expected to satisfy the escalating demands in terms of throughput and reliability as well as latency, is still not a ubiquitous reality at the time of writing and it is outright banned in protected historical architectural regions [2]. To address this issue, XG.fast [3] as shown in Fig. 1.1, the new digital subscriber line (DSL) technology, is associated with fiber-to-the-frontage (FTTF) architecture, which has been conceived for supporting high-quality broadband network access, relying on already-installed twisted pairs and the so-called home-passed fiber network.

Particular to the physical-layer implementation, the design of both modulation and coding schemes requires the detailed characterization of the channel and noise properties. The most crucial factors degrading the DSL performance include frequency-dependent attenuation as well as multi-path propagation and noise. In contrast to the wireless communication scenario, the noise in DSL cannot be simply characterized by an additive white

Gaussian noise (AWGN) model [4]. Hence, a particular investigation of the typical DSL impairments constitutes inevitable prerequisite for accommodating the afore-mentioned escalating demands.

The noise components in DSL can be generally classfied into crosstalk as well as impulsive and background noise. Crosstalk is the phenomenon by which a signal transmitted over a specific cable contaminates the signal in another cable. The multi-user crosstalk can be entirely averted by the fiber-to-the-frontage (FTTF) architecture [3] or efficiently mitigated by the transmit preprocessing techniques of vectoring and dynamic spectrum management [5]. However, the effects of impulsive noise continue to impose a substantial deleterious impact on DSL systems. Therefore, the feature of the impulsive noise in DSL needs to be explicitly characterized for analyzing its deleterious influence to DSL systems. Moreover, an efficient mitigation technique is a prerequisite for ensuring a reliable backbone for the forthcoming smart home. These two aims constitute the motivation of this thesis.

1.2 An Introduction to Digital Subscriber Lines

Digital subscriber lines constitute a technique that allows broadband signals to be delivered over twisted pairs. In order to support home area network access, numerous alternative media have been conceived, typically including optical fiber, coaxial cable, wireless access and satellite services, whose strengths and weakness are discussed below.

- Optical fiber: the FTTH concept resulted in excitement during the late 1980s, when the operators planed to upgrade all twisted pairs to fiber. The motivation came from the notion that twisted pairs were incapable of providing high-speed data delivery. Fortunately, both HDSL and ADSL demonstrated the substantial potential of the access network of twisted-pairs. Nonetheless, there is little doubt that fiber will be eventually laid to support all customers and the only question is when.

- Coaxial cable: Service providers can potentially provide DSL-like services over the coaxial cable network originally designed for broadcasting television signals. However, on average, 90% of the cables installed are only unidirectional for signal delivery [6]. Although there are some trials which upgrade the coaxial network to bidirectional tele-traffic in some selected areas, its roll-out remains limited by the expensive cost, caused by replacing the infrastructure.

- Wireless access: The rapid development of wireless access is potentially capable of supporting enhanced mobile broadband services via wireless links in the forthcoming 5G network in most scenarios. However, in some particular scenarios, e.g.,

the wireless links experience severe blockage in high-rise buildings. Furthermore, its deployment cost cannot be justified in remote rural areas, where only limited tele-traffic is generated.

- Satellite services: Digital satellite broadcast has seen fast growth, with millions of subscribing customers. However, no upstream capability to the satellite is available for most customers.

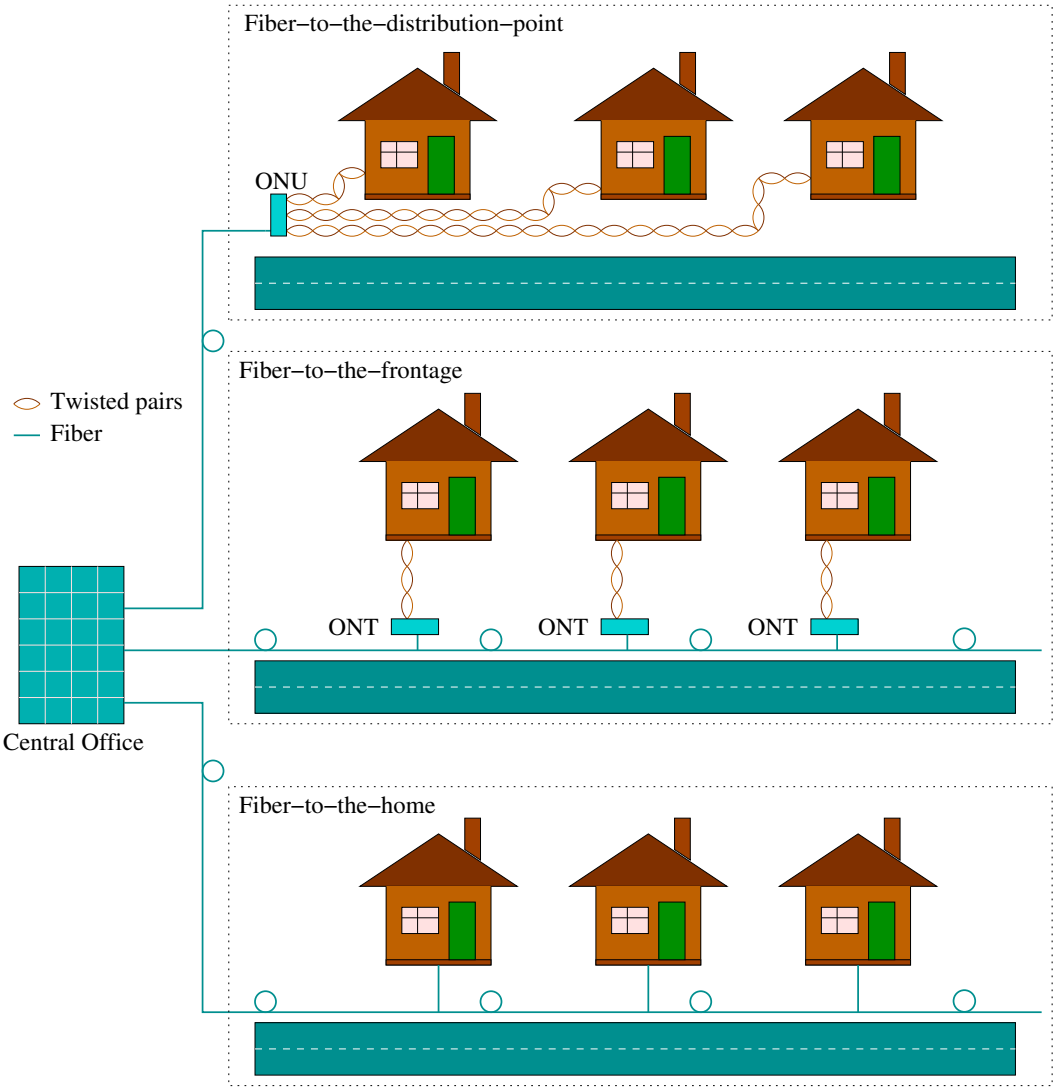

Figure 1.1: Illustration of the wireline based broadband network architecture. The abbreviations are as follows: optical network unit (ONU) and optical network terminal (ONT).

In a nutshell, relying on the existing telephone lines, DSL techniques are capable of supporting broadband network access at a low cost and high quality, before the wide-spread full-optical network is rolled out. At the time of writing, the operational DSL is typically used up to the fiber-to-the-distribution-point (FTTdp). As shown in Fig. 1.1, an optical network unit (ONU) is deployed at the curb, which acts as a relay station between the fiber

and twisted pairs. In other words, the central office and ONUs are connected using fiber, while ONUs are linked with multiple customer premise equipments (CPEs) by twisted pairs. As a result, the high-cost installation of fiber can be avoided and yet high-quality network access is attained. Furthermore, the concept of fiber-to-the-frontage (FTTF) was conceived [3] for the next generation of DSL. As shown in Fig. 1.1, the FTTF is supplemented by installing an optical network terminal (ONT) at the frontage, which connects only to a CPE. As a consequence, the multi-user crosstalk can be entirely eliminated, which is more explicitly discussed in Section 1.2.1. Moreover, the shorter twisted pair link results in a reduction of channel attenuation, hence enabling more bits to be successfully delivered using the same transmit power. In the rest of this section, we will outline the channel impairments that restrict the system performance and then provide a historical perspective on DSL. Moreover, the techniques in DSL are discussed from a physical-layer perspective.

1.2.1 Overview of Channel Impairments in DSL

The detailed characterization of both the channel and noise constitute a prerequisite for designing an appropriate transceiver. In this section, we present an overview of the channel impairments encountered in DSL. Typically, the channel impairments in DSL include a frequency-dependent channel, crosstalk as well as background and non-stationary noise, which are briefly introduced in this subsection.

Channel Characteristics

The early analysis of DSL channel properties dates back to 1991 [7], where the authors have revealed that the increasing operational frequencies results in a hostile environment for data transmission, because the infrastructure that was originally designed for voice-band signal transmission is far from ideal for data transmissions. Fig. 1.2 depicts a typical DSL channel in the frequency domain and the channel characteristics are summarized as follows.

Firstly, impedance matching in electrical wires is not designed at the data transmission frequency and hence the signal is reflected at the junctions of cables and sockets, resulting in *multi-path propagation*.

Secondly, since the impedance varies as a function of frequency, the channel exhibits *frequency-dependent attenuation*. Moreover, *low-pass* characteristics are observed in DSL systems, because high-frequency signals suffer from more hostile reflections.

Thirdly, the channel of DSL systems exhibit a *slowly time-variant nature*, which can be modeled as a linear time-invariant system.

Fourthly, the DSL channel exhibits *path loss*, which depends on the operating frequen-

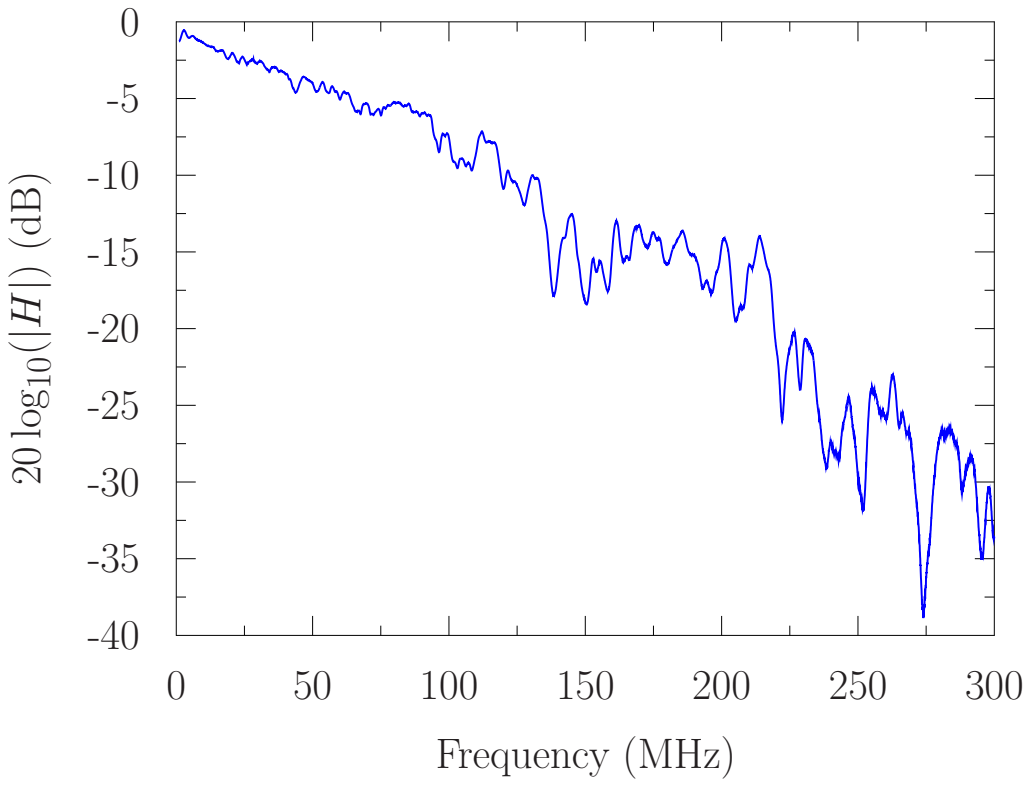

Figure 1.2: The frequency-domain channel transfer function (FDCHTF) of DSL upto 300 MHz.

cies, voltage, type of cables, loading, weather, etc. Typical values of the path loss range from $0.1 - 200$ dB/km and it tends to increase with the operating frequencies.

Multi-User Crosstalk

Crosstalk is a phenomenon by which a signal transmitted on one circuit imposes an undesired effect on another circuit. Historically, Bell's twisting of the telephone lines substantially reduced the electromagnetic coupling among twisted units. However, the crosstalk cannot be totally eliminated, hence it remains a major impairment [8], especially at high operational frequencies. As depicted in Fig. 1.3, the crosstalk in DSL is classified into near-end crosstalk (NEXT) and far-end crosstalk (FEXT).

- As shown in Fig. 1.3a, NEXT occurs in the scenario that User 1 is transmitting data in the uplink spanning from the home to the CO, whereas other users bonded with User 1 are receiving data, when they use the same frequencies in the downlink.
- FEXT occurs, when the collocated customers simultaneously transmit or receive signals using the same frequency band. Considering the upstream in Fig.1.3b as an example, we observe that all users are transmitting signals to the ONU. In this case, the receiver of User 2 also receives the signals from User 1. Here we term this type

of interference by FEXT.

In this system operating at a low frequency band, the crosstalk is not a challenging issue because the direct channel gain is usually over 100 times of the crosstalk channel gain. However, in order to enhance the throughput, we consider an ultra-broadband based solution, where the crosstalk becomes increasingly deleterious due to the reduction of the direct channel gain.

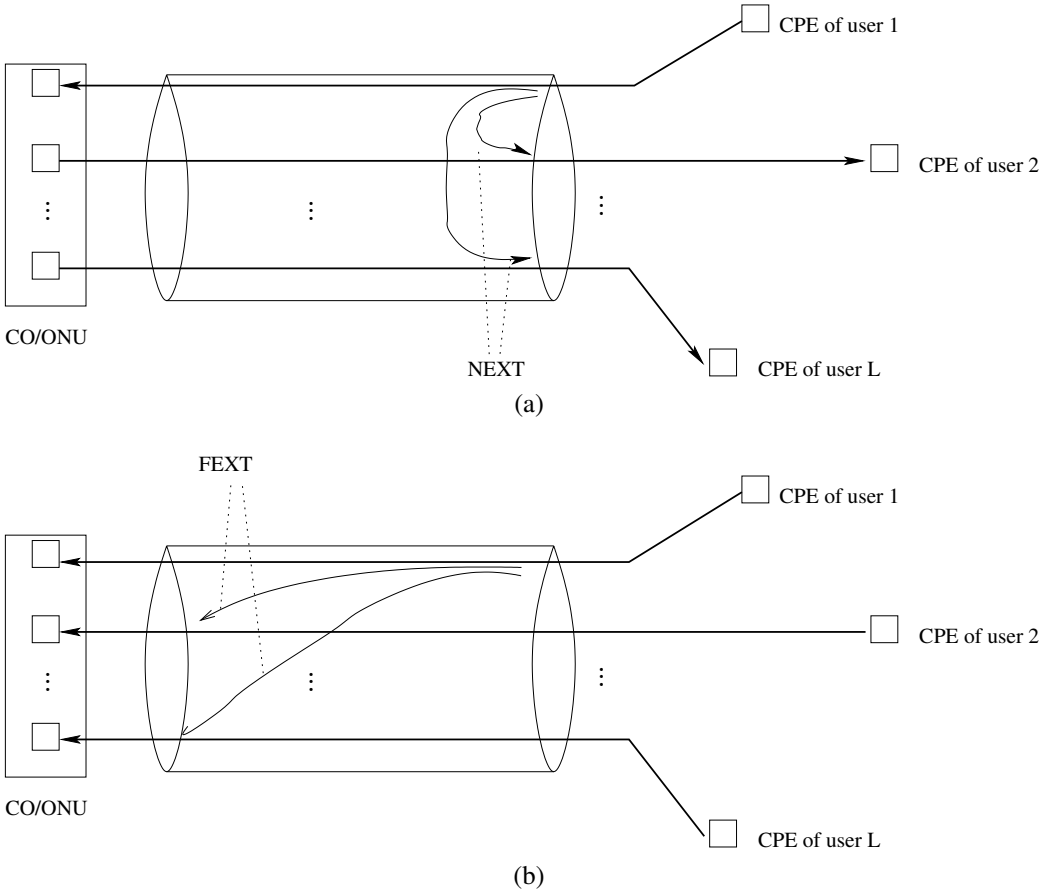

Figure 1.3: Illustration of Far-end and near-end crosstalk. a) NEXT, b) FEXT.

Non-stationary Noise

The non-stationary noise in DSL can be categorized into internally and externally induced classes [9]. Externally induced impulses are inflicted by high-voltage devices, railways, fluorescent tubes, lightning, etc. whereas the internal ones are caused by dialing pulses, busy signals, ringing, etc. In general, they are also categorized into narrow-band interference and impulsive noise as follows.

- *Narrow-band interference* originates from both the uncoordinated DSL devices and the ingress of broadcast radio stations in the form of sinusoidal signals, resulting in a high-power impairment, which may saturate at the analog front-end electronics.

Fortunately, this ingress is usually restricted to a narrow-band, hence sophisticated transmission methods may attempt to notch the bands occupied by this interference, essentially avoiding the noise rather than try to transmit in the face of it.

- *Impulsive noise* is caused by electromagnetic disturbances in the vicinity of twisted-pairs. Deleterious impulses may be generated by the opening of a refrigerator door, control voltages of elevators, and the ringing of the tele-phones on lines sharing the same binder. The voltage induced can be as high as 100 mV and span time intervals as long as 3 ms, which may overwhelm the desired signal and causes unreliable data transmission.

1.2.2 DSL Evolution

Telephone lines date back to Alexander Graham Bell's invention of the telephone in 1875, when a single voice signal was transmitted within a 3.4kHz-bandwidth channel [6]. With the ever-increasing demand for data service since the 1970s, the feasibility of the twisted copper pair to convey data has drawn a huge amount of attention. Nowadays, DSL technologies have enabled high-speed digital transmission over the conventional telephone line.

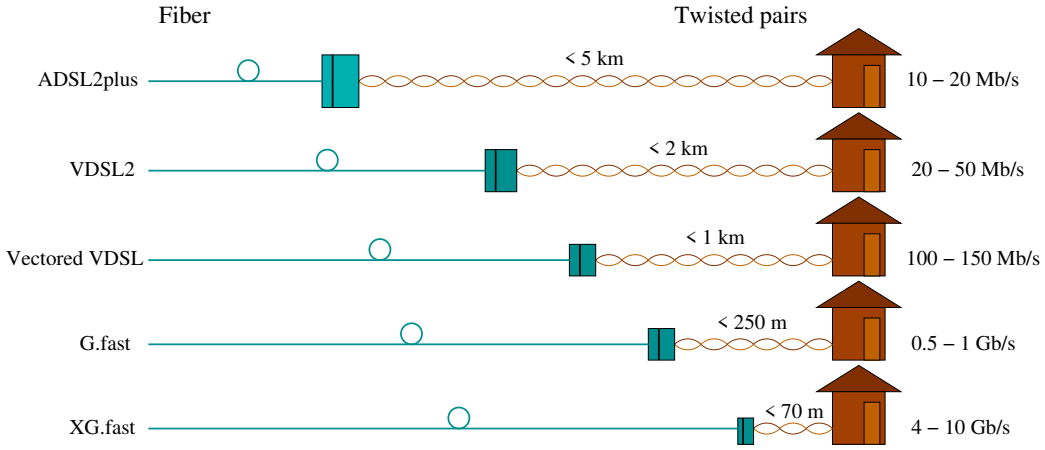

Figure 1.4: Illustration of the evolution of DSL.

The throughput of DSL can be improved in three approaches: reducing the distance of twisted pair links and expending the bandwidth as well as adopting more advanced communication and signal processing techniques. In this subsection, we focus on the first and second approaches, with the aid of Fig. 1.4 and Fig. 1.5, which present the evolution of DSL from the perspective of the distance of twisted pairs as well as operational spectrum, respectively. The initial modem was not designed for supporting simultaneous telephone services and data services. This problem was solved by the integrated services digital network (ISDN). Designed for short range data services, the high-rate digital subscriber

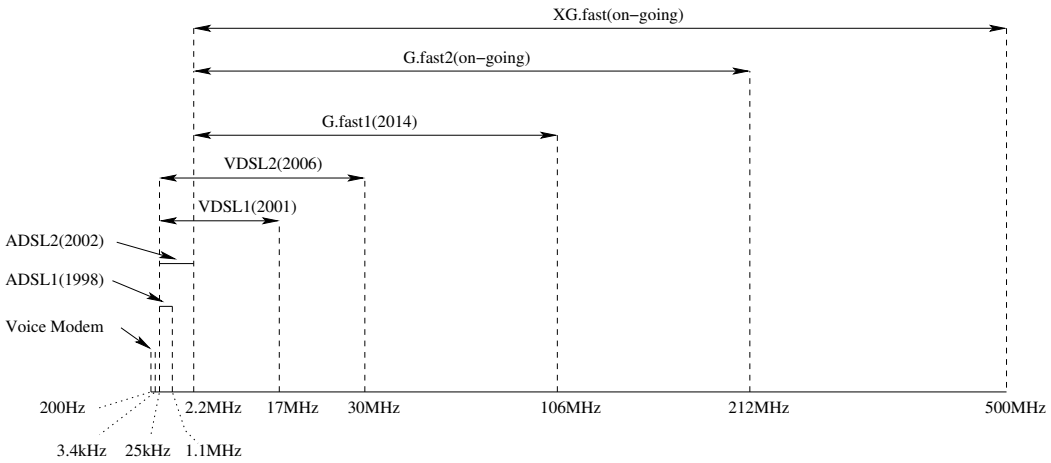

Figure 1.5: Illustration of the evolution of DSL.

line (HDSL) was capable of supporting data traffic amongst buildings within a campus network. Asymmetric DSL (ADSL) was developed to support asymmetric data transmission by sharing the bandwidth between downstream and upstream. With data rate of upto 8Mbit/s for the downstream, the true broadband era has arrived at the end of the 20th century. ADSL2 improved the peak downstream rate to 12Mbit/s by extending the bandwidth from 1.1MHz to 2.2MHz and by introducing the digital subscriber line access multiplexer (DSLAM), which is deployed near the CPEs. Very high-speed DSL (VDSL) extended the bandwidth further, upto 17MHz and 30MHz for the most recent edition termed as VDSL2. However, with the increase of the operating frequencies, crosstalk among copper pairs becomes a challenge. Hence the so-called vectoring techniques were designed for reducing the influence of crosstalk, hence boosting the data rate upto 150Mbit/s. Later on, DSL under the standard of G.fast, is capable of providing 500Mbit/s to 1000Mbit/s over copper wires within a distance of 250 meters for FTTdp architecture. At the time of writing, experts from industry and academia are working on a new standard for DSL, namely XG.fast, which aims to enable 10-Gb/s data transmission over a 70 m twisted pair link, using the frequencies upto 500 MHz.

1.2.3 DSL Techniques

During the evolution of DSL, an increasing number of both advanced communication and signal processing techniques have been gradually implemented, as summarized in Fig. 1.6. As shown in Fig. 1.7, we categorize them into five classes, including modulation, channel coding, impulsive noise reduction, vectoring and spectrum management. In this subsection, we will briefly review them.

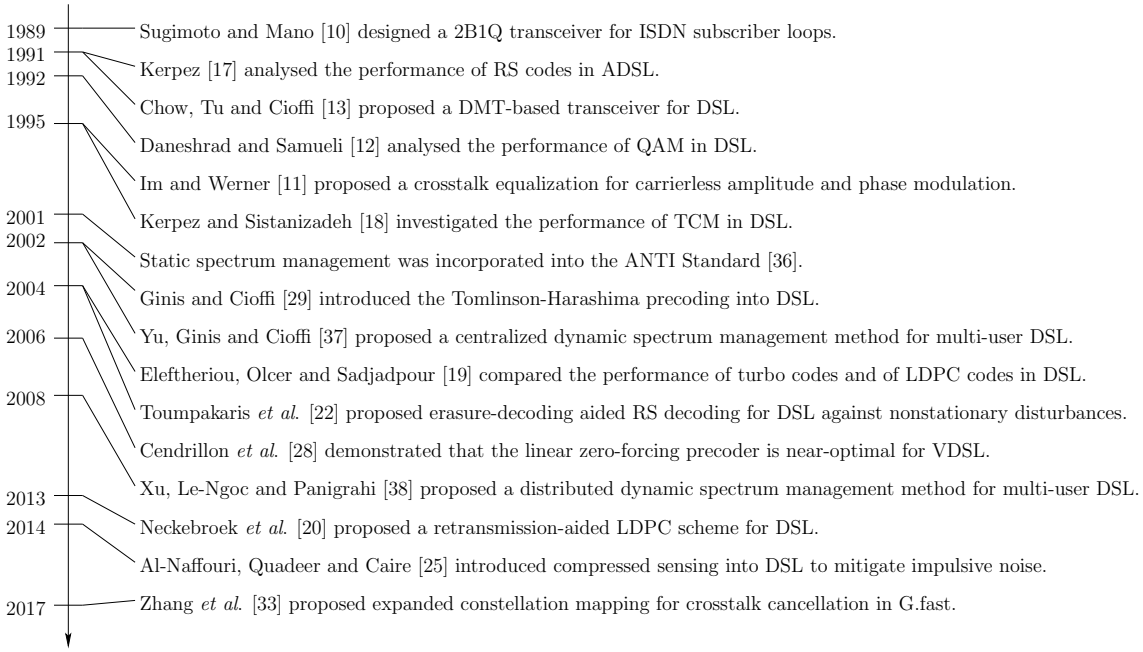

Figure 1.6: Illustration of time-line of DSL techniques from a physical-layer perspective.

Modulation

Modulation is used to transform groups of bits to points on the constellation diagram. In DSL, the binary information bits are mapped to the symbols of either discrete multitone (DMT) or of single-carrier modulation (SCM) known as two-binary one-quaternary (2B1Q), carrierless AM/PM (CAP) and quadrature amplitude modulation (QAM). Sugimoto *et al*. designed the transceiver of 2B1Q for ISDN [10], which relies on a four-level pulse amplitude modulation (PAM). Im and Werner proposed a crosstalk equalization technique for the CAP [11], which is a two-dimensional passband transmission scheme. Daneshrad and Samueli analysed the performance of QAM in DSL [12], which is based on baseband spectral shaping techniques, while Chow *et al*. proposed the classic DMT [13]. Shim and Shanbhag compared the complexity of the above single-carrier and multicarrier modulation schemes in the high-rate VDSL scenario [14].

Channel Coding

The low-power received signals are susceptible both to channel impairments in DSL. Hence they are fundamentally protected using forward error correction (FEC) codes, for improving the attainable system performance. Reed-Solomon (RS) codes and trellis coded modulation (TCM) have been incorporated into the recommendations of ADSL and VDSL. The specific benefit of this FEC combination is that TCM has been designed to have a modulated signal constellation, where the unprotected bits are mapped to phaser points having the largest possible Euclidean distance. They are also capable of exploiting soft detection,

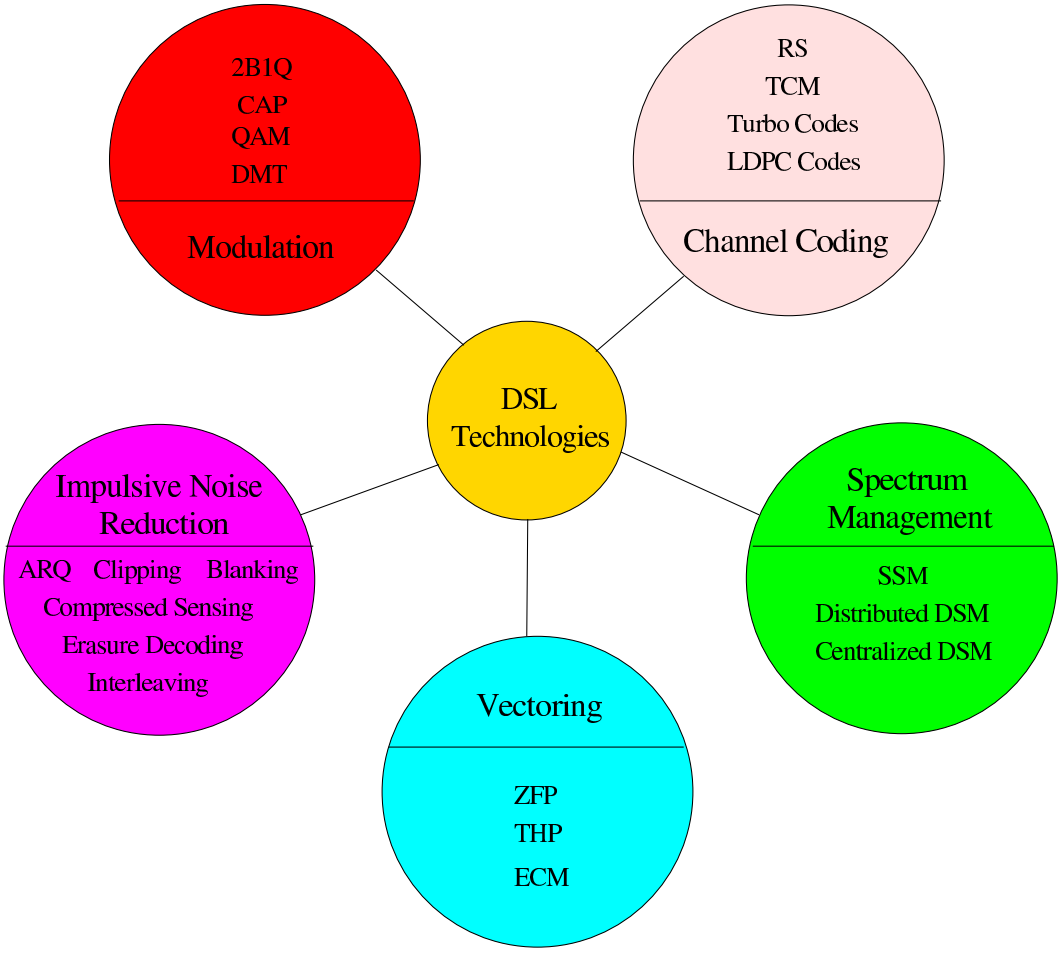

Figure 1.7: Illustration of DSL techniques from a physical-layer perspective. The abbreviations are defined as follows: two-binary one-Quaternary (2B1Q), carrierless AM/PM (CAP), quadrature amplitude modulation (QAM). discrete multitone (DMT), Reed-Solomon codes (RS), trellis coded modulation (TCM), low density parity-check (LDPC), automatic repeat request (ARQ), zero-forcing precoding (ZFP), Tomlinson-Harashima precoding (THP) and expanded constellation mapping (ECM), static spectrum management (SSM), dynamic spectrum management (DSM).

when the received signal is contaminated by AWGN. The resultant long burst of errors can be readily corrected by a powerful long external RS code. This code-family has the highest possible minimum Hamming distance amongst the codewords, but unfortunately its soft-decision-based Chase-decoder typically has a limited extra gain. At the time of writing the intention is to replace them by more powerful codes, such as turbo codes [15] or low density parity-check (LDPC) codes [16]. Kerpez examined the performance of RS codes in ADSL [17] in the presence of impulsive noise. Later Kerpez and Sistanizadeh investigated the performance of TCM in DSL [18]. Eleftheriou *et al.* discussed both the performance and latency as well as complexity both of turbo codes and of LDPC codes in DSL [19].

Impulsive Noise Reduction

High-power impulsive noise causes deleterious influence to DSL systems' reliability and hence it has drawn substantial attention [20–26]. Assuming that the impulsive noise does not occur frequently, Neckebroek *et al*. proposed retransmission schemes in [20] for DSL. Interleaving [21] is another low-complexity technique of reducing the effects of impulsive noise, albeit at the cost of increasing the delay. Toumpakaris and Cioffi designed erasure decoding aided RS decoding [22] for reducing the interleaving delay. To mitigate the effect of impulsive noise, Zhidkov conceived various low-complexity schemes, such as clipping and blanking, for a general OFDM scenario [23]. Quite recently, compressed sensing has also been proposed for impulse-noise mitigation [25] [26].

Vectoring

The increase of the operating frequencies results in a higher attenuation of the channel and a larger the power of far-end crosstalk (FEXT). In this case, the crosstalk from other cables may severely overwhelm the intentionally transmitted signal. As a result, the intentional signal cannot be successfully distinguished from the noise. To tackle this issue, transmit precoding (TPC) is applied to the transmitted signal for the downstream transmission, so that it arrives at customers without crosstalk, thanks to the co-located transmitter structure [27]. Specifically, Cendrillon *et al*. proposed linear zero-forcing precoding (ZFP) and demonstrated that it was near-optimal under the scenario of low operating frequencies in DSL [28]. Ginis and Cioffi introduced the nonlinear TPC concept of Tomlinson-Harashima precoding (THP) [29] into DSL [30], which has a better performance than ZFP. Recently, Zhang *et al*. proposed a vector perturbation [31] [32] based method, namely the expanded constellation mapping (ECM) [33], which achieved a near-capacity performance.

Spectrum Management

To cope with the NEXT, frequency division duplex (FDD) or time division duplex (TDD) is employed [34], which enable the upstream and downstream transmissions operate in separate frequency bands or time slots, respectively and hence the NEXT problem is avoided. Power control is one of the most pivotal issues in the interference-limited multiuser DSL system, where each user's rate is dependent both on its own power allocation and on that of others', because the signals from others impose crosstalk in DSL, especially at the high frequencies, which causes a degradation of the sum rate [35]. In order to make use of the high frequencies, efficient spectrum management techniques must be employed. The very basic method is static spectrum management (SSM), which allocates an identical power to each user [36]. By contrast, dynamic spectrum management (DSM) adaptively allo-

cates a frequency-dependent power to the different users. Yu *et al*. proposed one of the first distributed DSM algorithms using iterative water-filling [37], which operates entirely autonomously. Xu *et al*. designed a low-complexity centralized DSM algorithm [38] for DSL, which is capable of finding the globally optimal solution, but requires a central hub supplied with full knowledge of the network's status. Since the recent time, a joint vectoring and dynamic spectrum management has drawn a growing interest [39], which is capable of achieving considerably higher bit rates than other schemes.

1.3 Necessity of Performance Analysis and Impairment Mitigation

Typical channel impairments in DSL include those inflicted by the frequency-selective channel, crosstalk and impulsive noise. As discussed in Section 1.2.3, DMT is capable of transforming the frequency-selective channel into a number of subchannels exhibiting a flat FDCHTF. The capacity can be approached with the aid of bit loading techniques [40], by allocating a larger number of bits to the specific subcarriers experiencing a high channel gain. Moreover, the crosstalk can be efficiently alleviated using so-called vectoring techniques [27] and dynamic spectrum management [35]. Meanwhile, in the next generation DSL where an ONT is supporting a single CPE, the multi-user crosstalk can be entirely avoided. However, impulsive noise continues to impose substantial detrimental effects on DSL systems. In this section, we commence by elaborating on the behavior of impulsive noise and on its deleterious impacts on the system performance. Then we outline challenges of both the associated performance analysis and of the available impairment mitigation techniques in the face of impulsive noise, respectively.

1.3.1 The Impacts of Impulsive Noise on DSL Systems

The behavior of impulsive noise is predominantly characterized by the following four aspects. Firstly, the impulses are usually of *high power*, hence the desired *signals are likely to be overwhelmed* in the DSL relying on low-power transmitters. For example, impulsive noise in certain frequencies may be up to 50 dB above the background noise. Secondly, impulsive noise samples commonly exhibit *non-Gaussian distribution*, hence *the optimality of the detector* originally optimized for Gaussian noise environments no longer holds. Thirdly, the impulsive noise often *occurs in bursts*, which may *obliterate an entire packet*, because the bursts of errors may exceed the error correction capability of FEC codes. For instance, the average duration of an impulse amounts to 35 µs, i.e. potentially lasting for the duration of two consecutive DMT symbols [41]. Fourthly, the impulsive noise is of high occurrence probability, which leads to the fact that DSL transmission links are

frequently under the risk of contamination, hence *degrading the reliability* of DSL. For example, typical noise bursts account for 3.29% of the total time interval in DSL [20].

1.3.2 Why the Performance Analysis is Important and Challenging?

From the discussions in Section 1.3.1, we may conclude that the occurrence of impulsive noise severely degrades the DSL system performance. However, it is desirable to quantify the degradation, for examining the gap between the attainable system performance and the requirements of services. The performance analysis of DSL systems in the face of impulsive noise plays an important role in addressing this issue [42]. The challenges of performance analysis are as follows. The first one hinges on *the trade-off between the feasibility of performance analysis and its accuracy*, as determined by the noise model selected. To elaborate, the accuracy of the selected impulsive noise model directly determines the accuracy of the performance analysis results. Therefore, it is desired to analyze the system performance based on an accurate empirical noise model. However, some of the functions characterizing an accurate model are often mathematically intractable. In this way, we have to strike on trade-off between the accuracy and the feasibility of tractable performance analysis. The second one is *the trade-off between the feasibility of tractable performance analysis and the complexity of the transmission system considered*. To elaborate, different tools have to be invoked for uncoded and coded systems. In the family of coded systems, the analysis based on infinite codeword length and finite length leads to diverse performance results. These challenges have to be carefully tackled.

1.3.3 Why the Impulsive Noise Mitigation is Important and Challenging?

As elaborated on in Section 1.3.1, the noise severely deteriorates the performance of DSL systems, hence noise mitigation plays a crucial role. More explicitly, the conventional transceiver design, including detection and coding, has to be modified for accommodating the noise in DSL. Furthermore, even when equipped with the optimal transceiver, the system cannot achieve the same performance as in AWGN environments, at a given noise level. Additionally, the influence of noise should be explicitly considered when conceiving channel estimation strategies. The noise mitigation challenges are as follows. The first one is the noise *mitigation efficiency*. A well-designed mitigation technique has to mitigate the impulsive noise as much as possible for establishing a reliable transmission link. The second is *computational complexity*. The third one is *processing delay*. Low-latency transmission is desirable for many mission-critical applications for supporting home automation and health care for example. The fourth one is *spectral efficiency*.

1.4 The State-of-the-Art in Impulsive Noise Mitigation

In order to alleviate the deleterious influence of impulsive noise, DSL systems have invoked sophisticated noise mitigation techniques both at the transmitter and at the receiver sides. These mitigation techniques can be adopted individually or in combination, depending on the specific nature of the impulsive noise, as detailed below.

Mitigation techniques at the transmitter side mainly include channel coding [], interleaving [43] and Automatic-Repeat-and-reQuest (ARQ) [44]. Mitigation employed at the receiver side may be classified into *parametric* and *non-parametric approaches* [45], depending on the requirements concerning the noise's statistical knowledge. More particularly, parametric processing techniques used at the receiver side mainly include nonlinear processing [46], adaptive filtering [47], and iterative decoding [48]. Specifically, assuming that the noise obeys a particular statistical model, parametric approaches estimate its parameters during the training stage and then optimize the receiver accordingly. The advantage of parametric methods accrues from exploiting the above-mentioned statistical knowledge. However, its spectral efficiency is reduced due to the training overhead imposed. Furthermore, some performance degradation arise, when the estimated long-term statistics do not match the short-term statistics. By contrast, non-parametric approaches [45] mitigate the impulsive noise effects based on the short-term observation results. They do not degrade the bandwidth efficiency, but they tend to require a higher signal power. Non-parametric approaches typically rely on erasure decoding [49] as well as sparse reconstruction and mitigation [50]. Table 1.1 compares these techniques, in terms of their mitigation efficiency, processing delay, computational complexity and spectral efficiency. These mitigation techniques are detailed below.

Table 1.1: Comparison of Impulsive Noise Processing Techniques.

Tx/Rx	Processing Techniques	Targeted Noise	Mitigation Efficiency	Computational Complexity	Processing Delay	Spectral Efficiency
Transmitter	Channel Coding	Discontinuous	Moderate	Moderate	Moderate	Moderate
	Interleaving	Bursty	Moderate	Moderate	Moderate	High
	ARQ	Any	High	Low	High	Moderate
Parametric Receiver	Nonlinear Preprocessing	Any	Moderate	Low	Low	Low
	Adaptive Filtering	Colored	Moderate	Moderate	Low	Low
	Symbol Detector	Any	Moderate	Low	Low	Low
	Iterative Decoding	Any	Moderate	High	High	Low
Nonparametric Receiver	Erasure Decoding	Any	High	High	Moderate	High
	CS-aided mitigation	Discontinuous	Moderate	Moderate	Moderate	Moderate

1.4.1 Mitigation at the Transmitter

In this subsection, we review the family of impulsive noise mitigation techniques applied at the transmitter sides, including channel coding and interleaving as well as ARQ. Note

that our literature is not limited to the DSL, it covers all copper-based transmission systems for providing broader insights.

Channel Coding

In order to correct the errors caused by impulsive noise, numerous channel coding candidates have been considered [49,51–55], ranging from maximum-minimum-distance Reed-Solomon codes [56] to the advanced turbo codes [57], LDPC codes [16] and Polar codes [58]. To elaborate, Toumpakaris *et al.* proposed a Reed-Solonmon code scheme [49], where erasure decoding was applied to the symbols corrupted by impulsive noise. Inspired by the erasure decoding scheme of [49], Ardakani *et al.* optimized LDPC codes in [51]. Guerrieri *et al.* characterized the performance of turbo coded HomePlug AV systems [52], concluding that turbo codes are indeed capable of significantly improving the BER performance of the PLC channel suffering from narrow-band interference, especially when the decoder uses a sufficiently high number of iterations. Hadi *et al.* investigated the performance of Polar-codes in the presence of Middleton's Class A (MCA) noise in [55], where the simulation results also demonstrated that Polar codes outperformed LDPC codes in the face of MCA noise. Furthermore, both concatenated coding [59] and multi-level coding [60] were also investigated. As a further advance, Raptor codes, concatenating the Luby transform codes with LDPC codes were shown to be capable of achieving near-capacity performance [54]. Hormis *et al.* conceived a pulse-amplitude modulation (PAM)-based coset-coding scheme for counteracting the deleterious effects of impulsive noise [53].

Naturally, each channel coding scheme has a limited error correcting capability. For example, a Reed-Solomon codeword having a block length of n symbols and encoding k information bytes is capable of correcting $(n-k)/2$ error symbols. However, the impulsive noise typically exhibits in a bursty nature and hence often leads to error precipitation after the decoding, because the excessive number of errors misleads the decoding process, which hence corrects the symbols in the wrong positions, resulting in avalanche-like error prorogation. Hence, channel coding is usually invoked in the combination with interleaving, as discussed below.

Interleaving

Interleaving is a well-known techniques of randomizing the channel-induced errors by dispersing them. Interleavers can be categorized into bit interleavers [43, 61–65] and symbol interleavers [66–68], where the bit interleavers spread the bits to be transmitted while the symbol interleavers disperse the symbols. They can also be classified into block interleavers and convolutional interleavers [69].

As mentioned in Section 1.4.1, interleaving is usually utilized *in combination with channel coding* in communication systems, as shown in Fig. 1.8a. It is plausible that a binary channel decoder should ideally be combined with a binary interleaver, while a non-binary RS decoder should rely on a symbol-based interleaver, because a bit-interleaver would potentially map the bits of an erroneous symbol to another symbol, hence increasing the symbol error probability. This would in turn increase the symbol error probability to be mitigated by the symbol decoder.

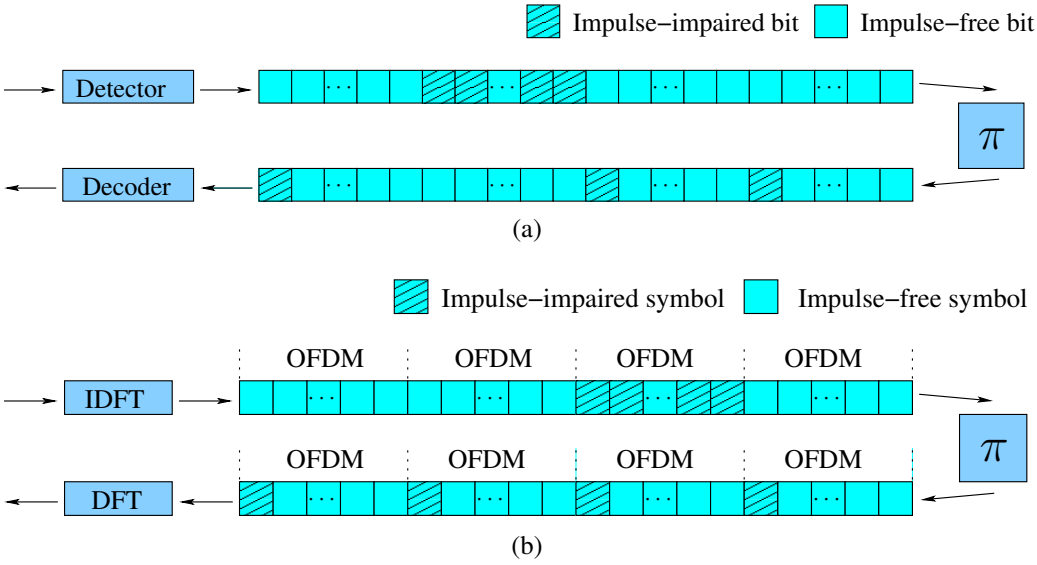

Figure 1.8: Illustration of the interleaver. (a) Interleaver for impulse-impaired bits; (b) Interleaver for impulse-impaired OFDM.

Interleavers also play a role in terms of *eliminating error floors* not only in coded but also in uncoded systems, as shown in Fig. 1.8b. To elaborate in the particular context of systems relying on multi-carrier modulation, once a time-domain sample is corrupted by an impulse in an OFDM symbol, the impulse is spread over the whole OFDM symbol after DFT-based demodulation. This way, the impulsive noise power becomes averaged over all subcarriers of the OFDM symbol. As a result, the noise level of different OFDM symbols tends to fluctuate because the impulsive noise tends to occurs not uniformly. This in turn results in an error floor, because the BER performance is predominantly determined by those OFDM symbols, which suffer from a high noise power. In order to mitigate the error floor, a time-domain interleaver (TDI) was proposed in [67], where the interleaver was placed after the inverse discrete Fourier transform (IDFT) based modulator. Accordingly, the interleaver was positioned before DFT based demodulator, so that the impulses could not only be spread within an OFDM symbol but also among the OFDM symbols. As a result, the noise power after demodulation is expected to be maintained at a similar level. The TDI based solution of [67] was further extended in [68] and [70]. Specifically, the authors conceived a time-domain interleaver in conjunction with an additional orthogonal transform (TDI-OT) [68], which was achieved by inserting another IDFT-DFT block

between the interleaver and deinterleaver of the TDI. As a benefit, the interleaver depth was quadratically increased, compared to that of [67], albeit at the cost on increasing the complexity. Given this interleaver depth, the noise power of MC systems equipped with TDI-OT became almost identical among the OFDM symbols and hence the error floor was mitigated. Note, however, that the BER performance improvement brought about by TDI and TDI-OT remains limited when the noise pulses are near-uniformly distributed.

ARQ

ARQ has been widely adopted in communication systems [71–76], thanks to its high robustness to sudden perturbations and low-complexity implementation. If a packet is correctly received at the receiver side [44], a positive acknowledgement (ACK) is sent back to the transmitter and then the next packet is transmitted. By contrast, if corrupted is received, a negative ACK (NACK) is fed back to the transmitter and then the packet is sent continuously, until the transmitter receives an ACK or the affordable number of retransmissions reaches its maximum limit.

Although it was originally designed for the MAC layer, ARQ can also be combined with channel coding in the physical layer, reaching to the concept of hybrid ARQ (HARQ), which is classified into conventional HARQ [77], Chase-combining aided HARQ [78] and incremental-redundancy assisted HARQ [79]. More explicitly, as shown in Fig. 1.9a, conventional HARQ relies on the same principle as ARQ. As depicted in Fig. 1.9b, the most recently received packet is jointly detected with the previously received copies in the context of Chase-combining aided HARQ. As seen in Fig. 1.9c, additional parity is transmitted for each transmission attempt in incremental-redundancy assisted HARQ. Typically, once a packet is corrupted, additional redundancy is requested for joint decoding at the receiver. The performance of the above-mentioned three HARQ schemes was compared in [80] in an impulsive noise environment, which revealed that the outage probability is highest for the conventional HARQ and lowest for incremental-redundancy based HARQ.

A disadvantage of HARQ techniques is their increased delay imposed by the processes of feedback, re-transmission, decoding and interleaving. If DSL systems are operated in a hostile environment, the delay caused by ARQ is substantial. Therefore, ARQ is typically used as an outer protection mechanism, compensating the failure of other impulsive noise mitigation techniques.

1.4.2 Parametric Mitigation at the Receiver

In this section, we present a comprehensive review of the parametric impulsive noise mitigation at the receiver side, including non-linear pre-processing, adaptive filtering, symbol

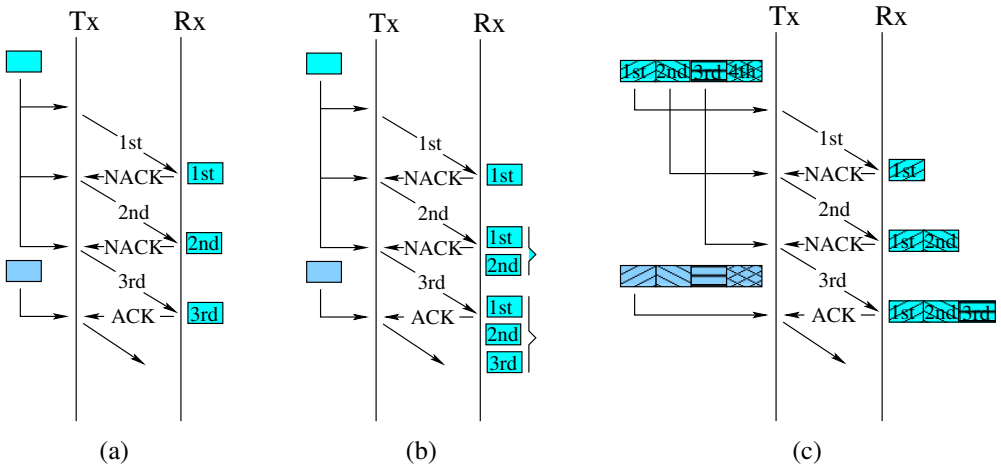

Figure 1.9: Illustration of three types of HARQ. (a) Simple HARQ; (b) Chase-combining HARQ; (c) Incremental-redundancy HARQ.

detection and iterative decoding, which are detailed below.

Nonlinear Pre-processing at the Receiver's Input

Thanks to its conceptual simplicity and ease of implementation, nonlinear preprocessing has been widely adopted in practice [46, 81, 82]. Nonlinear preprocessing is carried out at the receiver's input and typically includes blanking [46], clipping [46], replacement [82] and their combination, in order to blank out, clip or replace the received signal corrupted by impulsive noise, which are detailed as follows. Let us denote the received signal at time instant k by $y_k = x_k + n_k$. As for the low-complexity *blanking* technique shown in Fig. 1.10a, if the amplitude of y_k exceeds the pre-set threshold denoted by T_b, y_k is forced to zero, which is expressed as [46]:

$$r_k^b = \begin{cases} y_k, & \text{if } |y_k| \leq T_b, \\ 0, & \text{if } |y_k| > T_b. \end{cases} \tag{1.1}$$

In terms of the *clipping* technique [46] depicted in Fig. 1.10b, if the amplitude of y_k exceeds the pre-set threshold denoted by T_c, y_k is forced to T_c, while the phase remains unaltered, which is formulated as [46]:

$$r_k^c = \begin{cases} y_k, & \text{if } |y_k| \leq T_c, \\ T_c \exp\left(j \arg(y_k)\right), & \text{if } |y_k| > T_c. \end{cases} \tag{1.2}$$

As plotted in Fig. 1.10c, blanking and clipping can also be combined in the form of a *joint clipping and blanking* function is given by [46]:

$$r_k^{cb} = \begin{cases} y_k, & \text{if } |y_k| \leq T_c, \\ r_T^b \exp\left(j \arg(y_k)\right), & \text{if } T_c < |y_k| \leq T_b, \\ 0, & \text{if } |y_k| > T_b. \end{cases} \tag{1.3}$$

As an intermediate form of conventional clipping and blanking techniques, the so-called deep clipping shown in Fig. 1.10d, was applied to mitigate the destructive effects of impulsive noise in [81], which cut the received signal linearly under a threshold βT_{dc} and blanked the signal that exceeds the threshold, which is formulated as [46]:

$$r_k^{dc} = \begin{cases} y_k, & \text{if } |y_k| \leq T_{dc}, \\ (T_{dc} - \alpha) e^{j \arg(y_k)}, & \text{if } T_{dc} < |y_k| \leq \beta T_{dc}, \\ 0, & \text{if } |y_k| > \beta T_{dc}, \end{cases} \tag{1.4}$$

where we have $\alpha = \mu(|y_k| - T_{dc})$, μ is the clipping slope and $\beta = (1+\mu)/\mu$. Furthermore, Papilaya and Vinck [82] proposed an additional action termed as *replacement* as depicted in Fig. 1.10e, which replaced y_k by the average magnitude of noiseless OFDM samples denoted by $|\overline{x}|$, if y_k exceeded the replacement threshold denoted by T_r. The *replacement* function is expressed as:

$$r_k^{r} = \begin{cases} y_k, & \text{if } |y_k| \leq T_r, \\ |\overline{x}| \exp\left(j \arg(y_k)\right), & \text{if } |y_k| > T_r, \end{cases} \tag{1.5}$$

where $|\overline{x}|$ can be obtained by $|\overline{x}| = \sqrt{(\pi E_s)/4}$ and E_s corresponds to the signal power per symbol. Replacement can also be inserted between the clipping and blanking stages, as seen in Fig. 1.10f. The corresponding *clipping-replacement-blanking* function is formulated as [82]:

$$r_k^{crb} = \begin{cases} y_k, & \text{if } |y_k| \leq T_c, \\ T_c \exp\left(j \arg(y_k)\right), & \text{if } T_c < |y_k| \leq T_r, \\ |\overline{x}| \exp\left(j \arg(y_k)\right), & \text{if } T_r < |y_k| \leq T_b, \\ 0, & \text{if } |y_k| > T_b. \end{cases} \tag{1.6}$$

The threshold used in nonlinear receiver preprocessing has to strike a trade-off between a high detection and low false alarm probability, so that useful signals are preserved as much as possible, while the impulsive noise is mitigated as best as possible. The threshold can be simply determined experimentally by simulation based on the minimum BER [83]. However, it requires long-term experiments and it remains only suitable for the specific

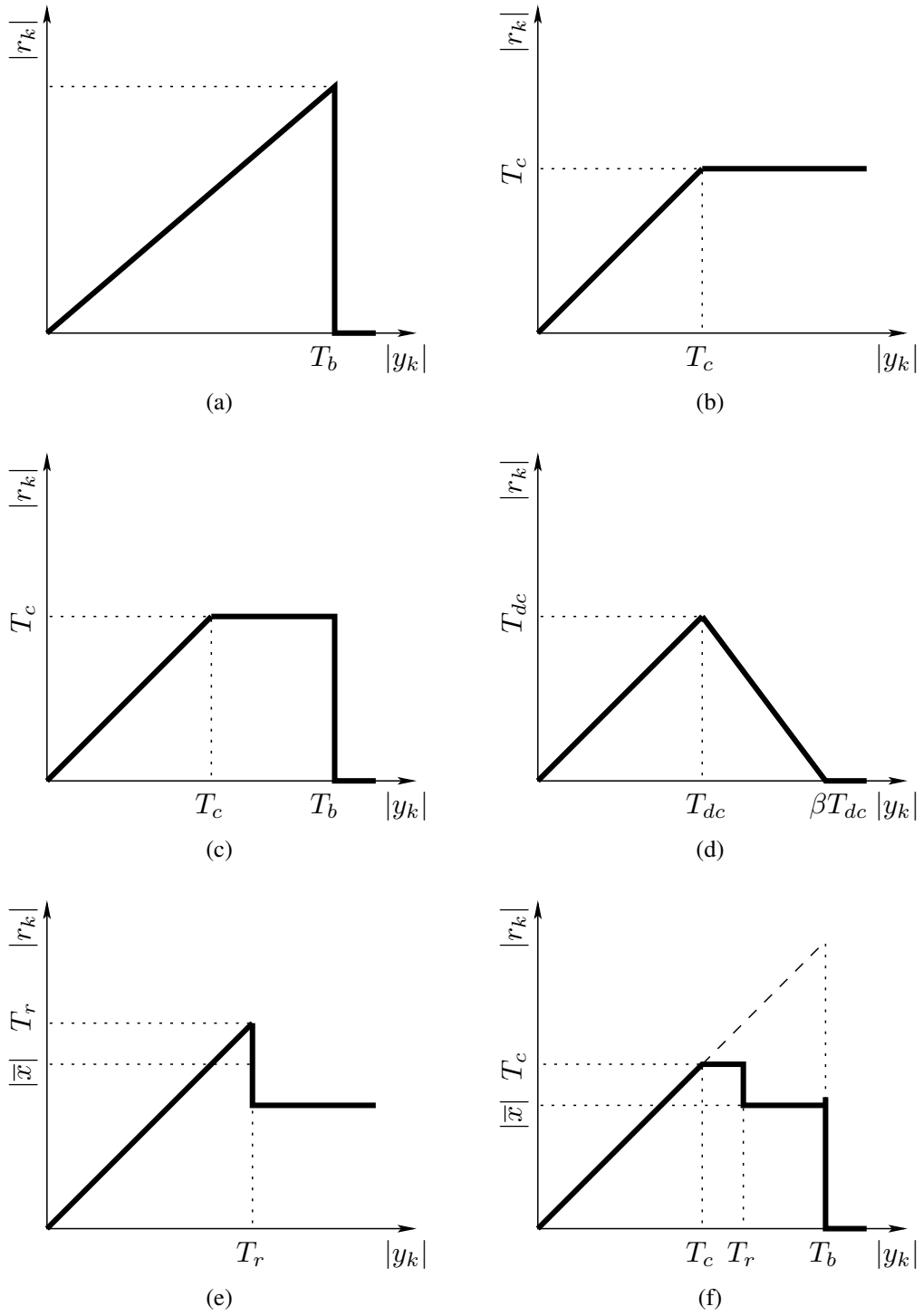

Figure 1.10: Illustration of nonlinear preprocessing at the receiver side. (a) Blanking; (b) Clipping; (c) Clipping and blanking; (d) Deep clipping; (e) Replacement; (f) Clipping-replacement-blanking.

impulsive noise scenarios. Zhidkov derived the closed-form of SNR after nonlinear preprocessing with the aid of Bussgang's Theorem [46], albeit the threshold optimization still requires extra numerical software tools. Moreover, Ndo *et al.* [84] proposed a threshold optimization technique based on signal detection theory and then examined the thresh-

old optimization in a closed form [85]. The above two threshold optimization techniques in [46, 85] require the long-term statistics of impulsive noise, which is usually difficult to obtain in practice. In order to address this issue, Tseng *et al.* [86] determined the threshold using the approximate range of impulsive noise arrival probability and derived an adaptive LLR metric for turbo decoding for mitigating the clipping effect. Moreover, Alsusa and Rabie proposed a peak-based threshold decision method for OFDM-based systems [87], which attained approximately $0.5 - 2.5$ dB gain, dependent on the accuracy of signal-to-noise ratio estimate acquired.

The disadvantages of nonlinear receiver pre-processing manifest themselves in at least two aspects. Firstly, the performance of nonlinear receive pre-processing is not only dependent on the threshold selection but also on the average peak-to-average-power ratio (PAPR) of the transmitted signal. Specifically, if the transmitted signals exhibit different power levels, it is a challenge to distinguish whether a signal is impaired by impulsive noise or not. Therefore, the employment of PAPR reduction is desired at the transmitter side, for ensuring that the power of transmitted signals remains at a similar level. Since high PAPR in multicarrier modulation typically prevails, its reduction has attracted substantial attention [88–93]. In general, PAPR reduction in multicarrier modulation can be loosely categorised as follows, signal clipping [88] and peak cancellation [89], which impose signal distortion on. By constrast, coding [90], tone reservation [91], selective mapping [92] and constant envelope design [93] do not impose any signal distortion. To elaborate, the techniques operating without distortion tend to be more complex than those imposing distortion. However, despite their higher complexity, they tend to be more attractive, because the distortion caused by PAPR reduction may outweigh the benefits gleaned from the reduced PAPR. Moreover, some single carrier schemes were proposed as a benefit of their intrinsically lower PAPR, such as. the SC-FDMA scheme of [94]. Secondly, nonlinear preprocessing causes inter-carrier interference in multicarrier modulation. To overcome this impediment, Yih proposed an iterative interference cancellation schemes [95], while Mengi and Vinck [96] advocated a successive interference cancellation scheme in OFDM systems, which relied on clipping and blanking as well on a syndrome decoder and exhibited an improved convergence speed.

Finally, the above nonlinear preprocessing techniques can also be integrated into other modules, namely, into TDI [70], bit-loading [97] and amalgamated with channel coding [84, 98].

Adaptive Filtering

Cyclostationry noise tends to occur periodically in communication systems, which typically exhibits deterministic spectral characteristics, hence it can be alleviated by adaptive

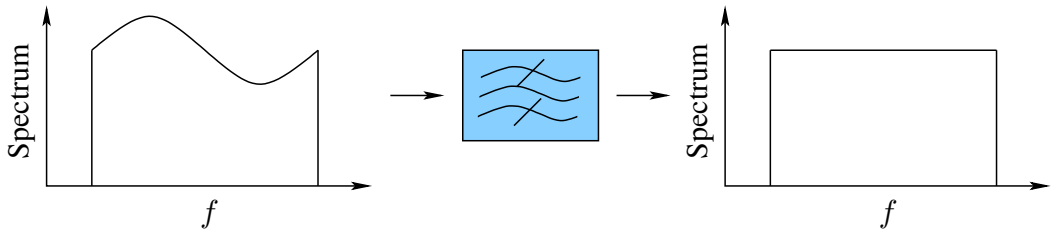

Figure 1.11: Illustration of adaptive filter for equalization. The colored noise is whitened through the adaptive filter.

filtering. In general, the adaptive filter is used for *equalization* and *prediction*. More explicitly, as shown in Fig. 1.11, assuming that the noise obeys an auto-regressive moving average (ARMA) model, it can be whitened by passing the received signals through an adaptive filter for the equalization of this frequency-domain characteristic. For example, using the so-called linear periodic time variant model of [99] for the noise, Lin *et al.* conceived a filtering scheme for whitening the colored noise [47], whose parameters were estimated using Bayesian learning. In a further contribution, Yoo and Cho proposed a linear minimum mean square error (MMSE) based method for estimatiing the parameters of correlated noise and designed an equalizer for the noise [100]. As for the prediction filter based approach, García *et al.* [101] extracted the parameters of the colored periodic noise using Yule-Walker methods based on pilots and then designed a linear prediction filter predicting and mitigating the noise effects. Similarly, Llano *et al.* [102] proposed a prediction filter for quasi-stationary noise and extracted the desired signal by subtracting predicted noise from the received signal. In their recent work, Talebi *et al.* [103] proposed an adaptive filter for the α-stable signal, which was capable of filter out the signal in an optimal pattern.

Noise-Mitigation Symbol Detection

As shown in Fig. 1.12, since conventional detectors are usually optimized for the ubiquitous AWGN environment, the non-Gaussian nature of impulsive noise in DSL degrades their *optimality*, as it has been demonstrated under the Middleton's Class A noise environment in [104] and in a radio frequency interference contaminated environment in [105]. To address the above issue, Fukami *et al.* [106] designed a noncoherent frequency shift keying (FSK) detector for the Middleton's Class A channel. Furthermore, both optimum and near-optimum detectors were designed for Middleton's Class A noise and general performance bounds were derived in [107]. In their contribution, Nassar *et al.* [108] proposed a low-complexity expectation-maximization (EM) based detector for the Middleton's Class A channel. The above three investigations were conceived for mitigating the discontinuous Middleton's Class A noise. As for the bursty impulsive noise, the memory of the channel has to be taken into account. Specifically, Fertonani *et al.* [109] proposed a noise-

mitigating symbol detector for the channel contaminated by Markov-Gaussian impulsive noise, by appropriately modifying the maximum *a posteriori* (MAP) criterion, which was able to attain the optimum performance. Similarly, Ndo *et al.* [110] extended the optimum MAP detector of [109] to the Markov-Middleton impulsive noise model.

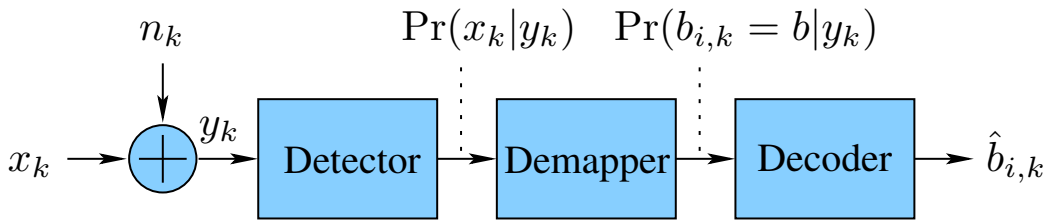

Figure 1.12: Illustration of the symbol detector, where $\Pr(x_k|y_k)$ is adjusted according to the non-Gaussian nature of the noise process.

Iterative Decoding

As the inherent counterpart of channel coding used at the transmitter, iterative decoding employed at the receiver is capable of supporting communication systems in attaining the near-capacity performance. For example, Bahl *et al.* [111] proposed the Max A Posterior (MAP) decoding strategy as early as 1974. Since this bit-by-bit decoder was much more complex than Viterbi's Maximum Likelihood sequence estimator (MLSE), but failed to outperform it, this remained almost unused, until 1993, when Berrou's turbo decoder required bit-by-bit soft-metric based detection [57]. The turbo became capable of approaching the Shannon limit. To elaborate, during the process of turbo decoding, as depicted in Fig. 1.13, Log-likelihood ratio (LLRs) of the *a posteriori* symbol probability is constituted by three parts [112], namely, the extrinsic value, channel output value and the *a priori* value. Since it was designed for the AWGN channel, the original channel output value calculation in [111] is not suitable for the impulsive noise channel in DSL, which imposes a performance degradation. To overcome this problem, Umehara *et al.* [48] modified the LLR calculation expression according to the MCA noise statistics, which enhanced the reliability of LLRs during the decoding iterations and hence significantly improved the BER performance compared to the conventional decoder. As for the LDPC decoding, the optimal initial channel output LLR calculation formulas under MCA environmental statistics were proposed for the sum-product decoding algorithm in [113]. As a further advance, upon assuming that the noise obeys a two-state Markov-Gaussian model and assuming perfect knowledge of both the noise variance and of the state transition probabilities, Mitra and Lampe [114] proposed a joint iterative estimation and decoding algorithm. When considering the classic trellis-based decoding of convolutional codes, the expressions of the soft-metric play a crucial role in predetermining the attainable performance. Specifically, the conventional soft-metric based on the Euclidean distance between the channel-imposed

received signal samples and legitimate symbol values, requires no knowledge about the noise statistics but sacrifices the performance compared to the more advanced metrics requiring more statistical knowledge about the noise. Accordingly, Mitra and Lampe [115] theoretically analyzed both the cut-off rate and the BER associated with various metrics in a Markov-Gaussian noise scenario for convolutionally coded systems.

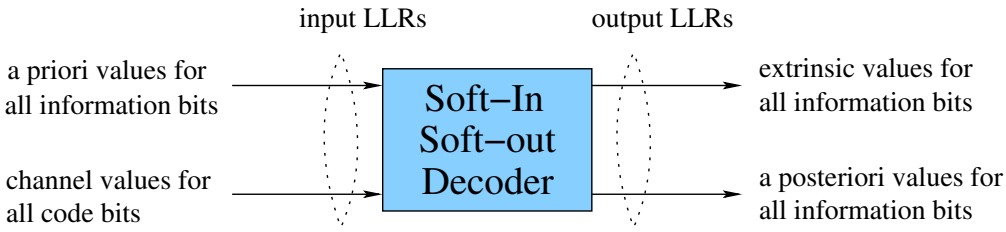

Figure 1.13: Illustration of the soft-in/soft-out decoder [111].

Block codes have also been involved for minimizing the effects of impulsive noise. For example, Haring and Vinck [116] proposed iterative decoding aided block codes for impulsive noise channels. More explicitly, the codes were optimized for spreading the noise impulses, which had a similar mitigating effects to the DFT block. The simulation results revealed that the errors caused by impulsive noise were substantially mitigated, leading to a performance close to that under an AWGN channel. Moreover, a RS coded OFDM system was conceived in [117].

Additionally, iterative decoding can also be invoked in combination with other processing techniques. For example, the combinations between clipping and both LDPC as well as turbo codes were investigated in [98] and [84], respectively. Moreover, Bai *et al.* [118] conceived an iterative impulsive noise estimation and data detection scheme, where the symbols at the output of the iterative decoder were compared to the received signals in order to improve the accuracy of impulsive noise estimation.

1.4.3 Non-Parametric Mitigation at the Receiver

In this section, we present a brief review of non-parametric impulsive noise mitigation carried out at the receiver side, including erasure decoding [49, 51, 54, 119–123] and compressed-sensing-aided mitigation [26, 45, 50, 124–128], which are detailed below.

Erasure Decoding

The noise-mitigation symbol detection and iterative decoding require the statistical knowledge of impulsive noise, which is however difficult to obtain in practice. In the case where the noise statistics are unknown, once a symbol is corrupted by impulsive noise, the corresponding LLRs gleaned from the soft detector become unreliable due to the soft metric

mismatch and in case of iterative detection the errors may also be propagated to the symbols in the vicinity during the iterative decoding stage. A promising solution is to identify the low-confident symbols impaired by impulsive noise and erase them during decoding. More explicitly, the large amplitude and bursty occurance of impulsive noise allow us to spot the impaired symbols, which are then marked as erasures [119]. In this way, the LLRs corresponding to these symbols are not involved in the decoding process and hence the impulse-free symbols are protected from the noise impulse. This leads to *improved BER performance* [49]. Naturally, the erased symbols have to be filled. A beneficial technique is to exploit the position knowledge of these symbols, which can be achieved for example by RS codes. Explicitly, this is achieved by exploiting the specific property of RS codes that they can correct $t = (h-k)/2$ errors or fill $2t = (h-k)$ erasures. This explicitly doubles their erasure-filling capability.

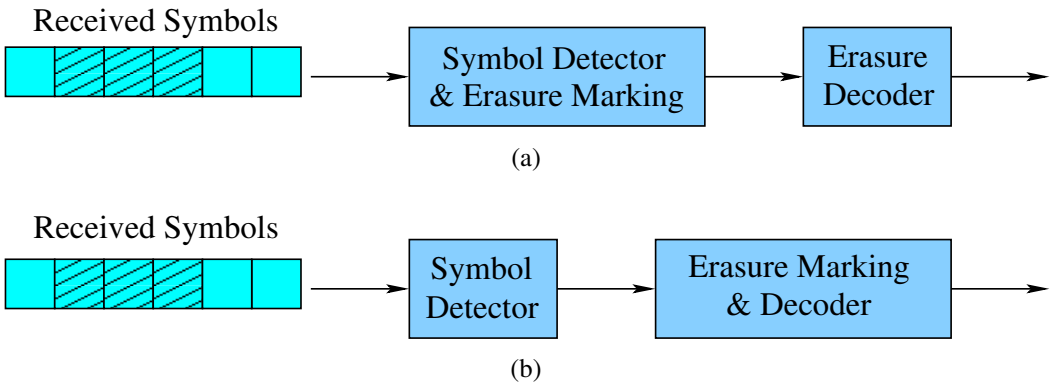

Figure 1.14: Illustration of the erasure decoding. (a) Separate erasure and decoding; (b) Joint erasure and decoding.

To elaborate, the erasure-filling techniques of copper-based communications can be classified into *separate erasure and decoding* [51, 54, 120] as well as *joint erasure and decoding* [121–123]. As for the separate erasure and decoding shown in Fig. 1.14a, the decoding used for correction excludes the symbols that are impaired by impulsive noise. For example, Ardakani *et al.* [51] proposed a separate erasure and decoding scheme, where the corrupted symbols were detected using a distance-based detection technique [129], while their LDPC decoder was optimized for the erasure channel contaminated by AWGN. As a further solution, Andreadou and Tonello proposed a concatenated coding scheme [54], where LDPC codes were employed as the inner code to identify the catastrophically error-infested packets, while Luby transform (LT) codes [130] were used as the outer code for correcting errors. Since the inner code and the outer code do not perform both erasure marking and decoding at the same time, this method of [54] is termed as separate erasure and decoding. A disadvantage of the solution in [54] is that the erasure detection relies on the value of LLRs received from the soft demapper, while some large impulses may lead to large yet erroneous LLRs, which potentially result in wrong decisions. To overcome this issue, Elgenedy *et al.* [120] conceived a technique for appropriately scaling the LLRs

obtained upon weighting the PSD of impulses, which improved the erasure detection reliability. As for joint erasure and decoding, this relies on erasure and decoding within the same decoding block. For example, Li *et al.* [122] proposed a joint erasure marking and Viterbi algorithm (JEVA), where the decoding process was composed of two steps. The first step decided the positions to be erased, while the second step determined the number of erasures. The schemes of [122] were later extended to the joint erasure marking and list Viterbi algorithm (JELVA) [123] by invoking the list Viterbi algorithm of [131] in order to improve the erasure marking accuracy.

Compressed-Sensing-Aided Impulse Noise Mitigation

Training-based impulsive noise estimation relying on compressive sensing (CS) constitutes an attractive method, since it has several distinct advantages for OFDM systems. Firstly, in practical DSL, the high-attenuation frequency sub-bands of an OFDM symbol may be disabled for data transmissions [132, 133]. As a benefit, some of these deactivated tones can be used as training symbols for supporting training-based impulsive noise estimation. Secondly, it is possible to disperse the prolonged impulsive bursts affecting numerous time-domain samples by simply using an interleaver. In this way, the asynchronous impulsive noise can be estimated at a low complexity with the aid of CS, as shown in Figure. 1.15. Finally, since the power of asynchronous impulsive noise is usually much higher than that of the background noise, accurate impulsive noise estimation becomes attainable by using CS.

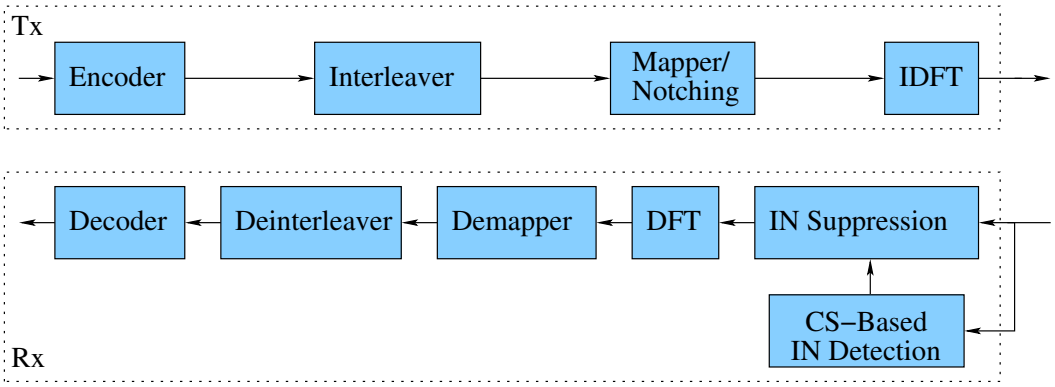

Figure 1.15: Illustration of compressive-sensing-aided mitigation.

The idea of applying CS to mitigate the impulse noise in OFDM systems was originally proposed in [50], where the impulse noise estimation was formulated as an ℓ_1-minimisation problem. Later in [124], the mixed ℓ_2/ℓ_1-minimisation has been employed for impulse noise estimation, where the impulsive noises were assumed to appear in form of sparse blocks. It should be noted that in [50] and [124] the duration of impulse noise was assumed to be much lower than that of an OFDM symbol, which is however, not the

norm. Furthermore, although the ℓ_1-minimisation considered in [50] and the mixed ℓ_2/ℓ_1-minimisation of [124] can be carrierd out within polynomial rather than exponential time, the corresponding computational cost still remains excessive. It is important to emphasize that for both schemes substantial computational resources are required for estimating low-level impulsive noise, whose instantaneous power is lower than the modulation-dependent detection threshold. In [125], the so-called basis pursuit denoising technique relying on adaptive threshold detection was applied for coarsely estimating impulsive noise samples. The authors of [45] proposed a sparse Bayesian learning approach for mitigating impulsive noise, demonstrating that as expected, the performance can be improved upon increasing the number of pilot symbols in OFDM systems. In [127], an *a priori*-aided matching pursuit approach was proposed for mitigating the impulsive noise, where the time-domain support of the impulsive noise process is assumed to be partially known. Recently, in [26], a novel compressed impairment sensing assisted and Interleaved-Double-FFT (IDFFT) aided system was proposed, which has been shown to be capable of simultaneously mitigating both the multipath effects and the impulsive noise impairments. Finally, Korki *et al.* [128] proposed a block iterative Bayesian algorithm (Block-IBA) and a novel receiver.

1.5 Novel Contributions

The thesis is based on the publications [4, 80, 118, 134, 135]. The novel contributions of this thesis are listed as follows:

- Contribution 1 [134, 135]: An extensive review of the family of noise modeling and processing in DSL over the past thirty years is presented. In terms of noise modeling, we review both the empirical models and the simplified mathematical models of both discontinuous and bursty impulses. As for noise mitigation, we provide a survey from the perspectives of processing at the transmitter (including channel coding, interleaving and re-transmission), parametric processing at the receiver (i.e. nonlinear pre-processing, adaptive filtering, symbol detection and iterative decoding) and non-parametric processing at the receiver (including erasure decoding, compressed-sensing-aided mitigation).

- Contribution 2 [4]: The BER performance of DSL systems inflicting impulsive noise is quantitatively analyzed. In general, the accuracy of the performance analysis is dependent both on the noise model considered and on the system model invoked. Specifically in our work, an empirical noise model which characterizes the noise pulse amplitude, pulse duration and IAT as well as PSD is invoked. Finally, a closed-form BER formula is derived and its accuracy is verified using simulations conducted within the bandwidth of the most recent DSL standard. Based on our

analytical results, we demonstrate the necessity of impulsive noise mitigation.

- Contribution 3 [80]: HARQ constitutes an efficient technique of alleviating the deleterious effects of impulsive noise on the system's performance. Here we quantitatively analyze the performance of LDPC-coded OFDM-based HARQ-aided DSL systems in a finite block-length regime. Specifically, we have appropriately adapted the density evolution technique, which was originally conceived for analyzing LDPC-coded systems in stationary noise environments. Extensive simulation results verify the accuracy of our analysis and quantify the performance of two types of HARQ in the face of impulsive noise, both in terms of its outage probability as well as the average number of retransmissions and the effective throughput attained.

- Contribution 4 [118]: One of major challenges in coded DSL systems operating in the presence of impulsive noise is related to the acquisition of the reliable LLRs from the samples suffering from impulsive noise. To tackle this challenge, we have proposed a two-stage joint impulsive noise estimation and data detection algorithm. Specifically, first of all, we propose a semi-blind noise estimation method, which is capable of estimating the arrival of noise impulses by evaluating the power of noise impulses with an adequate accuracy. Secondly, in order to improve the accuracy of impulsive noise estimation, we propose a decision-directed method for the second stage of channel decoding and data detection with the aid of extrinsic information transfer (EXIT) charts. Our proposed two-stage scheme is capable of approaching the performance of the idealistic scenario of perfectly knowing both the arrival time and the instantaneous power of impulsive noise. Moreover, we analyze the mean square error (MSE) of the proposed schemes in order to quantify the estimation accuracy and to reduce the estimation complexity. Our simulation results demonstrate that the proposed scheme is capable of achieving a near-capacity performance in the context of LDPC-coded multi-carrier DSL systems in the presence of impulsive noise.

1.6 Thesis Outline

In this section, we provide an overview of the remainder of this thesis. We commence by analyzing the performance of DSL systems in the face of impulsive noise, in terms of its BER, outage probability, delay and effective throughput. We then propose a joint impulsive noise estimation and data detection algorithm. Let us now continue by highlighting the outline of of this thesis.

Chapter 2: We outline the parameters that are used to characterize the behavior of both the background and of the impulsive noise. In Section 2.2, including the amplitude,

impulse duration and IAT as well as PSD. In Section 2.3, we present the existing empirical noise modeling processes applied in DSL. The advantage of the empirical models is that they accurately reflect the nature of impulsive noise. However, the associated mathematically intractable functions impose challenges on the associated performance analysis. To overcome this problem, a range of simplified mathematical models have been proposed, which are reviewed in Section 2.4. Specifically, we classify them into discontinuous and bursty approaches, which are used for modeling the noise in systems both with and without interleaving, respectively.

Chapter 3: We analyze the performance of DMT-based DSL systems in the face of impulsive noise in this chapter. In Section 3.1, we discuss the relevant existing work. Our discussions indicate that the performance of DSL systems may be analyzed using an empirical noise model in the context of a DMT-based system. In Section 3.2, we describe the DMT signaling and the noise model that we considered. Since the BER performance is directly dependent on the number of samples that are contaminated by impulsive noise, in Section 3.3 we analyze the statistics of noise samples both in the time domain and in the frequency domain, with the aid of hidden-semi Markov model. Bearing in mind that the impulsive noise is colored in the frequency domain, we further investigated the feasibility of using the conventional bit error evaluation techniques in Section 3.4. Then, a closed-form BER formula is readily obtained for Q-ary QAM modulation schemes. The simulation results are presented in Section 3.5.

Chapter 4: In this chapter, we investigate the performance of two types of HARQ schemes, namely Type-I and Type-II HARQ, in the context of LDPC-coded OFDM-based systems in a finite block-length regime. In Section 4.1, we portray the existing work. The system model and the two types of HARQ schemes are described in Section 4.2. In Section 4.3, we analyze the outage probability of the systems equipped with no HARQ as well as the Type-I and Type-II HARQ, by modifying the classic density evolution technique that was originally designed for stationary noise processes. The accuracy of our analysis is verified by our simulation results. In Section 4.4, we further analyze the performance of these two types of HARQ schemes both in terms of the expected number of retransmissions and the goodput.

Chapter 5: We firstly discuss the related existing work and outline the motivation of conceiving joint impulsive noise estimation and data detection in Section 5.1. In Section 5.2, we describe both the transceiver and the noise model, which are similar to the recent DSL standard. In Section 5.3, we then present the two-stage impulsive noise estimation and data detection scheme conceived, followed by the MSE analysis of the estimator. In Section 5.4, we optimize the number of iterations in the

joint estimation and detection process with the aid of the EXIT chart. Then the BER performance is presented in diverse scenarios.

Chapter 6 : We summarize the entire thesis in Section 6.1 and a range of future research ideas are provided in Section 6.2.

Chapter 2

Impulsive Noise Modeling Preliminaries

2.1 Introduction

The accurate knowledge of noise characteristics in DSL is a prerequisite for designing a high-performance transceiver for establishing a reliable transmission link over twisted-pairs. However, the derivation of analytic expressions for empirical noise models in DSL is quite a challenge. Therefore, almost all existing models are established by curve fitting based on measurement results [136]. Empirical models have the advantages on accurately reflecting the characteristics of noise, but unfortunately they do not lend themselves to convenient performance analysis and system design, because often intractable functions have to be invoked for ensuring a high modeling accuracy. To overcome this hindrance, various simplified mathematical models have been proposed [70, 109, 110, 115, 137–142]. In this chapter, we briefly introduce the characteristic parameters of impulsive noise and then review both the empirical modeling and simplified mathematical modeling options, which are detailed below.

2.2 Characteristics of Impulsive Noise

As discussed in Section 1.2.1, the impairments in DSL may be categorized into crosstalk as well as background and impulsive noise. Owing to the sophisticated techniques of vectoring [27] and dynamic spectrum management [35] as well as the architecture of FTTF [2], the crosstalk may be mitigated for attaining a superb performance over twisted pairs. In this section, we focus our attention both on the background noise and on the impulsive noise encountered in DSL, by introducing their characteristic parameters, which are detailed below.

Fig. 2.1 depicts a noise instantiation over a time interval of 100 µs in DSL, which

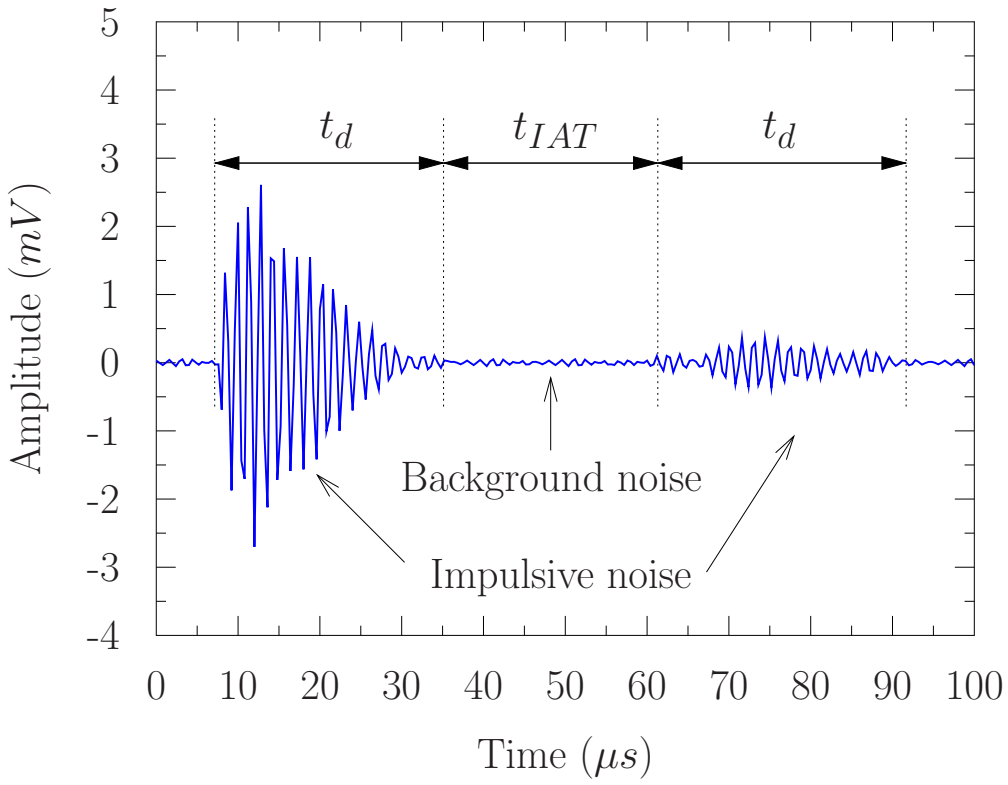

Figure 2.1: Illustration of an example of analog noise process in DSL [143]. t_d and t_{IAT} denote the duration and inter-arrival time of impulses, respectively.

comprises both background noise and impulsive noise. Specifically, the background noise can be regarded as a superposition of J_B sinusoids, given by [144]:

$$n_B(t) = \sum_{j=1}^{J_B} A_j^B \sin\left(2\pi f_j^B t + \alpha_j^B\right), \tag{2.1}$$

where A_j^B, f_j^B and α_j^B are the amplitude, "pseudo-frequency" and phase of the j-th sinusoid, respectively. Since the background noise exhibits a white spectrum over the frequency domain, its features can be understood by analyzing the impulse amplitude of A in (2.1).

The impulsive noise process is comprised of a collection of J_I damped sinusoids [53, 144, 145], expressed as [53]

$$n_I(t) = \sum_{j=1}^{J_I} A_j^I \sin\left(2\pi f_j^I (t - t_{\mathrm{arr}}) + \alpha_j^I\right) \times \exp\left(\frac{t - t_{\mathrm{arr}}}{\tau_j^I}\right) \sqcap \left(\frac{t - t_{\mathrm{arr}}}{t_w}\right), \tag{2.2}$$

where A_j^I, f_j^I and α_j^I are the amplitude, "pseudo-frequency" and phase of the j-th damped sinusoid, respectively. Furthermore, t_w and t_{arr} denote the width and arrival time of the sinusoid, respectively, while τ_j^I corresponds to the damping factor and $\sqcap(t)$ represents the square pulse duration of t_w having a constant amplitude in the interval of $0 < t \leqslant 1$ and the amplitude of 0 elsewhere. In contrast to background noise, impulsive noise exhibits a

non-flat frequency-dependent PSD [146] and it is not present all the time. Therefore, its features have to be further investigated by answering the following two questions:

1. Which frequencies are influenced by impulsive noise?
2. What is the temporal behavior of impulsive noise?

As for the first question, it is usually characterized by its power spectral density (PSD) denoted by $S_I(f)$. As exemplified in Fig. 2.1, let us now denote the duration of an impulse by t_d and the inter-arrival time (IAT) of two consecutive impulses by t_{IAT}. Then, the second question can be usually answered using t_d and t_{IAT}.

Based on the afore-mentioned basic variables, we can then derive high-order parameters, which may help to provide more insights for the associated performance analysis and system design. The first one is the background-to-impulsive noise power ratio, which is denoted by $\kappa(f)$. Then upon denoting the PSD of background noise by $S_B(f)$, we have

$$\kappa(f) = \frac{S_B(f)}{S_I(f)}. \tag{2.3}$$

The second one is impairment duration ratio, denoted by Λ, which is expressed as

$$\Lambda = \frac{\mathcal{E}[t_d]}{\mathcal{E}[t_{\mathrm{IAT}}] + \mathcal{E}[t_d]}, \tag{2.4}$$

where $\mathcal{E}[\bullet]$ refers to the expectation of $\bullet$. In this way, we may use $\kappa(f)$ and Λ for characterizing the spectral and temporal relationship between the background noise and impulsive noise, respectively.

2.3 Empirical Noise Modeling

The empirical noise modeling is capable of providing a straighforward understanding of the noise behavior and hence it has attracted substantial research attention [9, 41, 147]. In this section, the empirical modeling of both the background noise and of the impulsive noise encountered in DSL are reviewed in terms of the impulse amplitude, impulse duration, IAT and PSD. Moreover, we present an impulsive noise generation method that can be conveniently used for simulations.

2.3.1 Background Noise

Since the power spectrum of background noise is flat over all frequencies and the amplitude is Gaussian distributed [147], its probability density function (PDF) is expressed as

$$f(u_B) = \frac{1}{\sqrt{2\pi}\sigma_B} \exp\left(-\frac{|u_B|^2}{2\sigma_B^2}\right), \tag{2.5}$$

where u_B is real and σ_B^2 denotes the background noise variance.

2.3.2 Impulsive Noise

In contrast to the background noise, impulsive noise is usually colored in the frequency domain and the impulses tend to have a random duration and IAT. Hence, more variables have to be invoked for characterizing its duration, IAT and temporal correlation, as detailed below.

Amplitude of the Impulsive Noise

The seminal contribution on modeling the amplitude is [147] by Henkel and Kessler (termed by HK model in the following part) based on the measurement results collected from BT and DT, whose PDF is expressed as

$$f(u_I) = \frac{1}{240u_0} e^{|u_I/u_0|^{1/5}}, \tag{2.6}$$

where u_0 depends on the environment. Furthermore, the Weibull distribution was also shown to fit the measurement [41], and the associated PDF is formulated as

$$f(u_I) = \frac{1}{2} ab|u_I|^{a-1} \exp\left(-b|u_I|^a\right), \tag{2.7}$$

where u_I is real while a and b depend on the environment. We summarize the parameters of Weibull and HK amplitude histograms in Table. 2.1. Moreover, Fig. 2.2 depicts our comparison between the PDF of the amplitude modeled by Henkel and Kessler as well as that of the Gaussian distribution having the same mean and variance values. It is readily inferred that the empirical amplitude obeys a strongly non-Gaussian distribution.

Table 2.1: Typical model parameters for the Weibull and HK amplitude histograms.

	u_0	a	b
BT(CP)	9.12μV	0.263	4.77
DT(CP)	23.23μV	0.486	44.40
DT(CO)	30.67μV	0.216	12.47
PSTN	\	0.98	100

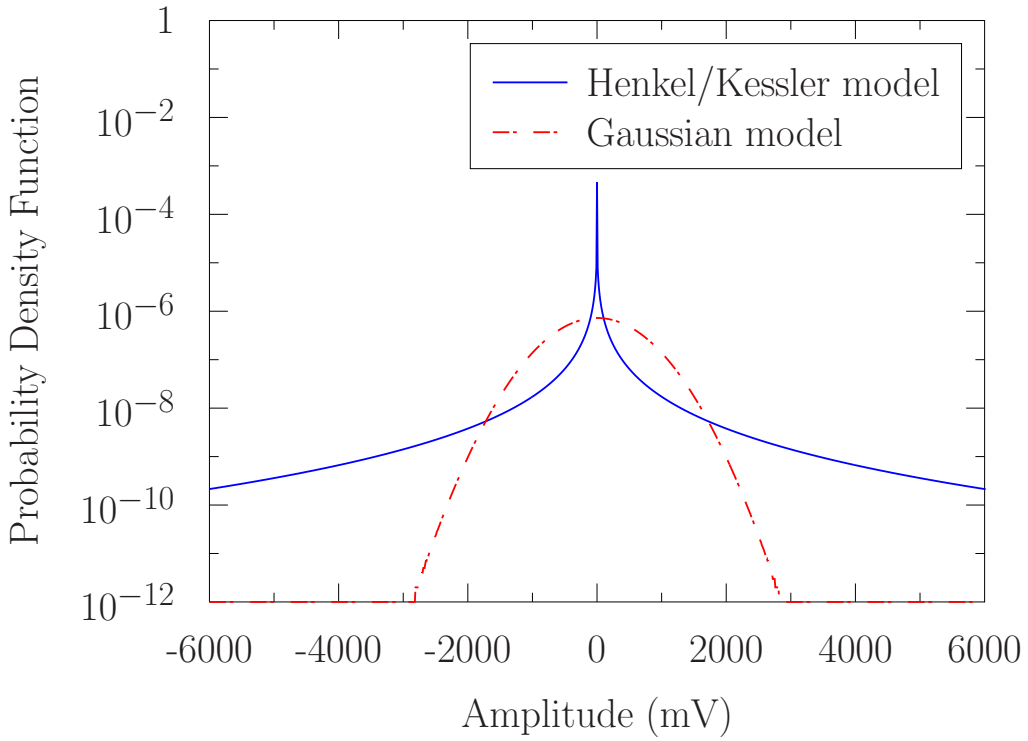

Figure 2.2: Illustration of probability density function of impulse amplitude which is modeled using (2.6). The Gaussian distribution yields the same values of the mean and the variance of the HK model. The corresponding abbreviations are as follows: IN (impulsive noise), IAT (inter-arrival time).

Duration of the Impulsive Noise

The PDF of the impulsive noise's duration is typically modeled by a two-term log-normal form formulated as in [41]

$$f(t) = \frac{B}{\sqrt{2\pi}v_1 t}\exp\left(-\frac{\ln^2(t/t_1)}{2v_1^2}\right) + \frac{1-B}{\sqrt{2\pi}v_2 t}\exp\left(-\frac{\ln^2(t/t_2)}{2v_2^2}\right). \quad (2.8)$$

Table 2.2 summarizes the typical parameters for both the customer premises (CP) and the central offices (CO) measured by DT, by BT and by the Italian Public Switched Telephone Network (PSTN) [41] [24].

Table 2.2: Typical model parameters for log-normal duration densities.

	u_0	a	b	B	v_1	t_1	v_2	t_2
BT(CP)	9.12μV	0.263	4.77	0.45	1.25	1.3 μs	21.5	129 μs
DT(CP)	23.23μV	0.486	44.40	1	1.15	18 μs	\	\
DT(CO)	30.67μV	0.216	12.47	0.25	0.75	8 μs	1.0	125 μs
PSTN	\	0.98	100	0.7	0.53	4.5 μs	0.8	60 μs

Inter-arrival Time of the Impulsive Noise

For daytime measurements, a generalization of the Poisson law was shown to be a suitable approximation of the IAT in [9] and its PDF is expressed as

$$f(t) = \frac{10^{a_1}}{\ln(10)} x^{a_4-1} 10^{-[a_4/\ln(a_2)]a_2^{[\log_{10}(t)-a_3]}}, \tag{2.9}$$

where $a_2 = 2.22$, $a_3 = 5.15$, $a_4 = 1.26$, $x = t/100\text{ns}$. Moreover, a_1 is a normalization constant and has to be chosen for ensuring that the integral over the density equals one. Clearly, the impulse duration in (2.9) is assumed to be independent and identically distributed. However, the occurrence of impulses was shown to exhibit self-similarity [148].

As a further advance, Levey and MaLaughlin [149] proposed a Markov renewable process based model, which is capable of capturing the IAT memory. More explicitly, each of these two inter-arrival time ranges is represented by a specific set as Markov states. To elaborate, s_0 represents the inter-arrival times lower than 1 ms, which is exponentially-distributed, while s_1 represents the inter-arrival time longer than 1 ms, which is Pareto-distributed. Then the PDF of the two states of the inter-arrival times can be expressed as:

$$f(t|s_j) = \begin{cases} \frac{1}{1-\exp(-\lambda t_s)} \lambda \exp(-\lambda t), & \text{if } j = 0 \ (t < t_s) \\ \theta t_s^{\theta} / t^{\theta+1}, & \text{if } j = 1 \ (t \geq t_s), \end{cases} \tag{2.10}$$

where $t_s = 1$ ms, which is the switching threshold between the two states, while we have $\lambda = 0.16s^{-1}$ and $\theta = 1.5$ [41]. Moreover, the Markov state-transition probability matrix is a (2×2) - element matrix

$$\mathbf{P}_{s_0}(1) = \begin{bmatrix} p_{s_0}^{00} & p_{s_0}^{01} \\ p_{s_0}^{10} & p_{s_0}^{11} \end{bmatrix}, \tag{2.11}$$

and the typical state transition probabilities are shown below, which were confirmed by χ^2-

type hypothesis testing in [41] based on the experimental measurement results, yielding:

$$\mathbf{P}_{s_0}(1) = \begin{bmatrix} 0.8 & 0.2 \\ 0.4 & 0.6 \end{bmatrix}. \tag{2.12}$$

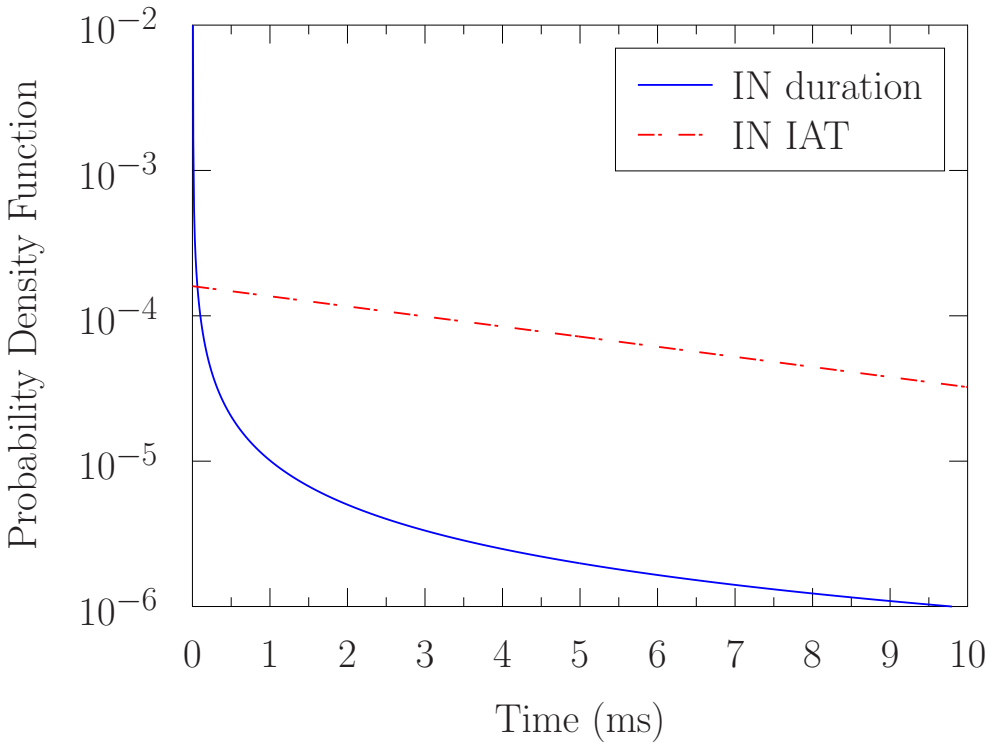

Figure 2.3: Illustration of PSD of impulse duration and IAT, where the duration is modeled using the log-normal distribution in (5.16) while IAT is modeled using the Markov process (5.17).

Fig. 2.3 shows the PDF of the impulse duration and IAT. Bearing in mind that the duration of a DMT symbol was set to 20.83 μs in the recent G.fast standard, we observe that the impulse duration ranges from microsecond to milliseconds, which is long enough to contaminate several consecutive DMT symbols, potentially leading to dropping an entire packet. Moreover, the normalized time interval inflicting impulsive noise is about 3.29% of the total time-duration. Hence, the impulsive noise is of relatively high occurrence probability, resulting in an unreliable DSL transmission link, which cannot satisfy the backbone requirements of supporting high-integrity smart home networks.

Spectral Characteristics of Impulse Noise

The PSD of impulse noise was [147], formulated as

$$S_I(f)(\text{dB}) = \begin{cases} -15\log_{10}\frac{f}{\text{Hz}} + 80, & 5\,\text{kHz} \leq \text{f} \leq 1.64\,\text{MHz} \\ -29\log_{10}\frac{f}{\text{Hz}} + 167, & 1.64\,\text{MHz} \leq \text{f} \leq 4\,\text{MHz}. \end{cases} \tag{2.13}$$

The weakness of the model in (2.13) is that it lacks flexibility and that it cannot be utilized for impulse generation in simulations. In order to overcome this impediment, the auto-correlation function (ACF) of the impulsive noise was formulated in [41], as an exponentially decaying cosine function:

$$R(t) = cos(2\pi\alpha t)\exp\big(-\beta|t|\big), \tag{2.14}$$

where α obeys the Gaussian distribution, while β is a randomly generated Gaussian variable related to the duration of impulsive noise spikes [150]. In the following, we will introduce an impulsive noise generation method based on the so-called zero-memory non-linearity technique [151].

Impulsive Noise Generation

It can be inferred from the above discussion that the impulsive noise is a correlated non-Gaussian signal. The generation of a random sequence having a jointly specified marginal distribution and auto-correlation has attracted substantial research attention [151–153]. One of the most popular methods is the so-called zero-memory non-linearity technique [151], which transforms a zero-mean unit-variance Gaussian sequence associated with the corresponding ACF to another sequence having a specific target cumulative density function (CDF) and target ACF.

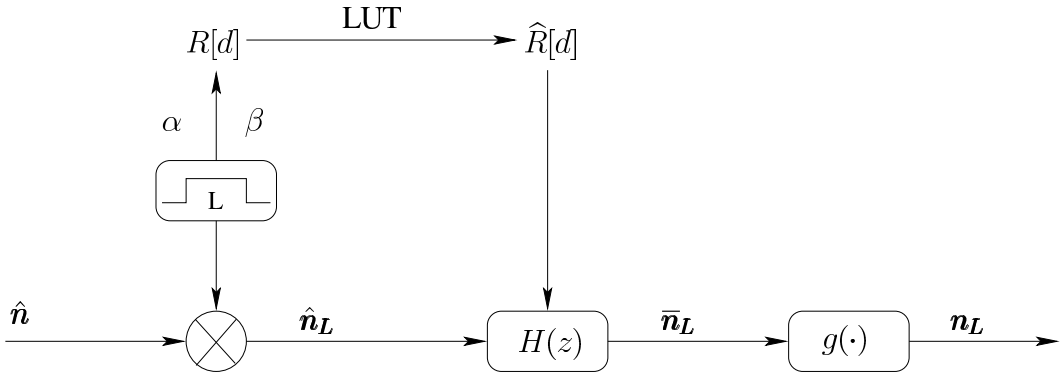

Figure 2.4: Illustration of the impulsive noise generation scheme.

Since our signals are processed at discrete time instants, we denote the discrete time index by d. The generation of impulsive noise is detailed step-by-step, as illustrated in Fig 2.4.

1. Generate a white Gaussian sequence $\hat{\boldsymbol{n}}_{\boldsymbol{L}}$ obeying $\mathcal{N}(0,1)$ with the duration L, which is randomly generated according to the duration-PDF of every impulse;

2. Obtain the discrete target ACF $R[d]$ with α and β adjusted according to the their distribution;

3. Obtain the corresponding discrete ACF $\hat{R}[d]$ for the Gaussian sequences by matching $R[d]$ to the look-up table (LUT), which is detailed later in this section;

4. Design a filter $H(z)$ with the aid of the Levinson algorithm of [154] to generate the output signal obeying the ACF of $\hat{R}[d]$;

5. Pass the white Gaussian sequence $\hat{\boldsymbol{n}}_{\boldsymbol{L}}$ through the filter and normalize the variance of the output $\overline{\boldsymbol{n}}_{\boldsymbol{L}}$ to unity;

6. Pass the correlated Gaussian sequence $\overline{\boldsymbol{n}}_{\boldsymbol{L}}$ through the zero-memory non-linearity function $g(\cdot)$ to get the correlated target Weibull distributed sequence $\boldsymbol{n}_{\boldsymbol{L}}$.

In the following, we will characterize the zero-memory non-linearity function and the relationship between $R[d]$ and $\hat{R}[d]$. Let us denote the CDF of $\boldsymbol{n}_{\boldsymbol{L}}$ as F_{n_L} and CDF of $\overline{\boldsymbol{n}}_{\boldsymbol{L}}$ as $F_{\overline{n}_L}$. Then, we have [151]

$$F_{n_L} = \int_{-\infty}^{n_L} f(u_I)\mathrm{d}u_I = \begin{cases} \frac{1}{2}\exp\left[-b(-n_L)^a\right], & n_L \leq 0 \\ 1 - \frac{1}{2}\exp\left[-b(n_L)^a\right], & n_L > 0. \end{cases} \tag{2.15}$$

Then, for the standard normal distribution, we have:

$$F_{\overline{n}_L} = \frac{1}{2}\Big[1 + \mathrm{erf}\Big(\frac{\overline{n}_L}{\sqrt{2}}\Big)\Big]. \tag{2.16}$$

The zero-memory non-linearity function is expressed as [151]

$$g(x) = F_{n_L}^{-1}\big[F_{\overline{n}_L}(x)\big] = \begin{cases} -\left[\frac{1}{b}\ln\left(\frac{1}{\mathrm{erfc}(-x/\sqrt{2})}\right)\right]^{\frac{1}{a}}, & x \leq 0 \\ \left[\frac{1}{b}\ln\left(\frac{1}{\mathrm{erfc}(x/\sqrt{2})}\right)\right]^{\frac{1}{a}}, & x > 0. \end{cases} \tag{2.17}$$

In order to obtain the discrete target ACF $R[d]$, the corresponding discrete ACF $\hat{R}[d]$ has to be the solution of [151]

$$R[d] = \sum_{k=1}^{\infty} c_k^2 \big(\hat{R}[d]\big)^k, \tag{2.18}$$

where we have

$$c_k^2 = \frac{1}{k!}\Big[\int_{-\infty}^{\infty} g(x)H_k(x)\phi(x)\,\mathrm{d}x\Big]^2, \tag{2.19}$$

and $H_k(x)$ is the kth physicists' Hermite polynomial [155], while $\phi(x)$ is the unit-variance normal PSD. In this way, a look-up table (LUT) can be generated, matching $R[d]$ to the corresponding $\hat{R}[d]$.

Fig 2.5 depicts the desired and simulated PSD of the impulsive noise. The background

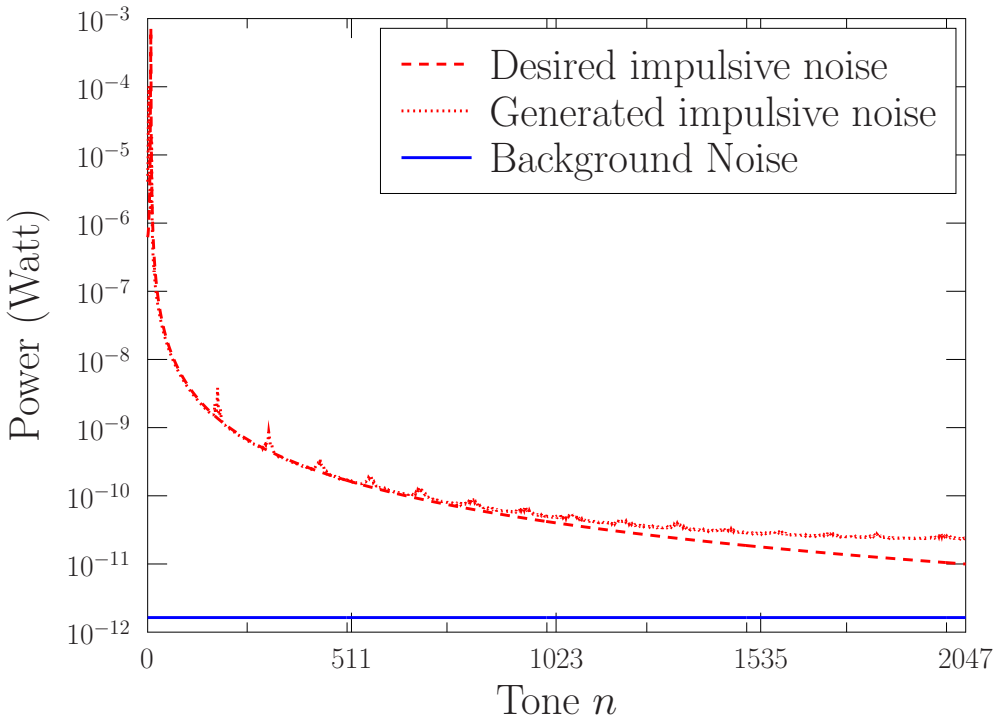

Figure 2.5: Spectrum of the impulsive noise and the background noise, with the bandwidth of up to 106 MHz and multicarrier spacing of 51.75 kHz. For the background noise, the power spectral density is set as -135 dBm/Hz.

noise amplitude is modeled by the ubiquitous white Gaussian noise process, with the power spectral density being -135 dBm/Hz. For the impulsive noise, the voltage amplitude and impulse duration is represented by the DT(CP) seen in Table 2.2. The inter-arrival time and the spectral characteristics are set according to Section II.B. For the LUT generation, we have dropped c_k beyond the ninth term in (2.18), because they are indeed negligible.

It can be inferred from the figure that the impulsive noise power has a maximum value at low frequencies, which is about 80 dB higher than the background noise floor, and decreases rather sharply with the frequency. Nonetheless, at high frequencies, the impulsive noise power is still about 10 dB higher than the stationary noise floor. Compared to Fig .14 of [41], the simulated results seen in Fig. 2.5 demonstrates a substantial improvement: the simulated power is quite close to the analytical one according to our proposed method, while there is at least 10 dB gap between the desired and simulated impulsive noise power at the peak values in [41].

2.4 Simplified Mathematical Modeling

The empirical modeling detailed in Section 2.3 allows us to characterize the noise in a straightforward manner. However, due to the usage of uncommon functions, empirical modeling may not lend itself to convenient mathematical analysis. To tackle this problem, simplified mathematical noise models have also been proposed [70, 109, 110, 115, 137–142]. Fig. 2.6 provides a rudimentary classification of the popular noise modeling techniques. From the perspective of impulse duration, simplified mathematical modeling may be applied to discontinuous impulses and bursty impulses, which are detailed below.

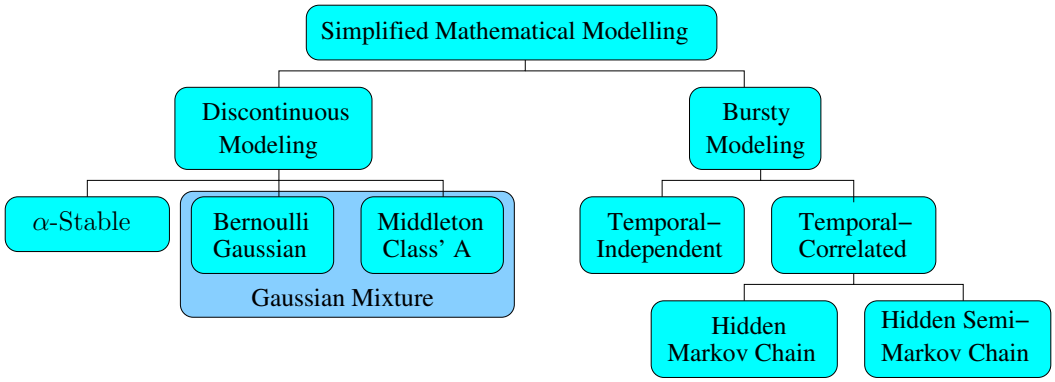

Figure 2.6: Family tree of simplified mathematical impulse noise models.

2.4.1 Discontinuous Impulses

Discontinuous impulse modeling is the simpler one of the above-mentioned pair of modeling approaches, which is not concerned with the temporal correlations and tends the impulse noise as an independent and identically distributed (i.i.d.) variable. As shown in Fig. 2.6, discontinuous impulsive noise modeling typically includes the Middleton's Classes [140], the Bernoulli Gaussian [137], the Gaussian Mixture [138] and α-stable [141] scenarios, which are introduced individually below.

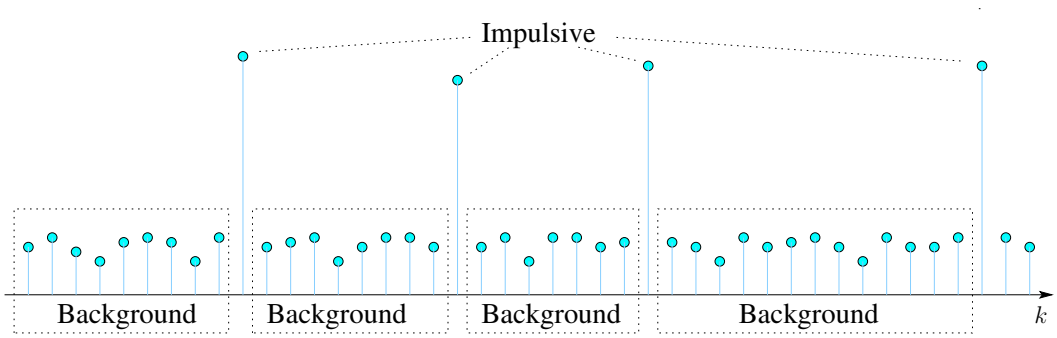

Figure 2.7: Illustration of discontinuous impulses.

Middleton has categarized the natural or man-made electromagnetic impairments into

three broad classes, namely, Class A, Class B and Class C [139, 140], according to the ratio between the interference bandwidth and receiver bandwidth. Specifically, Class A represents the scenario, when the impulsive noise is spectrally narrower than the receiver's bandwidth. By contrast, Class B represents the case when the impairment exhibits a wider spectral occupation than the receiver's bandwidth. Finally, Class C represents the combination of impairments belonging to Class A and Class B. Among these three classes, Middleton's Class A scenario is the most popular one for three reasons. Firstly, it requires the lowest number of parameters. Secondly, it exhibits the most analytically convenient PDF. Thirdly, it is capable of characterizing a wide range of impairments in reality. The PDF of a real-valued Middleton's Class A noise sample n_k, where k represents the noise index, is given by [139]:

$$f_{\text{MCA}}(n_k) = e^{-\Lambda} \sum_{m=0}^{\infty} \frac{\Lambda^m}{m!\sigma_m\sqrt{2\pi}} \exp\Big(-\frac{n_k^2}{2\sigma_m^2}\Big), \tag{2.20}$$

where we have $\sigma_m^2 = \sigma^2 \cdot (m/\Lambda + \kappa)/(1+\kappa)$. Here Λ denotes the impairment-duration ratio, while $\kappa = \sigma_{n,B}^2/\sigma_{n,I}^2$ is the background to impulsive power ratio [110]. The overall power of the noise process is expressed as $\sigma_{n,\text{all}}^2 = \sigma_{n,B}^2 + \sigma_{n,I}^2 = (1+1/\kappa)\sigma_{n,B}^2$. To elaborate a little further in physically tangible terms, the Middleton Class A scenario may be interpreted as the superposition of statistically independent noise components, whose sources obey the Possion distribution in both space and time [140]. More explicitly, at the time instant k, the destination receives noise impulses from m sources of impairments, with the result of n_k obeying the Gaussian distribution having the mean value of 0 and the variance value of σ_m^2.

Bernoulli-Gaussian Model [156] of Fig. 2.7 is widely invoked in the performance analysis and design of communications systems, which is an explicit benefit of its simplicity and capability of characterizing the random occurrence of high-power impulses [157]. It simply models the impulse noise by a two-term Bernoulli process, where both the background and impulsive noise obey a Gaussian distribution, i.e. we have $n_k = w_k + b_k i_k$, where $w_k \sim \mathcal{N}(0, \sigma_{n,B}^2)$, $i_k \sim \mathcal{N}(0, \sigma_{n,I}^2)$ and b_k is the Bernoulli random variable. Then, the PDF of the real-valued noise relying on Bernoulli-Gaussian Model is expressed as [137]:

$$f_{\text{BGM}}(n_k) = \frac{1-p}{\sigma_{n,B}\sqrt{2\pi}} \exp\Big(-\frac{n_k^2}{2\sigma_{n,B}^2}\Big) + \frac{p}{\sigma_{n,I}\sqrt{2\pi}} \exp\Big(-\frac{n_k^2}{2\sigma_{n,I}^2}\Big), \tag{2.21}$$

where $p = \Pr(b_k = 1)$, which represents the occurrence probability of impulsive noise. Similar to Middleton's Class A, let us define $\kappa = \sigma_{n,B}^2/\sigma_{n,I}^2$, which represents the ratio between the background and impulsive noise.

The Gaussian Mixture Model [156] represents a more generalized technique of model-

ing the impulse noise as a mixture of several Gaussian-distributed components. The PDF of the real-valued noise in Gaussian Mixture Model is formulated as [138]:

$$f_{\mathrm{GMM}}(n_k) = \sum_{m=0}^{M-1} \frac{p_m}{\sigma_m \sqrt{2\pi}} \exp\Big(- \frac{n_k^2}{2\sigma_m^2} \Big), \tag{2.22}$$

where $\sum_{m=0}^{M-1} p_m = 1$ and p_m refers to the occurrence probability of the m-th component which yields $\mathcal{N}(0, \sigma_m^2)$. Note that Gaussian Mixture Model includes the Middleton's Class A and Bernoulli-Gaussian Model as a special case, i.e. $p_m = e^{-A} A^m / m!$ and $M-1 = \infty$ for Middleton's Class A while $p_0 = 1-p$, $p_1 = p$ and $M-1 = 1$ for Bernoulli-Gaussian Model.

The Alpha-Stable distribution [156] constitues the generalization of the Gaussian distribution and it is also suitable for impulsive noise modeling. The PDF of the real-valued noise in the Alpha-Stable model is given by [141]:

$$f_{\alpha S}(n_k) = \exp\Big(i\delta n_k - |\gamma n_k|^{\alpha} (1 - i\beta \mathrm{sgn}(n_k) \Phi \Big) \tag{2.23}$$

and

$$\Phi = \begin{cases} \tan\big(\frac{\pi\alpha}{2}\big), & \text{if } \alpha \neq 1, \\ \frac{2}{\phi} \log |n_k|, & \text{if } \alpha = 1. \end{cases} \tag{2.24}$$

where we have $-\infty < \delta < +\infty$, $\gamma > 0$, $0 < \alpha \leqslant 2$, $-1 \leqslant \beta \leqslant 1$. Furthermore, γ is a scaling parameter, which calibrates the spread of the samples, while α sets the degree of impulsiveness. Explicitly, the smaller the value of α, the higher the frequency and the amplitude of extreme pulses. When $\beta = 0$, the distribution is symmetric about the center δ. In this case, the distribution is said to be symmetric α-stable (SαS) [141].

2.4.2 Bursty Impulses

The discontinuous modeling technique of Section 2.4.1 can only be used for modeling the impulsive noise after the process of interleaving and de-interleaving. In order to apply impulse noise modeling to a wider range of systems, diverse bursty models have been proposed [4, 70, 109, 110, 115, 142, 158–160]. Specifically, the noise impulses are assumed to occur in a burst of consecutive time instants. Generally, bursty impulse modeling can be classified into temporally-independent and temporally-correlated scenario, which are discussed as follows.

The noise impulses in the temporally-independent modeling scenarios can be presented by a gated Bernoulli process [70], consisting of impulse-free and impulse-impaired bursts alternatively, whose time durations are independent of each other. Assuming that the l-th

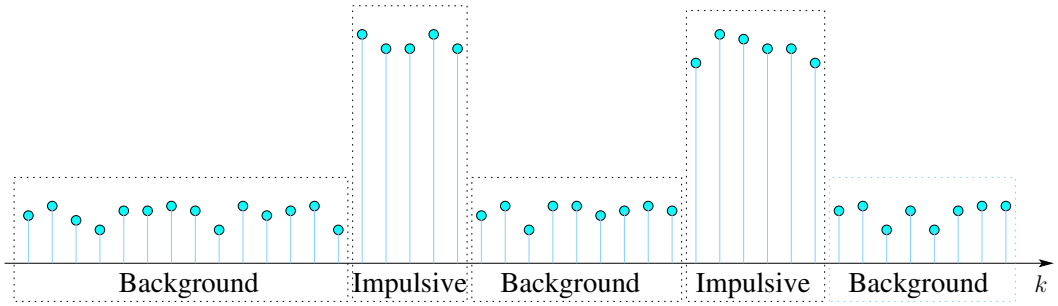

Figure 2.8: Illustration of noise impulse burst.

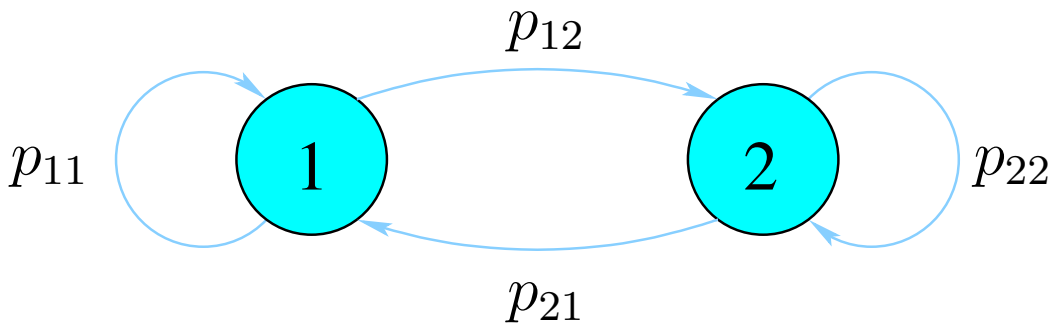

Figure 2.9: Illustration of Gilbert-Elliot model, a two-state Markov noise model, where State 1 corresponds to impulse-free instants while State 2 represents impulse-impaired instants. The transition probability p_{ij} refers to the occurrence probability of State j given the current state as State j.

burst spans over t_l time intervals, the l-th noise burst is expressed as [70]:

$$\boldsymbol{n}_l = \boldsymbol{w}_l + b_l \boldsymbol{i}_l. \tag{2.25}$$

and

$$t_l = \begin{cases} t_d, & \text{if } b_l = 0, \\ t_{\text{IAT}}, & \text{if } b_l = 1, \end{cases} \tag{2.26}$$

where b_l is Bernoulli distributed random variable, while $\boldsymbol{w}_l$ and $\boldsymbol{i}_l$ are the vectors with length of t_l, whose elements obeys the Gaussian distribution. To elaborate, t_d and t_{IAT} are deterministic for periodic impulsive noise, while they obey certain distributions in aperiodic impulsive noise scenarios, such as uniform [70], exponential [142] or log-normal [4] distribution.

In temporally-correlated modeling, the impulse duration and the IAT are temporally correlated, obeying the classic Markov chains. Specifically, Gilbert and Elliott modeled the noise using the simplest form of Markov chains in [158, 159], relying on a two-state Hidden Markov Model (HMM). Specifically, the impulse noise process was represented by a pair of two states, namely the impulse-free state and impulse-impaired state. The

noise voltage obeys the Gaussian distribution during both states. Therefore, the Gilbert-Elliott model is also often referred to as the Markov-Gaussian model. To elaborate a little further with the aid of Fig. 2.9, the Gilbert-Elliott model is introduced as an example for the temporally-correlated modeling. Let us denote the state of noise at the k-th time instant by s_k, the state without impulsive noise by S_1 and the state contaminated by impulsive noise by S_2. Then, the PDF of the noise conditioned on s_k is given by:

$$p(n_k|s_k = S_1) = \frac{1}{\sqrt{2\pi\sigma_{n,B}^2}} \exp\left(\frac{-|n_k|^2}{2\sigma_{n,B}^2}\right), \tag{2.27}$$

$$p(n_k|s_k = S_2) = \frac{1}{\sqrt{2\pi\sigma_{n,I}^2}} \exp\left(\frac{-|n_k|^2}{2\sigma_{n,I}^2}\right). \tag{2.28}$$

As shown in Fig. 2.9, the evolution of noise states can be represented by $p_{ij} = \Pr(s_{k+1} = S_j|s_k = S_i)$, which corresponds to the probability of transition from state S_i to state S_j. Then the ergodic probability of S_1 and S_2 can be expressed as:

$$\Pr(s_k = S_1) = \frac{p_{21}}{p_{12} + p_{21}}, \tag{2.29}$$

$$\Pr(s_k = S_2) = \frac{p_{12}}{p_{12} + p_{21}}, \tag{2.30}$$

which is eminently suitable for performance analysis and system design [109, 115]. However, the drawback of the Gilbert-Elliott model is that the associated small number of states fails to accurately characterize a wide variety of impulsive noise scenarios. To address this problem, Ndo *et al.* [110] introduced a four-state HMM, where one state corresponded to the impulse-free intervals, while the other three states characterized the impulse-impaired intervals associated with different parameter settings. Meanwhile, the amplitude of the four states were modeled to yield a Middleton's Class A scenario. Accordingly, Ndo's model is also termed as the Markov-Middleton model. Furthermore, inspired by [110] and [146], Zhang *et al.* [142] modeled the noise using a two-state Hidden Semi-Markov model (HSMM), where the duration of the impulse-free states and the impulse-impaired states obeying an exponential distribution associated with different emission rates and transition probability between the two states was 1.

2.5 Chapter Summary

In this chapter, we have introduced the characteristic parameters of impulsive noise in DSL. Then, the family of empirical noise modeling has been reviewed, with particular attention dedicated to the variables of amplitude, impulse duration and IAT as well as

spectral characteristics. We have also proposed a zero-memory non-linearity technique based impulsive noise generation method, which is capable of representing the impulsive noise in simulations. In order to support the performance analysis of the forthcoming chapters, we have summarized the simplified mathematical modeling techniques, from the perspective of both discontinuous and bursty impulses. These discussions on noise modeling constitute the basis of understanding the impulsive noise behavior in DSL, which is a prerequisite for the performance analysis of the following chapters.

Chapter 3

Performance Analysis of DMT-Based DSL Systems In the Face of Impulsive Noise

The deleterious influence of impulsive noise inflicted upon the DSL systems has to be quantified for determining the overall system performance. Hence in this chapter we present our performance analysis of DMT-based DSL systems in the presence of impulsive noise. Based on these results, we may conclude that the attainable system performance is inadequate without impulsive noise mitigation.

3.1 Introduction

The performance analysis of systems in the face of impulsive noise has drawn a substantial attention in the literature [161–163]. Ghosh [161] has analyzed the effect of impulsive noise on QAM and multi-carrier modulation (MCM) under the Bernoulli-Gaussian noise model of Section 2.4.1 by observing its analytical results, we may conclude that MCM is more resilient to impulsive noise because the noise sample are averaged after the DFT-based demodulation. However, the Bernoulli-Gaussian model invoked in [161] fails to reflect the bursty nature of the impulsive noise in DSL. Hence Chew *et al.* have analysed the performance of a binary single carrier system in the local loop [162]. Specifically, based on the noise model of Henkel and Keßler [9], the authors modified the error probability formula according to the PDF of impulsive noise amplitude where the temporal statistics were also taken into consideration. The study in [162] characterized a binary single-carrier system in an empirical manner. However, the single-carrier modulation has been replaced by DMT in the recent DSL standards. This is because the signal-reflection points imposed by the cable branching lead to dispersive propagation in the DSL channel. Moreover, mea-

surement results [7] show that the coherence bandwidth of the channel is rather limited and the DSL channel exhibits frequency-selective behaviors, which inevitably results in inter-symbol interference (ISI). In order to mitigate the ISI, DMT has been invoked by the standardized DSL transceivers, which is a baseband version of the classic orthogonal frequency division multiplexing (OFDM) [164]. Furthermore, based on the model by Mann *et al*. [41], the BER performance of both PAM as well as of single-carrier QAM and of multicarrier QAM was studied under the Bernoulli-Weibull model by Nedev *et al*. [163]. Since a more reliable IAT model was considered, this study accurately reflect the overall system performance. However, no closed-form BER formula was derived for MCM.

Against this background, we analyze the BER performance of DMT-based DSL systems under empirical DSL dispersion and noise modeling. Our main contributions are summarized as follows:

- We consider both stationary and impulsive noise for accurately reflecting both the temporal and spectral characteristics of practical channels.
- With the aid of the Hidden Semi-Markov model in Section 2.4.2, we derive the closed-form BER formula of DMT-based DSL systems relying on Q-ary QAM under the above noise model and a dispersive channel.
- We verify the accuracy of our BER formula by simulation results, where the dispersive channel is extended all the way upto 106 MHz, which is the bandwidth of the first version of G.fast.

The rest of the chapter is organized as follows. Section 3.2 details our DMT system and the noise model in a DSL context. In Section 3.3, we investigate the statistics of the noise samples both in the time domain and in the frequency domain. In Section 3.4, we analyze the impact of colored non-Gaussian noise on our DMT/OFDM system and derive closed-form BER expressions. In Section 3.5, the BER performance of DMT-based DSL systems under practical noise conditions and measurement-based dispersive channel conditions is presented. Finally, the chapter is concluded in Section 3.6.

3.2 DMT Signaling and Impulsive Noise Modeling

In this section, we describe the DMT signaling and noise procedure modeling in DSL systems.

3.2.1 DMT Signaling

Discrete multi-tone is invoked in DSL systems [13], in order to mitigate the ISI caused by frequency-selective channel. The transmission bandwidth is divided into a number of subchannels having a bandwidth lower than the coherence bandwidth of the channel, which ensures that the signals of each substream experience flat fading.

In DMT systems, $(N-2)/2$ Q-ary QAM symbols are used to form a block of symbols $\boldsymbol{X} = [X_0, X_1, \ldots, X_{N-1}]^{\mathrm{T}}$ having a Hermitian transpose structure, implying that we have $X_n = X^*_{N-n}$ for $n = \{1, \ldots, N/2-1, N/2+1, \ldots, N\}$ and $X_0 = X_{N/2} = 0$. The block of symbols is serial-to-parallel converted and the resultant parallel symbols are transformed to the time-domain with the aid of IDFT, resulting in the real-valued time-domain signals of $\boldsymbol{x} = [x_0, x_1, \ldots, x_{N-1}]^{\mathrm{T}}$, which can be expressed as

$$\boldsymbol{x} = \boldsymbol{\mathcal{F}}^H \mathbf{X}, \tag{3.1}$$

where $\boldsymbol{\mathcal{F}}$ is the normalized discrete Fourier transform (DFT) matrix [165], yielding $\boldsymbol{\mathcal{F}}\boldsymbol{\mathcal{F}}^H = \boldsymbol{\mathcal{F}}^H\boldsymbol{\mathcal{F}} = \boldsymbol{I}_N$, which means that $\boldsymbol{\mathcal{F}}$ is an orthogonal matrix.

In order to avoid ISI, cyclic prefices are added to the parallel-to-serial converted symbols, resulting in

$$\tilde{\boldsymbol{x}} = [x_{N-\mu}, x_{N-\mu+1}, \ldots, x_{N-1}, x_0, x_1, \ldots, x_{N-1}]^{\mathrm{T}}, \tag{3.2}$$

where μ is the length of the cyclic prefices, which should be selected by obeying the constraint of

$$\mu \Delta t \geq \tau_{max}, \tag{3.3}$$

where Δt is the sampling period at the baseband and τ_{max} is the maximum delay spread of the channel.

The time-domain signals $\tilde{\boldsymbol{x}}$ are passed through the dispersive DSL channel and are contaminated by the noise

$$\tilde{\boldsymbol{y}} = \boldsymbol{h}\tilde{\boldsymbol{x}} + \boldsymbol{u_S} + \boldsymbol{u_I}, \tag{3.4}$$

where $\tilde{\boldsymbol{y}}$ is a $(N+\mu)$-element vector, $\boldsymbol{h}$ is $(N+\mu) \times (N+\mu)$-element matrix, while the stationary noise $\boldsymbol{u_S}$ and the impulsive noise $\boldsymbol{u_I}$ are $(N+\mu)$-element vectors.

The cyclic prefices received are discarded, because they are contaminated by the ISI and (3.4) becomes equivalent to

$$\boldsymbol{y} = \tilde{\boldsymbol{h}}\boldsymbol{x} + \tilde{\boldsymbol{u}}_{\boldsymbol{S}} + \tilde{\boldsymbol{u}}_{\boldsymbol{I}}, \tag{3.5}$$

where $\boldsymbol{y}$ is an N-element vector, $\tilde{\boldsymbol{h}}$ is an $(N \times N)$-element matrix, while $\tilde{\boldsymbol{u}}_{\boldsymbol{S}}$ and $\tilde{\boldsymbol{u}}_{\boldsymbol{I}}$ are

N-element vectors.

Assuming that synchronization is perfectly achieved at the receiver, the received symbols can be recovered with the aid of a DFT based demodulator as:

$$\begin{aligned} \boldsymbol{Y} &= \boldsymbol{\mathcal{F}}\boldsymbol{y} = \boldsymbol{\mathcal{F}}(\tilde{\boldsymbol{h}}\boldsymbol{x} + \tilde{\boldsymbol{u}}_{\boldsymbol{S}} + \tilde{\boldsymbol{u}}_{\boldsymbol{I}}) \\ &= \boldsymbol{\mathcal{F}}(\tilde{\boldsymbol{h}}\boldsymbol{\mathcal{F}}^{H}\mathbf{X} + \tilde{\boldsymbol{u}}_{\mathbf{S}} + \tilde{\boldsymbol{u}}_{\boldsymbol{I}}) \\ &= \boldsymbol{\mathcal{F}}\boldsymbol{\mathcal{F}}^{H}\boldsymbol{H}\boldsymbol{\mathcal{F}}\boldsymbol{\mathcal{F}}^{H}\mathbf{X} + \boldsymbol{\mathcal{F}}\tilde{\boldsymbol{u}}_{\boldsymbol{S}} + \boldsymbol{\mathcal{F}}\tilde{\boldsymbol{u}}_{\boldsymbol{I}} \\ &= \boldsymbol{H}\boldsymbol{X} + \boldsymbol{U}_{\boldsymbol{S}} + \boldsymbol{U}_{\boldsymbol{I}}, \end{aligned} \tag{3.6}$$

where $\tilde{\boldsymbol{h}}$ can be diagonalized by the DFT matrix, giving $\tilde{\boldsymbol{h}} = \boldsymbol{\mathcal{F}}^{H}\boldsymbol{H}\boldsymbol{\mathcal{F}}$. The received symbols having an index spanning from 1 to $(\frac{N-2}{2})$ are used for detection. Since the DSL channel is only slowly time-variant [6], it is reasonable to assume perfect channel estimation. Hence $\boldsymbol{H}$ can be equalized by a one-tap frequency-domain channel equalizer (FEQ) at the receiver. $\boldsymbol{U}_{\mathbf{S}} = \boldsymbol{\mathcal{F}}\tilde{\boldsymbol{u}}_{\mathbf{S}}$ is the DFT of $\tilde{\boldsymbol{n}}_{\mathbf{S}}$, which is also an AWGN process since $\boldsymbol{\mathcal{F}}$ is unitary. $\boldsymbol{U}_{\boldsymbol{I}} = \boldsymbol{\mathcal{F}}\tilde{\boldsymbol{u}}_{\boldsymbol{I}}$ is the DFT of $\tilde{\boldsymbol{u}}_{\boldsymbol{I}}$ and represents the impulsive noise in the frequency domain.

3.2.2 Impulsive Noise Modeling

The noise in DSL can be categorized into stationary noise and impulsive noise, which can be modelled by a Hidden Semi-Markov Model (HSMM) [166] [167] [168], where the different states may have different durations and distributions. As shown in Fig 3.1, the noise in the time domain is represented by two states, where state s_0 refers to the absence of the impulsive noise, while state s_1 refers to the presence of both the stationary noise and the impulsive noise. It is reasonable to assume that the noise process starts from each state with an identical probability of 0.5.

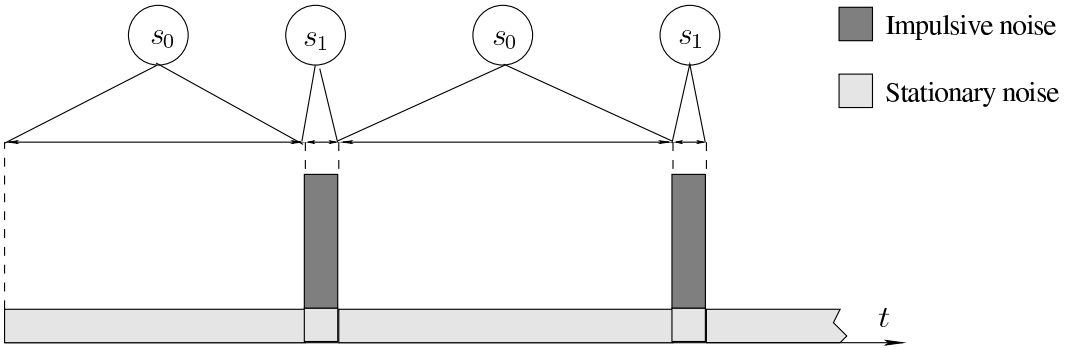

Figure 3.1: Illustration of noise process model, s_0 meaning states without impulsive noise and s_1 meaning states with impulsive noise.

As the measurement results of [41] illustrated, the duration of the impulse noise may be characterized by a two-term log-normal form. The probability density function (PDF)

of the duration can be expressed as

$$f(t|s_1)) = \frac{B}{\sqrt{2\pi}v_1 t}\exp\left(-\frac{\ln^2(t/t_1)}{2v_1^2}\right) + \frac{1-B}{\sqrt{2\pi}v_2 t}\exp\left(-\frac{\ln^2(t/t_2)}{2v_2^2}\right). \quad (3.7)$$

Setting the ranges of inter-arrival times as Markov states, as suggested in [41], the two-state MRP model is capable of characterising the impulsive noise inter-arrival times in DSL systems. To elaborate, $s_{0,0}$ represents the inter-arrival times lower than 1 ms, which is exponentially-distributed; $s_{0,1}$ represents the inter-arrival time longer than 1 ms, which is Pareto-distributed. Since only the inter-arrival time shorter than 1 ms obeys the exponential distribution, the PDF of state s_0 should be reformatted as a truncated distribution. Therefore, the PDF of the two states of the inter-arrival time can be expressed as

$$f(t|s_{0,j}) = \begin{cases} \frac{1}{1-\exp(-\lambda t_s)}\lambda\exp(-\lambda t), & \text{if } j=0 \ (t < t_s) \\ \theta t_s^{\theta}/t^{\theta+1}, & \text{if } j=1 \ (t \geq t_s), \end{cases} \quad (3.8)$$

where $t_s = 1$ ms, which is the switching threshold of the two states, while we have $\lambda = 0.16s^{-1}$ and $\theta = 1.5$ [41].

The Markov state-transition probability matrix of state s_0 is a (2×2) - element matrix

$$\mathbf{P}_{s_0}(1) = \begin{bmatrix} p_{s_0}^{00} & p_{s_0}^{01} \\ p_{s_0}^{10} & p_{s_0}^{11} \end{bmatrix}. \quad (3.9)$$

3.3 Statistics of Noise Samples

In this section, we analyze the noise characteristics in both the time domain and the frequency domain, by calculating the probability mass function (PMF). Then, the noise occurrence in a DMT symbol is investigated in the frequency domain. Finally, we obtain the probability corresponding to the fact that the number of infested samples in a DMT symbol happens to be n_I.

3.3.1 Impulsive Noise Characteristics in the Time Domain

Assuming that perfect synchronization is achieved at the receiver, the received samples are obtained at the time instant of $0, \Delta t, 2\Delta t, \ldots, (N-1)\Delta t$, where $\Delta t = T_{\text{DMT}}/N$ and T_{DMT} is the duration of a DMT symbol. The normalized state-duration d, which corresponds to the number of samples during that state is defined as $d = [t/\Delta t]$, where $[x]$ represents the integer closest to x. For convenience, let us denote $\frac{p_{s_0}^{10}}{p_{s_0}^{01}+p_{s_0}^{10}}$ and $\frac{p_{s_0}^{01}}{p_{s_0}^{01}+p_{s_0}^{10}}$ in (3.9) by $\pi_{0,1}$

and $\pi_{0,0}$, respectively. According to Appendix A, the PMFs of d conditioned on state s_0 and s_1 can be expressed as

$$p(d|s_0) = \begin{cases} \frac{\pi_{0,0}\left(e^{-\lambda\Delta t(d-0.5)} - e^{-\lambda\Delta t(d+0.5)}\right)}{1-e^{-\lambda t_s}}, & \text{if } d < [\frac{t_s}{\Delta t}] \\ \pi_{0,1}\left(\frac{t_s}{\Delta t}\right)^{\theta}\left(\frac{1}{(d-0.5)^{\theta}} - \frac{1}{(d+0.5)^{\theta}}\right), & \text{if } d \geq [\frac{t_s}{\Delta t}], \end{cases} \tag{3.10}$$

$$\begin{aligned} p(d|s_1) = B&\left[Q\left(\frac{\ln(\frac{(d-0.5)\Delta t}{t_1})}{v_1}\right) - Q\left(\frac{\ln(\frac{(d+0.5)\Delta t}{t_1})}{v_1}\right)\right] \\ &+ (1-B)\left[Q\left(\frac{\ln(\frac{(d-0.5)\Delta t}{t_2})}{v_2}\right) - Q\left(\frac{\ln(\frac{(d+0.5)\Delta t}{t_2})}{v_2}\right)\right]. \end{aligned} \tag{3.11}$$

3.3.2 Impulsive Noise Characteristics in the Frequency Domain

The noise in the frequency domain can also be categorized by two states: S_0 represents the absence of impulsive noise in a DMT symbol and S_1 refers to the presence of impulsive noise in a DMT symbol. In contrast to the time-domain, where the state transitions occur at multiplies of Δt, in the frequency-domain the state transitions occur at multiplies of the DMT symbol duration, because the impulsive noise effects are spread over the entire DMT symbol, when the signal is transformed from the time-domain back to the frequency-domain.

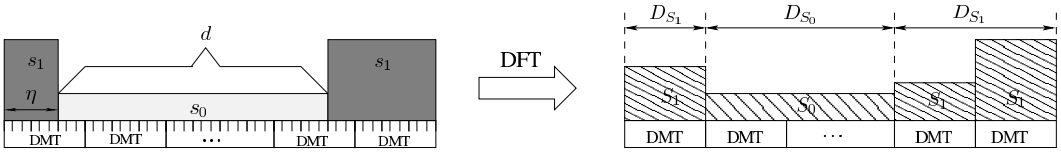

Figure 3.2: Illustration of the impulsive noise effect imposed DMT both in the time domain (left) and the frequency domain (right).

As shown in Fig 3.2, we define the duration of a state in the frequency-domain as D, which is a multiple of the DMT symbol duration. For convenience, we define the number of samples before time-domain state transition in the DMT symbol by η, where the frequency-domain state transition occurs. Since η is the offset relative to the start instant of a DMT symbol, η can be readily assumed to obey the uniform distribution of

$$p(\eta) = \frac{1}{N},\ \eta = 0, 1, \ldots, N-1. \tag{3.12}$$

Under the above assumptions, the relationship between the duration d of state s_i, where $i \in \{0, 1\}$ and the corresponding duration D of state S_i, where $i \in \{0, 1\}$, may be readily

shown. For state s_0, we have

$$D = \begin{cases} \lceil d/N \rceil - 2, & \text{if } \eta + d < \lceil d/N \rceil N \ \& \ \eta \neq 0 \\ \lceil d/N \rceil - 1, & \text{if } \eta + d \geq \lceil d/N \rceil N \ \& \ \eta \neq 0 \\ & \text{or } \eta + d > \lceil d/N \rceil N \ \& \ \eta = 0 \\ \lceil d/N \rceil, & \text{if } \eta + d = \lceil d/N \rceil N \ \& \ \eta = 0, \end{cases} \tag{3.13}$$

while for state s_1, we have

$$D = \begin{cases} \lceil d/N \rceil, & \text{if } \eta + d \leq \lceil d/N \rceil N \\ \lceil d/N \rceil + 1, & \text{if } \eta + d > \lceil d/N \rceil N, \end{cases} \tag{3.14}$$

where $\lceil x \rceil$ denotes the smallest integer larger than x.

As shown in Appendix B, the PMF $p(D|S_0)$ and $p(D|S_1)$ of D conditioned on state S_0 and S_1 can be readily derived.

3.3.3 Impulsive Noise Occurrence in a DMT Symbol

Let us assume that the noise process matches the statistical distribution required for the noise model sufficiently accurately. Here, we denote the total number of the states S_i as K_i, where $i \in \{0, 1\}$, during the noise process. Since the two states occur alternatively, we have $K_0 = K_1$. As shown in Fig. 3.2, let us denote the duration of the kth state S_i as $D_{S_i,k}$ and the expectation of $\cdot$ by $\mathcal{E}[\cdot]$. Then, we have $\sum_{k=1}^{K_i} D_{S_i,k} \rightarrow \mathcal{E}[D_{S_i,k}]K_i$. Hence, the posteriori probability of an observed DMT symbol $\mathbf{Y}$ in (3.6), which is corrupted by the noise in the state S_i can be expressed as

$$P(S_i|\boldsymbol{Y}) = \frac{\mathcal{E}[D_{S_i,k}]}{\mathcal{E}[D_{S_0,k}] + \mathcal{E}[D_{S_1,k}]}. \tag{3.15}$$

According to Bayes's rule, we have

$$\begin{aligned} P(D, S_i|\boldsymbol{Y}) &= \frac{P(D, S_i, \boldsymbol{Y})}{P(\boldsymbol{Y})} \\ &= \frac{P(D|S_i, \boldsymbol{Y})P(S_i, \boldsymbol{Y})}{P(\boldsymbol{Y})} \\ &= P(D|S_i, \boldsymbol{Y})P(S_i|\boldsymbol{Y}), \end{aligned} \tag{3.16}$$

where $P(D|S_i, \boldsymbol{Y})$ is the probability of having a given DMT symbol in state S_i, which happens to be in a set of D successive DMT symbols all being in state S_i. Let us denote the number of states S_i with the duration of D as $k_{S_i,D}$. Then we have $\sum_{D=1}^{\infty} k_{S_i,D} = K_i$

and $p(D|S_i) = \frac{k_{S_i,D}}{K_i}$. We can show that

$$P(D|S_i, \boldsymbol{\Upsilon}) = \frac{Dk_{S_i,D}}{\mathcal{E}[D_{S_i,k}]K_i} = \frac{Dp(D|S_i)}{\mathcal{E}[D_{S_i,k}]} \quad . \tag{3.17}$$

By substituting (3.15) and (3.17) into (3.16), we have

$$\begin{aligned} P(D, S_i|\boldsymbol{\Upsilon}) &= \frac{Dp(D|S_i)}{\mathcal{E}[D_{S_i,k}]} \frac{\mathcal{E}[D_{S_i,k}]}{\mathcal{E}[D_{S_0,k}] + \mathcal{E}[D_{S_1,k}]} \\ &= \frac{Dp(D|S_i)}{\mathcal{E}[D_{S_0,k}] + \mathcal{E}[D_{S_1,k}]} \, . \end{aligned} \tag{3.18}$$

3.3.4 $p(n_I)$ Study

Let us now denote the probability of having a received DMT symbol in which the number of samples in state s_1 in the time domain is n_I by $p(n_I)$. Based on the calculation in Appendix D, we then have

$$p(n_I) = \begin{cases} \frac{\mathcal{E}[D_{S_0,k}]}{\mathcal{E}[D_{S_0,k}]+\mathcal{E}[D_{S_1,k}]}, & \text{if } n_I = 0 \\ \mathcal{D}_1(n_I, B, v_1, t_1) + \mathcal{D}_1(n_I, 1-B, v_2, t_2), & \text{if } n_I = 1, 2, \ldots, N-1 \\ \mathcal{D}_2(B, v_1, t_1) + \mathcal{D}_2(1-B, v_2, t_2), & \text{if } n_I = N \end{cases} \tag{3.19}$$

Then, the Cumulative density function (CDF) of n_I at the location of DT central office (CO) and DT customer premises (CP) is accordingly plotted in Fig. 3.3.

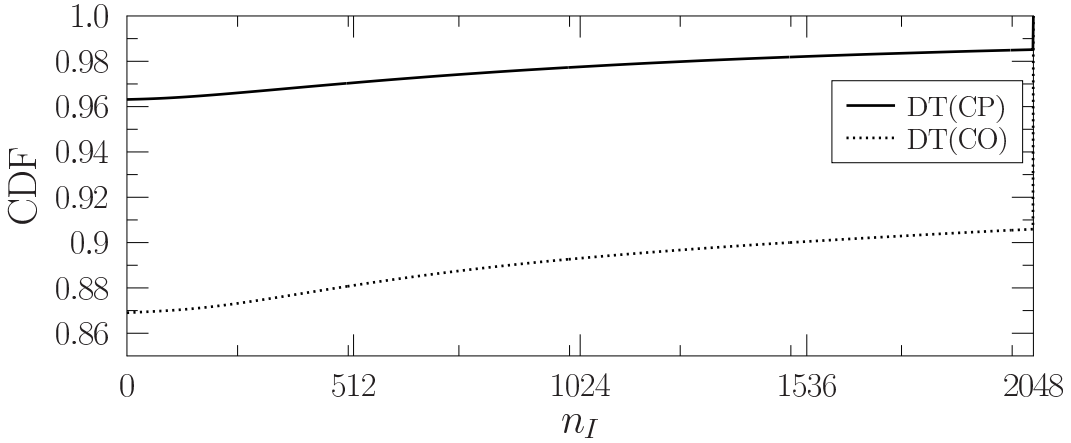

Figure 3.3: Cumulative density function of n_I at DT central offices (CO) and DT customer premises (CP).

3.4 Analysis of the Noise Power and of the Average Bit Error Ratio

In this section, we firstly investigate the behavior of colored non-Gaussian noise in DMT/OFDM systems, so as to obtain the noise power. Accordingly, we calculate the signal-to-noise ratio (SNR) in each subchannel and then formulate our BER formulas by integrating the $p(n_I)$ into the general BER expressions.

3.4.1 Colored Non-Gaussian Noise in the DMT/OFDM System

It is widely recognized that the performance of the communication system operating both with or without DMT/OFDM is identical in an AWGN channel. This is because during the DMT/OFDM demodulation the received signals are processed by the DFT-based demodulator, which is a linear process. Hence the linearly processed Gaussian distributed noise also yields a Gaussian distribution with an identical mean and variance after DFT and normalization. The stationary noise is characterized by the above situation. However, the situation is different for the case of the correlated Weibull-distributed impulsive noise in DSL.

There has been a number of publications discussing the Fourier transforms of both correlated and of non-Gaussian distributed signals [169–171]. Here let us denote a correlated Weibull distributed variable by $w[k]$ and its discrete Fourier transformed which of size N by

$$W[i] = \mathrm{DFT}\big[w[k]\big] = \sum_{i=0}^{N} e^{-j\frac{2\pi ik}{N}} w[k]. \tag{3.20}$$

The following convergence has been formally proved in [170]

$$\frac{1}{\sqrt{N}}\Big[\Re\big(W[i]\big), \Im\big(W[i]\big)\Big] \Rightarrow \Big[G[i], G[i]\Big], \tag{3.21}$$

where $G[i]$ is an independent identically distributed (i.i.d.) normal random variable with zero-mean and variance of $S[i]/2$, while $S[i]$ is the power spectral density associated with the ACF of the process, as stated by the Wiener-Khintchine theorem [172].

After DFT, the impulsive noise at the kth subcarrier has a variance of $\sqrt{N}$ times its spectral density and its distribution tends to the Gaussian distribution. Since the signal and the stationary noise are also amplified by the factor of $\sqrt{N}$ after DMT/OFDM demodulation, the factor $\sqrt{N}$ is eliminated by normalization, when considering the BER vs SNR performance.

3.4.2 SNR Calculation

Let us denote the power spectral density of the impulsive noise by $S(f)$, which can be calculated from the Fourier Transform (FT) of its ACF $R(t)$ as follows

$$\begin{aligned} S(f) &= \mathcal{F}\big[R(t)\big] \\ &= \frac{\beta}{\beta^2 + 4\pi^2(f+\alpha)^2} + \frac{\beta}{\beta^2 + 4\pi^2(f-\alpha)^2}. \end{aligned} \tag{3.22}$$

Furthermore, let us denote the impedance in DSL by Z and the power of the impulsive noise at the ith subchannel as $\sigma^2_{I,i}$, which can be calculated as:

$$\begin{aligned} \sigma^2_{I,i} &= \frac{1}{Z}\int_{i\Delta f}^{(i+1)\Delta f} S(f)\,\mathrm{d}f \\ &= \frac{1}{2\pi Z}\Bigg\{ \tan^{-1}\Big(\frac{2\pi\big[(i+1)\Delta f + \alpha\big]}{\beta}\Big) - \tan^{-1}\Big(\frac{2\pi\big[i\Delta f + \alpha\big]}{\beta}\Big) \\ &\quad + \tan^{-1}\Big(\frac{2\pi\big[(i+1)\Delta f - \alpha\big]}{\beta}\Big) - \tan^{-1}\Big(\frac{2\pi\big[i\Delta f - \alpha\big]}{\beta}\Big)\Bigg\}, \end{aligned} \tag{3.23}$$

where Δf is the multicarrier spacing of DMT.

Since the Fourier transform constitutes a linear process, the Fourier transform of the sum of stationary noise and impulsive noise is equivalent to the sum of Fourier transform of the stationary noise and that of the impulsive noise. Let us introduce $\kappa_i = \frac{\sigma^2_{I,i}}{\sigma^2_S}$ and denote the noise power at the ith subchannel by $\sigma^2_{N,i}$, which can be expressed as [21]

$$\sigma^2_{N,i} = \frac{N\sigma^2_S + n_I\sigma^2_{I,i}}{N} = \Big(1 + \frac{n_I\kappa_i}{N}\Big)\sigma^2_S. \tag{3.24}$$

According to (3.6) and (3.24), the instantaneous SNR per symbol for the ith subchannel is given by

$$\gamma_{i,n_I} = \frac{|H_i|^2 E_b \cdot M}{(1 + \frac{n_I\kappa_i}{N})\sigma^2_S} = \frac{|H_i|^2}{1 + \frac{n_I\kappa_i}{N}} \cdot \gamma_{s_0} \cdot M, \tag{3.25}$$

where H_i is the gain of the ith subchannel, E_b is the signal power per bit, M is the number of bits per symbol and $\gamma_{s_0} = E_b/\sigma^2_S$. The above equation shows that the SNR of a specific subchannel is affected by its gain, by SNR experienced in the absence of impulsive noise, by the number of samples encountered at state s_1 and by the power ratio between the impulsive noise to stationary noise.

3.4.3 BER Analysis

Bearing in mind the convergence of (5.11), the BER of Q-ary QAM relying on classic Gray mapping for the instantaneous SNR γ_{i,n_I} can be approximated according to the generalized superposition of Q functions [173]:

$$P_e(\gamma_{i,n_I}) \approx \sum_l p_l Q(\beta_l \sqrt{\gamma_{i,n_I}}), \tag{3.26}$$

where p_l and β_l are different for different modulation schemes, as shown in Table 3.1.

Table 3.1: Parameter values for different modems

	BPSK	QPSK	16QAM	64QAM
$[\rho_1, \beta_1]$	$[1, \sqrt{2}]$	$[1, 1]$	$[\frac{3}{4}, \sqrt{\frac{1}{5}}]$	$[\frac{7}{12}, \sqrt{\frac{1}{21}}]$
$[\rho_2, \beta_2]$	\	\	$[\frac{1}{2}, 3\sqrt{\frac{1}{5}}]$	$[\frac{1}{2}, 3\sqrt{\frac{1}{21}}]$
$[\rho_3, \beta_3]$	\	\	$[-\frac{1}{4}, 5\sqrt{\frac{1}{5}}]$	$[-\frac{1}{12}, 5\sqrt{\frac{1}{21}}]$
$[\rho_4, \beta_4]$	\	\	\	$[\frac{1}{12}, 9\sqrt{\frac{1}{21}}]$
$[\rho_5, \beta_5]$	\	\	\	$[-\frac{1}{12}, 13\sqrt{\frac{1}{21}}]$

Since the BER in (3.26) is conditioned on $p(n_I)$, the average BER of the system can be expressed as

$$P_{b,\text{OFDM}} \approx \frac{1}{N} \sum_{i=0}^{N-1} \sum_{n_I=0}^{N} P_e(\gamma_{i,n_I}) p(n_I). \tag{3.27}$$

Specifically, since the symbols of the subchannels with the index spanning from 1 to $(\frac{N}{2} - 1)$ are actually used for demodulation in DMT, the corresponding BER formula of DMT is expressed as

$$P_{b,\text{DMT}} \approx \frac{1}{N/2-1} \sum_{i=1}^{N/2-1} \sum_{n_I=0}^{N} P_e(\gamma_{i,n_I}) p(n_I). \tag{3.28}$$

Substituting (3.19) and (3.26) into (3.28), the average BER of the DMT system under impulsive noise in DSL can be expressed as in (3.29).

$$\begin{aligned} P_{b,\text{DMT}} \approx \frac{1}{N/2-1} \sum_{i=1}^{N/2-1} \Bigg\{ & P_e\big(|H_i|^2 \gamma_{s_0}\big) \cdot \frac{\mathcal{E}[D_{S_0,k}]}{\mathcal{E}[D_{S_0,k}] + \mathcal{E}[D_{S_1,k}]} \\ & + \sum_{n_I=1}^{N-1} P_e\Big(\frac{|H_i|^2 \gamma_{s_0}}{1 + \frac{n_I \kappa_i}{N}}\Big) \Big[\mathcal{D}_1(n_I, B, v_1, t_1) + \mathcal{D}_1(n_I, 1-B, v_2, t_2)\Big] \\ & + P_e\Big(\frac{|H_i|^2}{1+\kappa_i} \gamma_{s_0}\Big) \Big[\mathcal{D}_2(B, v_1, t_1) + \mathcal{D}_2(1-B, v_2, t_2)\Big] \Bigg\}. \end{aligned} \tag{3.29}$$

3.5 Performance Evaluation

This section first describes on simulation set up, including the DMT and the measured channel. Later, we present our analytical and simulation based BER performance for the DMT-aided DSL for a bandwidth of up to 106 MHz. For the BER performance evaluation, the noise process was arranged to have a sufficiently long duration for ensuring the statistical relevance of the noise model.

3.5.1 DMT, Channel and Noise Configuration

As proposed in G.fast [174], the DMT modulation employs Q-ary QAM on each tone, with the spacing of 51.75 kHz. The DMT symbol rate is 48 000 symbol/s, and again the duration T_{DMT} of a DMT symbol is 20.83 µs.

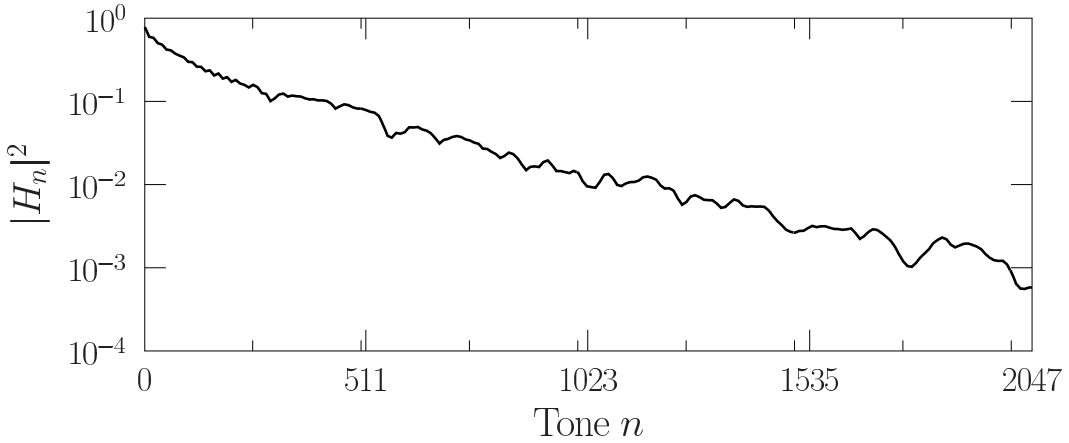

Figure 3.4: The frequency selective channel model in the frequency domain of DSL measured by BT, with a bandwidth of up to 106 MHz and multicarrier spacing of 51.75 kHz. The twisted pairs have a diameter of 0.5 mm and length of 100 m.

Since there is still no established channel model for the frequency range of G.fast at the time of writing, here we directly utilize the channel measured by BT, which is shown in Fig 3.4. The low-pass characteristics reflected in the figure are imposed by impedance mismatching, implying that the impedance was designed to be matched at the low frequencies for voice signals, hence the higher frequencies beyond the originally designed frequency range are severely attenuated.

3.5.2 BER Performance

In Fig 3.5, we investigate the BER performance of the DMT system considered under non-dispersive channel conditions while inflicting both stationary and impulsive noise in DSL. In this figure, three different modulation schemes, namely 4QAM, 16QAM and 64QAM

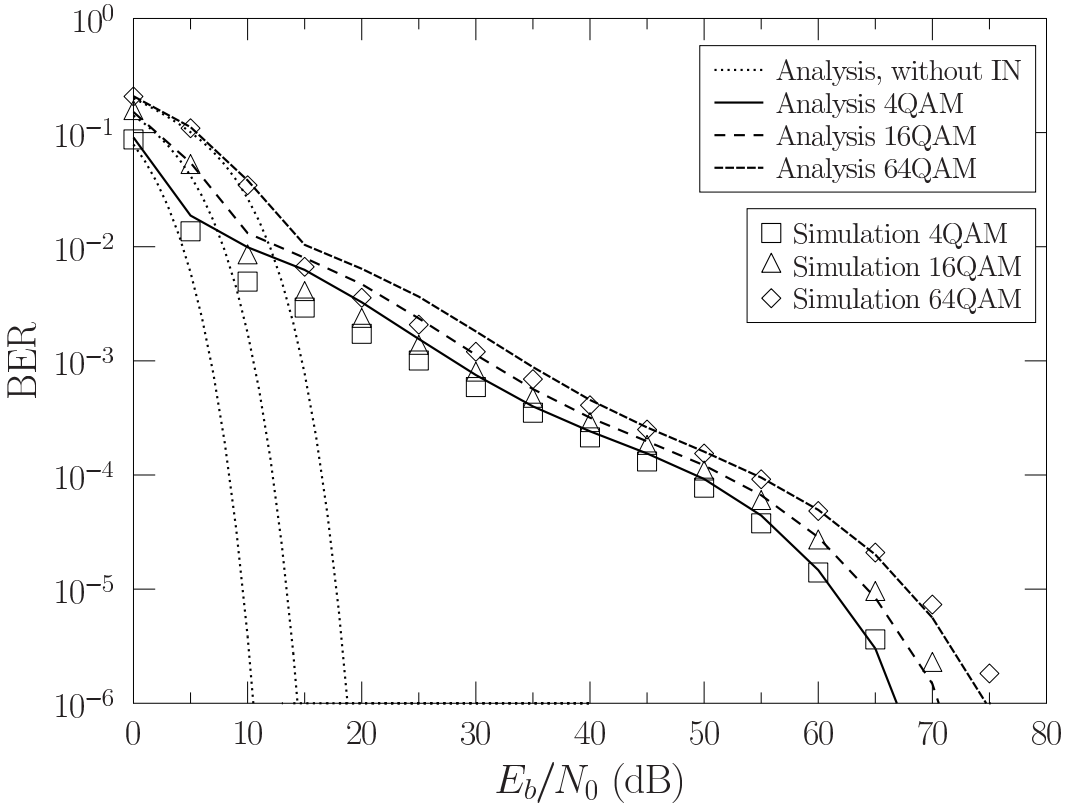

Figure 3.5: BER performance of the DMT system for Q-ary QAM with simulation results and theoretical analysis, when communicating over non-dispersive channels suffering from both stationary and impulsive noise. The theoretical results are calculated according to Eq. (3.29).

are considered. In addition to the well-known features of the different classic modulation schemes, our observations are as follows. Firstly, in comparison to the performance experienced over benign AWGN channels, there is a gradual slope change beyond a certain value of γ_{s_0}. This implies that when γ_{s_0} is lower than this value, the BER performance is dominated by the AWGN, while it is more dominated by the impulsive noise, when γ_{s_0} becomes higher. Secondly, in Fig 2.5, the maximum value of impulsive noise is about 80 dB higher than the stationary noise, while there is a γ_{s_0} gap of 60 dB between the system operating with and without impulsive noise for a given BER of 10^{-6}. The associated performance tends to be higher at higher γ_{s_0} values. This implies that at a high γ_{s_0}, the BER performance of the system is dominated by the maximum value of the impulsive noise.

In Fig 3.6, we study the BER performance of the DMT system considered, when communicating over dispersive channels using various M-QAM schemes. Firstly, when the channel becomes dispersive, the BER performance is severely degraded at the γ_{s_0} values, where the AWGN dominates the BER performance. In comparison to Fig 3.5, for a given BER of 10^{-2}, where the AWGN dominates the BER performance, the dispersive channel requires about 20 dB higher γ_{s_0} values, than communicating over non-dispersive channels in order to achieve the same BER performance. This can be explained by the frequency-

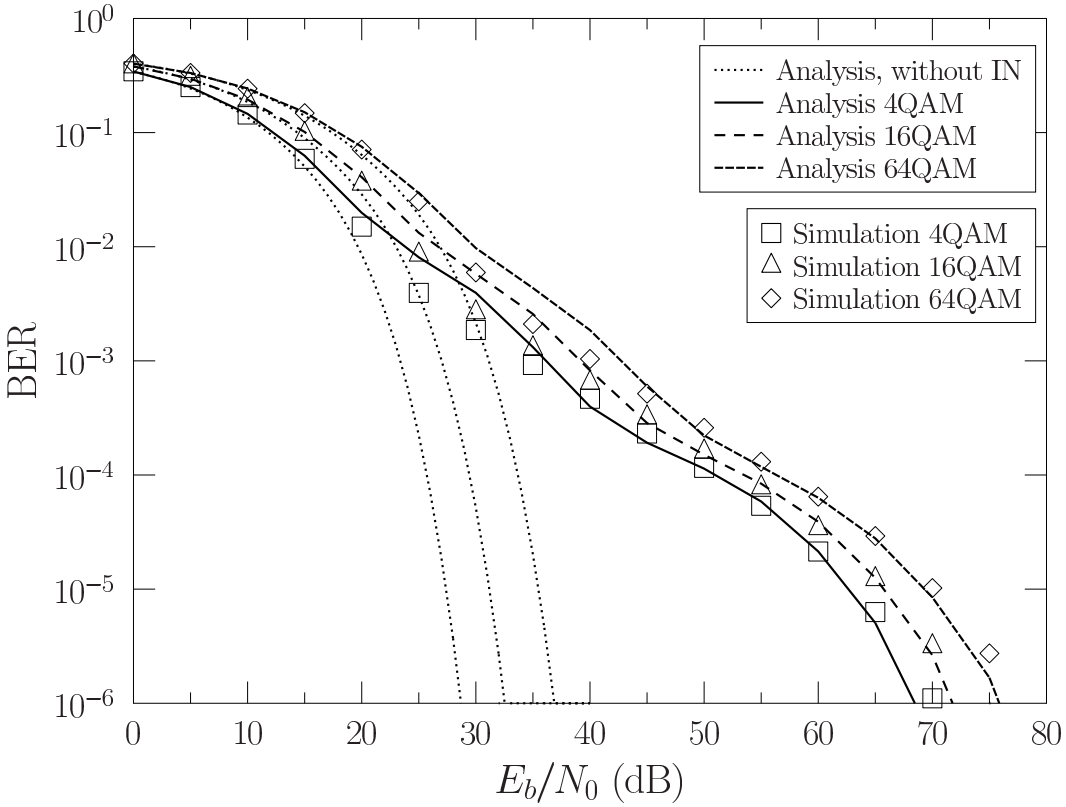

Figure 3.6: BER performance of the DMT system for Q-ary with simulation results and theoretical analysis, QAM when communicating over dispersive channels suffering from both stationary and impulsive noise. The theoretical results are calculated according to Eq. (3.29).

dependent attenuation shown in Fig 2.5. It should be noted that although the maximum attenuation is 30 dB in Fig 2.5, the extra γ_{s_0} required by the dispersive channel at BER of 10^{-2} is only about 20 dB. This is explained by the fact that all the tones with the index spanning from 1 to $(\frac{N}{2}-1)$ are utilized in DMT demodulation and the maximum attenuation is 20 dB in the first half of the tones in Fig 3.4. Secondly, the BER performance at high γ_{s_0} values, where the impulsive noise dominates the performance, is not degraded so severely. For a given BER of 10^{-6}, communicating over dispersive DSL channels requires only 2 dB higher γ_{s_0} than communicating over non-dispersive channels. As previously discussed, the BER performance at high γ_{s_0} values depends on the maximum value of impulsive noise power across the tones. As shown in Fig 2.5, the first half of the tones associated with the maximum value of the impulsive noise power are at low frequencies, where the channels' attenuation is low as shown in Fig 2.5, hence only resulting in a modest performance degradation.

In Fig 3.7, we explore the effect of the receiver location on the BER performance of DMT-based DSL systems contaminated both non-dispersive and dispersive channels, in the presence of both the stationary and the impulsive noise. In this figure, DT's central offices and DT's customer premises are considered. The corresponding impulsive noise

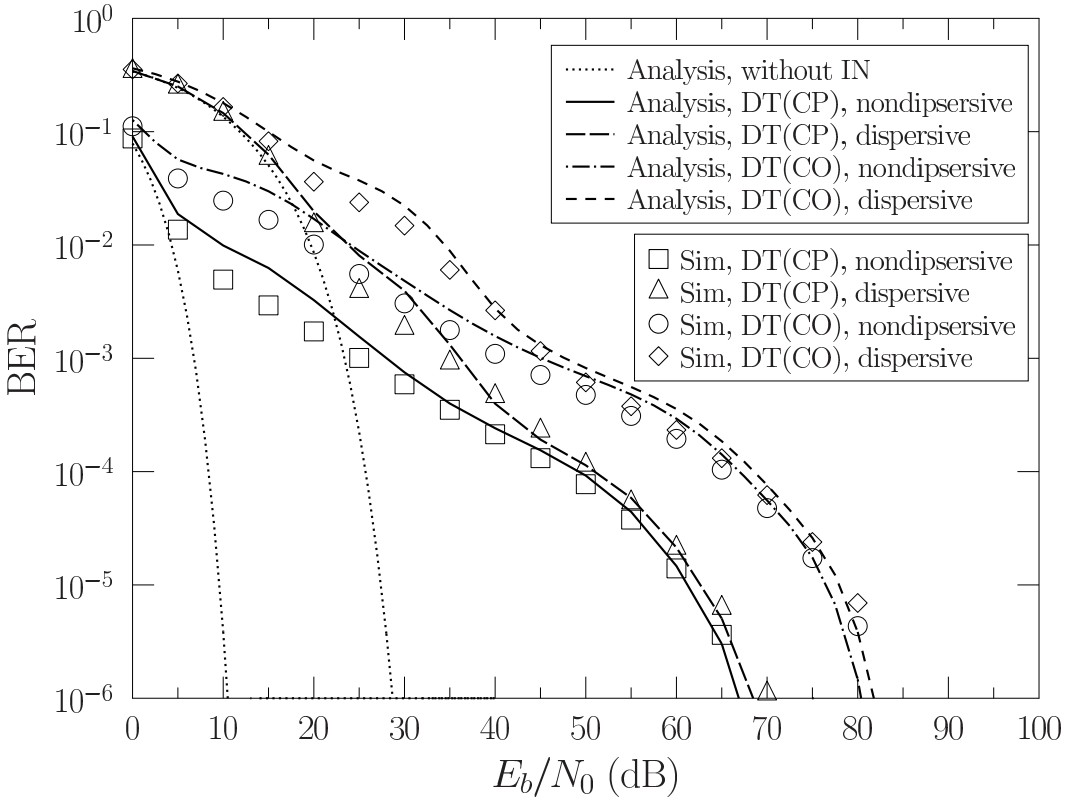

Figure 3.7: BER performance of the DMT system at the Deutsche Telekom central offices and customer premises with simulation results and theoretical analysis, when communicating over both non-dispersive and dispersive channels suffering both from stationary and impulsive noise. 4QAM is employed. The theoretical results are calculated according to Eq. (3.29).

characteristics are parametrized according to Table 2.2. Our observations are listed below. Firstly, for both non-dispersive and dispersive channels, the CO has a smaller γ_{s_0} value, where the impulsive noise dominates the BER performance. In other words, the CPs benefit from a better performance than the CO. As discussed in Section I, the receivers at the CO inevitably suffers from more dialling pulses, busy signals and ringing, which causes longer impulsive noise burst. Quantitatively, the mean value of the impulsive noise duration is 34.87 µs at DT(CP) and 157.22 µs at DT(CO) as calculated from the distribution in (5.16). According to (3.29), the probability of a DMT symbol becoming impaired by impulsive noise increases, when the impulse duration becomes longer, while keeping the inter-arrival time the same. Secondly, the γ_{s_0} gap between the CO and the CP becomes smaller upon aiming for achieving the same BER, when the maximum impulsive noise power dominates the BER performance. This can be explained by bearing in mind that at high γ_{s_0} the BER performance is mainly degraded, because the high-power impulsive noise requires a sufficiently high signal power to correct the errors, while at high γ_{s_0} the BER performance mainly depends on $\mathcal{E}[n_I]$ and $\sigma^2_{I,i}$, as seen with the aid of (3.29).

3.6 Chapter Summary

Observing the BER performance in Section 3.5.2, we may infer that the slope gradually changes beyond a certain value of SNR. This implies that when the SNR is below this certain value, the BER performance is dominated by the background noise, while when the SNR is above the value, the impulsive noise becomes dominating the performance. To elaborate, we compare throughput versus E_b/N_0 performance of systems contaminated by impulsive noise and that free of impulsive noise in Fig. 3.8. It can be inferred that the extra SNR required by the system contaminated by impulsive noise is around 10 dB for the BER of 10^{-3}, which is of our interest for the uncoded systems. The SNR gap become even larger upon decreasing the BER requirement. This in turn demonstrates necessity of impulsive noise mitigation in DSL system, which is the major concern of Chapter 4 and Chapter 5.

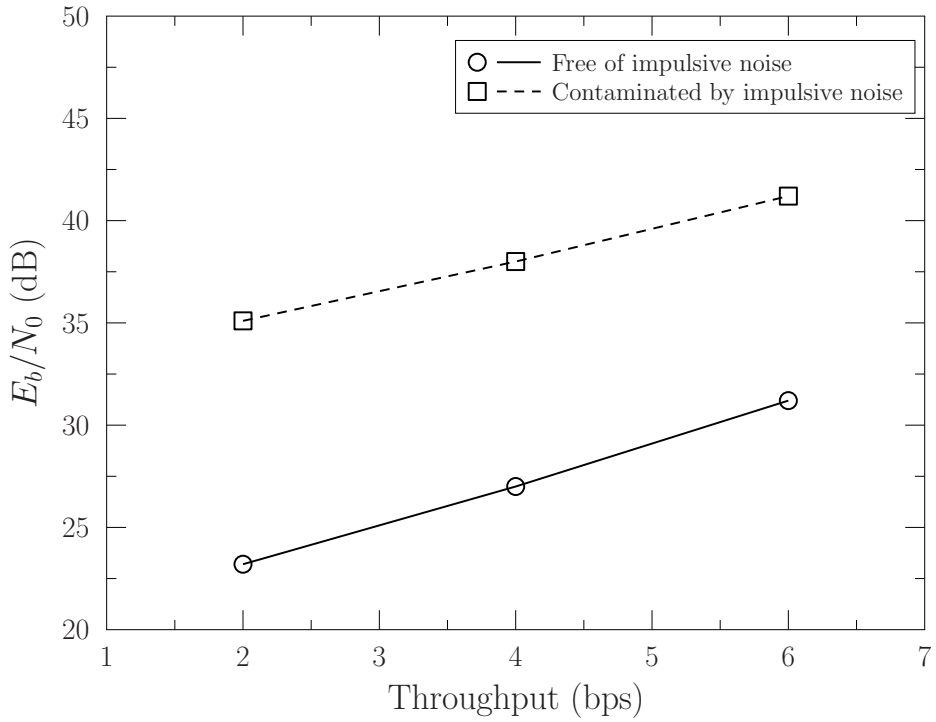

Figure 3.8: Throughput versus E_b/N_0 performance comparison between the systems free of impulsive noise and those contaminated by impulsive noise, when communicating over dispersive channels at BER of 10^{-3}. The results are obtained according to Fig. 3.6.

In a nutshell, in this chapter we have analyzed the performance of DMT systems both under practical noise conditions and under dispersive DSL channel conditions with the aid of a hidden semi-Markov model. A closed-form BER formula has been derived for DMT-based DSL systems. The simulation results demonstrated the accuracy of the BER formulas and showed that the BER performance of our DMT-based DSL systems is severely

degraded both by the impulsive noise and by dispersive channels.

3.7 Appendix

3.7.1 Derivation of $p(d|s_i)$

State s_0

For a Markov process having a one-step transition probability matrix of

$$\mathbf{P}_{s_0}(1) = \begin{bmatrix} p_{s_0}^{00} & p_{s_0}^{01} \\ p_{s_0}^{10} & p_{s_0}^{11} \end{bmatrix} \tag{3.30}$$

according to [156], we have

$$\lim_{n\to+\infty} \mathbf{P}_{s_0}^{00}(n) = \lim_{n\to+\infty} \mathbf{P}_{s_0}^{10}(n) = \frac{p_{s_0}^{10}}{p_{s_0}^{01} + p_{s_0}^{10}}, \tag{3.31}$$

$$\lim_{n\to+\infty} \mathbf{P}_{s_0}^{01}(n) = \lim_{n\to+\infty} \mathbf{P}_{s_0}^{11}(n) = \frac{p_{s_0}^{01}}{p_{s_0}^{01} + p_{s_0}^{10}}. \tag{3.32}$$

Since the probability matrix is a simple (2×2)-element matrix, the transition probability exhibit rapid convergence. Let us denote $\frac{p_{s_0}^{10}}{p_{s_0}^{01}+p_{s_0}^{10}}$ by $\pi_{0,0}$ and $\frac{p_{s_0}^{01}}{p_{s_0}^{01}+p_{s_0}^{10}}$ by $\pi_{0,1}$. For $d < [t_s/\Delta t]$, the PMF of state s_0 can be expressed as

$$\begin{aligned} p(d|s_0) &= \pi_{0,0} \int_{(d-0.5)\Delta t}^{(d+0.5)\Delta t} f(t|s_{0,0})\,\mathrm{d}t \\ &= \frac{\pi_{0,0}\big(e^{-\lambda\Delta t(d-0.5)} - e^{-\lambda\Delta t(d+0.5)}\big)}{1 - e^{-\lambda t_s}}, \end{aligned} \tag{3.33}$$

and for $d \geq [t_s/\Delta t]$, we have

$$\begin{aligned} p(d|s_0) &= \pi_{0,1} \int_{(d-0.5)\Delta t}^{(d+0.5)\Delta t} f(t|s_{0,1})\,\mathrm{d}t \\ &= \pi_{0,1}\Big(\frac{t_s}{\Delta t}\Big)^{\theta}\Big(\frac{1}{(d-0.5)^{\theta}} - \frac{1}{(d+0.5)^{\theta}}\Big). \end{aligned} \tag{3.34}$$

State s_1

$$\begin{aligned} p(d|s_1) &= \int_{(d-0.5)\Delta t}^{(d+0.5)\Delta t} f(t|s_1)\,\mathrm{d}t \\ &= B\Big[Q\Big(\frac{\ln(\frac{(d-0.5)\Delta t}{t_1})}{v_1}\Big) - Q\Big(\frac{\ln(\frac{(d+0.5)\Delta t}{t_1})}{v_1}\Big)\Big] \\ &\quad + (1-B)\Big[Q\Big(\frac{\ln(\frac{(d-0.5)\Delta t}{t_2})}{v_2}\Big) - Q\Big(\frac{\ln(\frac{(d+0.5)\Delta t}{t_2})}{v_2}\Big)\Big], \end{aligned} \tag{3.35}$$

where $Q(\cdot)$ is the tail function of the standard normal distribution.

3.7.2 Derivation of $p(D|S_i)$

State S_0

As shown in (3.13), the duration relationship between the state s_0 and the state S_0 is categorized into three cases. Let us denote by $p(D|d,s_i)$ the occurrence probability of a suitable η so that the state s_i with the duration of d results in state S_i with the duration of D, where we have $i \in \{0,1\}$. When exploiting that d and η are independent variables, we have

$$\begin{aligned} p(D|S_0) &= p(D|d,s_0)p(d|s_0)\big|_{d=DN} + \sum_{d=DN+1}^{(D+1)N-1} p(D|d,s_0)p(d|s_0) \\ &\quad + \sum_{d=(D+1)N}^{(D+2)N-2} p(D|d,s_0)p(d|s_0) \\ &= \frac{1}{N}p(d|s_0)\big|_{d=DN} + \sum_{d=DN+1}^{(D+1)N-1} \frac{d-DN+1}{N}p(d|s_0) \\ &\quad + \sum_{d=(D+1)N}^{(D+2)N-2} \frac{(D+2)N-d-1}{N}p(d|s_0), \end{aligned} \tag{3.36}$$

for $D = 1,2,3\ldots$.

For $d = (D+2)N-2 < [t_s/\Delta t]$, i.e. $D < \frac{[t_s/\Delta t]+2}{N} - 2$, substituting (3.33) into (3.36), we arrive at

$$p(D|S_0) \approx \frac{\pi_{0,0}}{1-e^{-\lambda t_s}}\frac{1}{\lambda\Delta t}\frac{1}{N}\Big(e^{-DN\lambda\Delta t} - 2e^{-(D+1)N\lambda\Delta t} + e^{-(D+2)N\lambda\Delta t}\Big). \tag{3.37}$$

For $d = DN \geq [t_s/\Delta t]$, i.e. $D \geq \frac{[t_s/\Delta t]}{N}$, substituting (3.34) into (3.36), we have

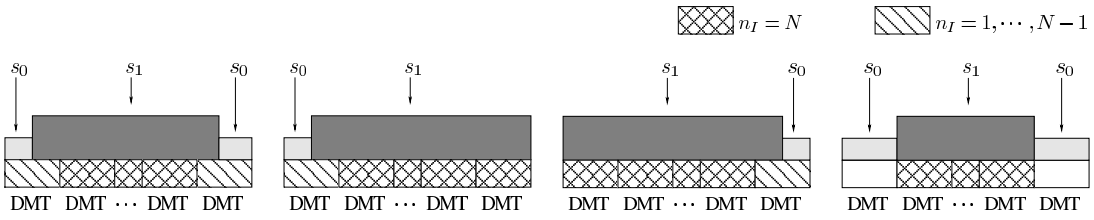

(a) Location 1 (b) Location 2 (c) Location 3 (d) Location 4

Figure 3.9: Illustration of the locations of $n_I = 1, 2, \ldots, N-1$ and $n_I = N$ in Appendix D.

$$p(D|S_0) = \frac{\pi_{0,1}}{N}\Big(\frac{t_s}{\Delta t}\Big)^{\theta}\frac{N^{1-\theta}}{\theta-1}\Big(D^{1-\theta} - 2(D+1)^{1-\theta} + (D+2)^{1-\theta}\Big). \tag{3.38}$$

Although the inter-arrival time is modelled by two states, the difference of $p(D|S_0)$ among the threshold values should be negligible. Therefore, it is reasonable to extend (3.37) to $D < \frac{t_s/\Delta t}{N} - 1$ and (3.38) to $D \geq \frac{t_s/\Delta t}{N} - 1$. In this case, $\sum_{D=0}^{\infty} p(D|S_0)$ is also extremely close to 1.0, which demonstrates the feasibility of the above approximation.

State S_1

The calculation of $p(D|S_1)$ is categorized into two types: one of is when is the duration of state s_1 in the time domain is shorter than N and occurs within one DMT symbol. Then, we have

$$\begin{aligned} p(D|S_1) &= \sum_{d=1}^{N} p(D|d, s_1)p(d|s_1) \\ &= \sum_{d=1}^{N} \frac{N-d+1}{N} p(d|s_1) \\ &= \mathcal{A}(B, v_1, t_1) + \mathcal{A}(1-B, v_2, t_2), \end{aligned} \tag{3.39}$$

for $D = 1$, where $\mathcal{A}(\cdot)$ is expressed as

$$\begin{aligned} \mathcal{A}(B, v_1, t_1) = B\Big\{ & Q\Big(\frac{\ln\left(\frac{0.5\Delta t}{t_1}\right)}{v_1}\Big) - \frac{1}{N}Q\Big(\frac{\ln\left(\frac{(N+0.5)\Delta t}{t_1}\right)}{v_1}\Big)\Big\} \\ & -\frac{B}{N}\Big\{(N-0.5)Q\Big(\frac{\ln\left(\frac{(N-0.5)\Delta t}{t_1}\right)}{v_1}\Big) - \frac{t_1}{\Delta t}\exp\Big(\frac{v_1^2}{2}\Big)Q\Big(\frac{\ln\left(\frac{(N-0.5)\Delta t}{t_1}\right)}{v_1} - v_1\Big) \\ & -1.5Q\Big(\frac{\ln\left(\frac{1.5\Delta t}{t_1}\right)}{v_1}\Big) + \frac{t_1}{\Delta t}\exp\Big(\frac{v_1^2}{2}\Big)Q\Big(\frac{\ln\left(\frac{1.5\Delta t}{t_1}\right)}{v_1} - v_1\Big)\Big\}. \end{aligned} \tag{3.40}$$

The other is the state s_1 which lasts more than 1 DMT symbols, when we have

$$\begin{aligned} p(D|S_1) &= \sum_{d=(D-1)N+1}^{DN} p(D|d,s_1)p(d|s_1) + \sum_{d=(D-2)N+1}^{(D-1)N} p(D|d,s_1)p(d|s_1) \\ &= \sum_{d=(D-1)N+1}^{DN} \frac{DN-d+1}{N} p(d|s_1) + \sum_{d=(D-2)N+1}^{(D-1)N} \frac{d-(D-2)N-1}{N} p(d|s_1) \\ &= \mathcal{B}(B,v_1,t_1) + \mathcal{B}(1-B,v_2,t_2), \end{aligned} \tag{3.41}$$

for $D = 2,3,4,\ldots$, where $\mathcal{B}(\cdot)$ is expressed as

$$\begin{aligned} \mathcal{B}(B,v_1,t_1) = B\Big\{ &-(D-2)Q\Big(\frac{\ln\big(\frac{(D-2)N\Delta t}{t_1}\big)}{v_1}\Big) + (2D-2)Q\Big(\frac{\ln\big(\frac{(D-1)N\Delta t}{t_1}\big)}{v_1}\Big) \\ &-DQ\Big(\frac{\ln\big(\frac{DN\Delta t}{t_1}\big)}{v_1}\Big)\Big\} + \frac{t_1}{\Delta t}\exp\big(\frac{v_1^2}{2}\big)\frac{B}{N}\Big\{Q\Big(\frac{\ln\big(\frac{(D-2)N\Delta t}{t_1}\big)}{v_1} - v_1\Big) \\ &-2Q\Big(\frac{\ln\big(\frac{(D-1)N\Delta t}{t_1}\big)}{v_1} - v_1\Big) + Q\Big(\frac{\ln\big(\frac{DN\Delta t}{t_1}\big)}{v_1} - v_1\Big)\Big\}. \end{aligned} \tag{3.42}$$

3.7.3 Expectation of $D_{S_i,k}$

State 0

When introducing $t_p = \Big\lfloor \frac{[t_s/\Delta t]}{N} - 1 \Big\rfloor$ and $t_q = \Big\lceil \frac{[t_s/\Delta t]}{N} - 1 \Big\rceil$, we have

$$\begin{aligned} \mathcal{E}[D_{S_0,k}] &= \sum_{D=0}^{\infty} Dp(D|S_0) = \sum_{D=0}^{t_p} Dp(D|S_0) + \sum_{D=t_q}^{\infty} Dp(D|S_0) \\ &= \frac{\pi_{0,0}}{1-e^{-\lambda t_s}} \frac{1}{\lambda\Delta t}\frac{1}{N}\Big\{e^{-N\lambda\Delta t} - (t_n+1)e^{-(t_p+1)N\lambda\Delta t} + t_p e^{-(t_p+2)N\lambda\Delta t}\Big\} \\ &\quad + \frac{\pi_{0,1}}{N}\frac{N^{1-\theta}}{\theta-1}\Big(\frac{t_s}{\Delta t}\Big)^{\theta}\Big\{(t_q)^{2-\theta} + (1-t_q)(t_q+1)^{1-\theta}\Big\}. \end{aligned} \tag{3.43}$$

State 1

The expectation of the duration of the state S_1 in the frequency domain can be expressed as

$$\begin{aligned}\mathcal{E}[D_{S_1,k}] &= \sum_{D=0}^{\infty} Dp(D|S_1) \\ &= Dp(D|S_1)\big|_{D=1} + \sum_{D=2}^{\infty} Dp(D|S_1) \\ &= \mathcal{B}(B, v_1, t_1) + \mathcal{B}(1-B, v_2, t_2) + B \cdot Q\Big(\frac{\ln\left(\frac{N\Delta t}{t_1}\right)}{v_1}\Big) \\ &\quad + (1-B) \cdot Q\Big(\frac{\ln\left(\frac{N\Delta t}{t_2}\right)}{v_2}\Big) + \frac{B}{N}\frac{t_1}{\Delta t}\exp\left(\frac{v_1^2}{2}\right)\Big\{2 - Q\Big(\frac{\ln\left(\frac{N\Delta t}{t_1}\right)}{v_1} - v_1\Big)\Big\} \\ &\quad + \frac{1-B}{N}\frac{t_2}{\Delta t}\exp\left(\frac{v_2^2}{2}\right)\Big\{2 - Q\Big(\frac{\ln\left(\frac{N\Delta t}{t_2}\right)}{v_2} - v_2\Big)\Big\}.\end{aligned} \tag{3.44}$$

3.7.4 $p(n_I)$ Study

$n_I = 0$

When the number samples in a DMT symbol at state s_1 is 0, we can say that this symbol is in the state S_0. Therefore, we have

$$p(n_I) = P(S_0|\boldsymbol{Y}) = \frac{\mathcal{E}[D_{S_0,k}]}{\mathcal{E}[D_{S_0,k}] + \mathcal{E}[D_{S_1,k}]},\ n_I = 0, \tag{3.45}$$

where $\mathcal{E}[D_{S_0,k}]$ and $\mathcal{E}[D_{S_1,k}]$ can be calculated according to Appendix C.

$n_I = 1, 2, \ldots, N-1$

The scenario of $n_I = 1, 2, \ldots, N-1$ is discussed for two specific cases. The first case is when D, namely the number of successive DMT symbols in the state S_1, is larger than 1. In this case, $n_I = 1, 2, \ldots, N-1$ occurs at three locations: 1) as shown in Fig. 3.9a, the first and the final symbols of the string of symbols in each state S_1 where $D \geq 3$ and the η values are not 0 for the state S_1 and the next state; 2) as shown in Fig. 3.9b, the first symbol in the each state S_1 where $D \geq 2$ and η value is not 0 for the state S_1 while η value is 0 for the next state; 3) as shown in Fig. 3.9c, the final symbol in each state S_1 where $D \geq 2$ and η value is 0 for the state S_1 while η value is not 0 for the next state;

$$\begin{aligned}\Pr_1(1 \le n_I \le N-1) = &\sum_{D=3}^{\infty} \frac{2}{D} P(D, S_1|\boldsymbol{\Upsilon}) \Big(\frac{N-1}{N}\Big)^2 \\ &+ \sum_{D=2}^{\infty} \frac{1}{D} P(D, S_1|\boldsymbol{\Upsilon}) \frac{1}{N} \frac{N-1}{N} \\ &+ \sum_{D=2}^{\infty} \frac{1}{D} P(D, S_1|\boldsymbol{\Upsilon}) \frac{1}{N} \frac{N-1}{N}. \end{aligned} \tag{3.46}$$

In this case, we have $n_I = (N - \eta)$ and η value yields to the uniform distribution. Therefore, the probability of n_I as one of the element in $n_I = 1, 2, \ldots, N-1$ is $(\frac{1}{N-1})$. Consequently, the probability of $n_I = 1, 2, \ldots, N-1$ in this case is given by

$$P_1(n_I) = \frac{1}{N-1} \Pr_1(1 \le n_I \le N-1). \tag{3.47}$$

The second case is $D = 1$ while $1 \le n_I \le N-1$. This case can be treated as a state s_1 with the duration $d = n_I$. In order to ensure $D = 1$, the η value has to be within the range $[0, N - n_I + 1]$, with the probability as $(\frac{N-n_I+1}{N})$ for each possible η value. Then, we have

$$P_2(n_I) = \frac{\mathcal{E}[D_{S_1,k}]}{\mathcal{E}[D_{S_0,k}] + \mathcal{E}[D_{S_1,k}]} \frac{N - n_I + 1}{N} p(n_I|s_1). \tag{3.48}$$

Therefore, the probability of $n_I = 1, 2, \ldots, N-1$ can be expressed as

$$\begin{aligned} P(n_I) &= P_1(n_I) + P_2(n_I) \\ &= \mathcal{D}_1(n_I, B, v_1, t_1) + \mathcal{D}_1(n_I, 1-B, v_2, t_2), \end{aligned} \tag{3.49}$$

for $n_I = 1, 2, \ldots, N-1$, where $\mathcal{D}_1(\cdot)$ is expressed as

$$\begin{aligned} &\mathcal{D}_1(n_I, B, v_1, t_1) \\ &= \frac{N-1}{N^2} \frac{2B}{\mathcal{E}[n_{S_0,k}] + \mathcal{E}[n_{S_1,k}]} \Bigg\{ -Q\Bigg(\frac{\ln\left(\frac{N\Delta t}{t_1}\right)}{v_1}\Bigg) + 2Q\Bigg(\frac{\ln\left(\frac{2N\Delta t}{t_1}\right)}{v_1}\Bigg) \\ &\quad + \frac{t_1}{\Delta t} \exp\left(\frac{v_1^2}{2}\right) \frac{1}{N} \Bigg[Q\Bigg(\frac{\ln\left(\frac{N\Delta t}{t_1}\right)}{v_1} - v_1\Bigg) - Q\Bigg(\frac{\ln\left(\frac{2N\Delta t}{t_1}\right)}{v_1} - v_1\Bigg) \Bigg] \Bigg\} \\ &\quad + \frac{1}{N^2} \frac{2B}{\mathcal{E}[n_{S_0,k}] + \mathcal{E}[n_{S_1,k}]} \Bigg\{ Q\Bigg(\frac{\ln\left(\frac{N\Delta t}{t_1}\right)}{v_1}\Bigg) + \frac{t_1}{\Delta t} \exp\left(\frac{v_1^2}{2}\right) \frac{1}{N} \Bigg[1 - Q\Bigg(\frac{\ln\left(\frac{N\Delta t}{t_1}\right)}{v_1} - v_1\Bigg) \Bigg] \Bigg\} \\ &\quad + \frac{\mathcal{E}[n_{S_1,k}]}{\mathcal{E}[n_{S_0,k}] + \mathcal{E}[n_{S_1,k}]} \frac{N - n_I + 1}{N} \Bigg\{ B \Bigg[Q\Bigg(\frac{\ln(\frac{(n_I-0.5)\Delta t}{t_1})}{v_1}\Bigg) - Q\Bigg(\frac{\ln(\frac{(n_I+0.5)\Delta t}{t_1})}{v_1}\Bigg) \Bigg] \Bigg\}. \end{aligned} \tag{3.50}$$

$n_I = N$

This situation occurs at four locations: 1) as shown in Fig. 3.9a, the symbols which are not at the first and final symbols in each state S_1 where $D \geq 3$ and the η values are not 0 for the state S_1 and next state; 2) as shown in Fig. 3.9b, the symbols which are not the first symbol in each state S_1 where $D \geq 2$ and η value is not 0 for the state S_1 while η value is 0 for the next state; 3) as shown in Fig. 3.9c, the symbols which are not the final symbol of each state S_1 where $D \geq 2$ and η value is 0 for the state S_1 while η value is not 0 for the next state; 4) as shown in Fig. 3.9d, all the symbols where $D \geq 1$ and η values are 0 for the state S_1 and the next state. Therefore, $p(n_I)$ can be expressed in (3.51),

$$\begin{aligned}
P(n_I) &= \sum_{D=3}^{\infty} \frac{D-2}{D} P(D, S_1|\boldsymbol{\Upsilon}) \frac{N-1}{N} \frac{N-1}{N} + \sum_{D=2}^{\infty} \frac{D-1}{D} P(D, S_1|\boldsymbol{\Upsilon}) \frac{N-1}{N} \frac{1}{N} \\
&\quad + \sum_{D=2}^{\infty} \frac{D-1}{D} P(D, S_1|\boldsymbol{\Upsilon}) \frac{1}{N} \frac{N-1}{N} + \sum_{D=1}^{\infty} P(D, S_1|\boldsymbol{\Upsilon}) \frac{1}{N} \frac{1}{N} \\
&= \frac{(N-1)^2}{N^2} \frac{1}{\mathcal{E}[D_{S_0,k}] + \mathcal{E}[D_{S_1,k}]} \Big\{ \sum_{D=3}^{\infty} D p(D|S_1) - 2 \sum_{D=3}^{\infty} p(D|S_1) \Big\} \\
&\quad + \frac{2(N-1)}{N^2} \frac{1}{\mathcal{E}[D_{S_0,k}] + \mathcal{E}[D_{S_1,k}]} \Big\{ \sum_{D=2}^{\infty} D p(D|S_1) - \sum_{D=2}^{\infty} p(D|S_1) \Big\} \\
&\quad + \frac{1}{N^2} \frac{1}{\mathcal{E}[D_{S_0,k}] + \mathcal{E}[D_{S_1,k}]} \Big\{ \sum_{D=1}^{\infty} D p(D|S_1) \Big\} \\
&= \mathcal{D}_2(B, v_1, t_1) + \mathcal{D}_2(1-B, v_2, t_2), \quad \text{for } n_I = N.
\end{aligned} \tag{3.51}$$

where $\mathcal{D}_2(\cdot)$ is expressed as

$$\begin{aligned}
&\mathcal{D}_2(B, v_1, t_1) \\
&= \frac{(N-1)^2}{N^2} \frac{B}{\mathcal{E}[D_{S_0,k}] + \mathcal{E}[D_{S_1,k}]} \Big\{ -Q\Big(\frac{\ln\left(\frac{N\Delta t}{t_1}\right)}{v_1}\Big) + \frac{1}{N} \frac{t_1}{\Delta t} \exp\left(\frac{v_1^2}{2}\right) Q\Big(\frac{\ln\left(\frac{N\Delta t}{t_1}\right)}{v_1} - v_1\Big) \Big\} \\
&+ \frac{2(N-1)}{N^2} \frac{B}{\mathcal{E}[D_{S_0,k}] + \mathcal{E}[D_{S_1,k}]} \Big\{ \frac{1}{N} \frac{t_1}{\Delta t} \exp\left(\frac{v_1^2}{2}\right) \Big\} \\
&+ \frac{1}{N^2} \frac{B}{\mathcal{E}[D_{S_0,k}] + \mathcal{E}[D_{S_1,k}]} \Big\{ Q\Big(\frac{\ln\left(\frac{0.5\Delta t}{t_1}\right)}{v_1}\Big) - \frac{1}{N} Q\Big(\frac{\ln\left(\frac{(N+0.5)\Delta t}{t_1}\right)}{v_1}\Big) \\
&- \frac{1}{N} \Big[(N-0.5) Q\Big(\frac{\ln\left(\frac{(N-0.5)\Delta t}{t_1}\right)}{v_1}\Big) - \frac{t_1}{\Delta t} \exp\left(\frac{v_1^2}{2}\right) Q\Big(\frac{\ln\left(\frac{(N-0.5)\Delta t}{t_1}\right)}{v_1} - v_1\Big) \\
&- 1.5 Q\Big(\frac{\ln\left(\frac{1.5\Delta t}{t_1}\right)}{v_1}\Big) + \frac{t_1}{\Delta t} \exp\left(\frac{v_1^2}{2}\right) Q\Big(\frac{\ln\left(\frac{1.5\Delta t}{t_1}\right)}{v_1} - v_1\Big) \Big] \\
&+ Q\Big(\frac{\ln\left(\frac{N\Delta t}{t_1}\right)}{v_1}\Big) + \frac{1}{N} \frac{t_1}{\Delta t} \exp\left(\frac{v_1^2}{2}\right) \Big[2 - Q\Big(\frac{\ln\left(\frac{2N\Delta t}{t_1}\right)}{v_1} - v_1\Big) \Big] \Big\}.
\end{aligned} \tag{3.52}$$

Chapter 4

Performance of HARQ-Assisted OFDM Systems Contaminated by Impulsive Noise: Finite-Length LDPC Code Analysis

As a benefit of their iterative decoding structure, LDPC codes [16] are capable of achieving a near-capacity performance and are expected to be employed in next-generation of DSL systems, in cooperation with Hybrid Automatic Repeat reQuest (HARQ). This system configuration is expected to be eminently suitable for impulsive noise environments in the random event, when a packet cannot be successfully received due to the occurrence of an impulsive noise event, the transmitter will re-send the packet until it is correctly received. The benefit of this design philosophy is that the sophisticated HARQ mentioned is only activated, when it is required, because the channel coding mechanism was overwhelmed by a large noise impulse. This sophisticated design philosophy is attractive owing involving just sufficient redundancy and due to its controlled delay. Hence in this chapter, we analyze the performance of LDPC-coded HARQ schemes, in terms of its outage probability, number of retransmissions and effective throughput, in a practical finite block-length regime. This quantitative analysis enables us to examine the performance of HARQ schemes in the face of the impulsive noise.

4.1 Introduction

In order to alleviate the detrimental influence of impulsive noise, a plethora of schemes discussed in Section 1.4 have been proposed both for the transmitter and receiver. Specifically, at the transmitter side, both channel coding [51] and interleaving [67] as well as

ARQ [73] may be involved.

In this chapter, we focus our attention on the impulsive noise mitigation techniques applicable to the transmitter side, from the perspective of HARQ. Although it was originally designed for the MAC layer, ARQ can also be combined with channel coding in the physical layer, reaching to the concept of HARQ, which is classified into conventional HARQ [77], Chase-combining aided HARQ [78] and incremental-redundancy assisted HARQ [79]. More explicitly, as shown in Fig. 1.9a, conventional HARQ relies on the same principle as ARQ. As depicted in Fig. 1.9b, the most recently received packet is jointly detected with the previously received copies in the context of Chase-combining aided HARQ. As seen in Fig. 1.9c , additional parity is transmitted for each transmission attempt in incremental-redundancy assisted HARQ. Typically, once a packet is corrupted, additional redundancy is requested for joint decoding at the receiver. In the literature, HARQ has been widely investigated in non-static channels from the aspect of information theory [175–177] or code design [178–180]. However, the analysis of HARQ-assisted systems in impulsive noise environments is still in its infancy.

LDPC codes have been considered to be a potent candidate for next-generation DSL systems, as a benefit of their near-capacity performance and low-complexity parallel decoding structure. In order to analyse the performance of LDPC codes, Richardson *et al.* proposed the density evolution (DE) concept [181], which is an analytical tool conceived for characterizing the performance of LDPC codes by evaluating the PDF of the LLRs during the iterations between the variable nodes and check nodes. To further extend the performance analysis of LDPC codes, Yazdani *et al.* conceived the waterfall performance analysis concept [182]. However, unfortunately this approach cannot be directly utilized in our system, because it assumes that the noise variance is constant.

Against this background, we analyze the performance of LDPC-coded HARQ-assisted OFDM systems contaminated by impulsive noise in terms of their outage probability, the average number of retransmission attempts and the effective throughput. The main contributions are summarized as follows.

- We conceive an LDPC-coded HARQ-assisted OFDM system for communications in impulsive noise environments. Specifically, we design a soft demodulator, which is intrinsically amalgamated with our Type-II HARQ scheme for operation in hostile impulsive noise environments.

- We then propose a methodology for analyzing the outage probability, the average number of transmissions and the effective throughput of our system, in a realistic finite-length codeword regime. Specifically, as for the outage probability analysis, we modify the DE concept for determining the LDPC codes's waterfall performance SNR and then extend our solution to the finite-length LDPC regime. In order to

characterize the error floor of our system, we propose an algorithm for calculating the outage probability of our system.

- We verify the accuracy of the proposed analysis technique through extensive simulation results for further quantifying the impact of impulsive noise on our LDPC-coded HARQ-assisted OFDM system.

The chapter is organized as follows. The system model and noise model are described in Section 4.2. Then the outage probability is analyzed mathematically and verified experimentally in Section 4.3. In Section 4.4, both the average number of retransmissions and the effective throughput are quantified. Finally, we present conclusions in Section 4.5.

4.2 System Description

As mentioned in Section 4.1, HARQ schemes are generally categorized into three types. Specifically, the Type-I and Type-II HARQ schemes have a wide range of applications in diverse systems owing to their constructional simplicity [20, 74–76]. Therefore, this chapter focuses on the analysis of Type-I and Type-II HARQ schemes. In this section, we describe the general LDPC-coded OFDM systems, the noise model and the pair of considered retransmission schemes considered.

4.2.1 LDPC-Coded OFDM Systems

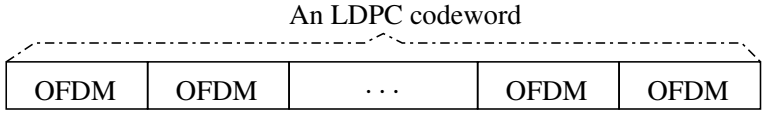

Figure 4.1: An LDPC codeword is comprised of L_B OFDM symbols, each of which conveys M subcarriers.

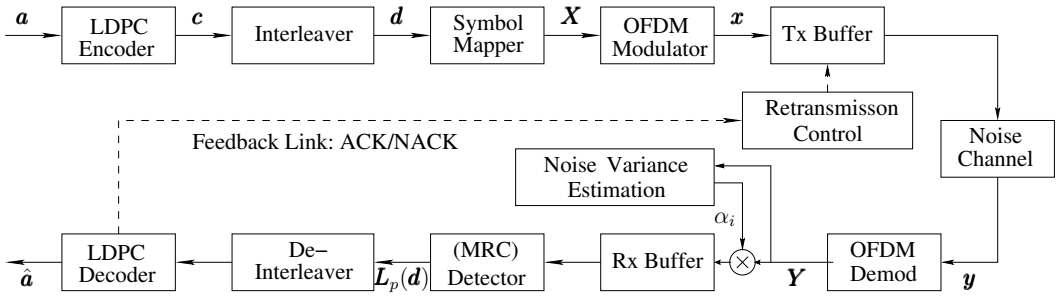

Figure 4.2: Illustration of the structure of HARQ-assisted LDPC-coded OFDM systems in impulsive noise environments.

Transmitter

As illustrated in Fig. 4.1, we consider an LDPC-coded OFDM system, where an LDPC codeword spans over L_B OFDM symbols, whereas an OFDM symbol consists of M subcarriers. More explicitly, as shown in Fig. 5.1, a bit sequence denoted by $\boldsymbol{a}$ and having the elements $a \in \{0,1\}$ is encoded by an LDPC encoder, leading to the sequence $\boldsymbol{c}$. The interleaved bits denoted by $\boldsymbol{d}$ are mapped to a particular constellation, e.g. BPSK, having the alphabet $\boldsymbol{\mathcal{X}}$ in the modulator, resulting in samples denoted by $\boldsymbol{X} = [\boldsymbol{X}_1, \boldsymbol{X}_2, \cdots, \boldsymbol{X}_{L_B}]$. Each element is processed by an OFDM modulator and we denote the l_B $^{\text{th}}$ OFDM symbol obtained in the time-domain by $\boldsymbol{x}_{l_B}$, where we have $l_B \in [1, L_B]$. For simplicity, we omit the process of adding a cyclic prefix. The signals are processed with the aid of channel inversion based frequency-domain equalization to compensate for the dispersive channel impulse response and then passed through the channel. The received signal is contaminated by both the time-domain background and impulsive noise denoted by $\boldsymbol{n}_{l_B}$. Then, the received signals is expressed as:

$$\boldsymbol{y}_{l_B} = \sqrt{\rho}\boldsymbol{x}_{l_B} + \boldsymbol{n}_{l_B}, \tag{4.1}$$

where ρ is the power of received signals, while $\boldsymbol{y}_{l_B}, \boldsymbol{x}_{l_B}, \boldsymbol{n}_{l_B}$ are vectors having the dimension of M.

Noise Model

Again, we consider both the background noise and impulsive noise. The background noise is modelled by an Additive White Gaussian Noise (AWGN) process [183]. As for the impulsive noise, it generally consists of short pulses, whose amplitude, duration and arrival time are all random variables. The amplitude is mainly modelled by either Gaussian [184] or Middleton's Class A [185] or alternatively Weibull PDFs [42]. The main models routinely used for the impulse duration are either the partitioned Markov Chain (PMC) [146] or the log-normal PDFs [42]. The common distribution of the arrival time is typically modelled by PMC [146], Poisson [186] and gated Bernoulli-Gaussian (GBG) PDFs [137].

Bearing both the analytical tractability and empirical characteristics in mind, in this treatise the bursty GBG model is invoked for representing the noise process. To elaborate, gated Bernoulli-Gaussian is widely adopted in the literature [137, 187], where the IN is modelled as a sequence of independent, Bernoulli distributed pulses, each of whose width exactly covers the duration of a single time-domain OFDM sample. However, the disadvantage of the GBG model is its inability to reflect the bursty nature of impulsive noise. To overcome this shortcoming, here the impulsive noise is modelled using the bursty GBG model of [188]. Specifically, the impulsive noise process consists of a sequence of in-

dependent bursts, each of which is constituted by M pulses. In this case, any impulsive noise burst may contaminate an OFDM symbol. Here let us denote the background noise component without impulsive noise by $\boldsymbol{w}_{l_B}$ and the noise component containing both the background and impulsive noise by $\boldsymbol{i}_{l_B}$. Then, the total received noise is expressed as $\boldsymbol{n}_{l_B} = (1-b)\boldsymbol{w}_{l_B} + b\boldsymbol{i}_{l_B}$, where $\boldsymbol{w}_{l_B}$ and $\boldsymbol{i}_{l_B}$ are complex-valued Gaussian vectors of the dimension of M, while the binary flag of $b \in \{0,1\}$ is used to specify the presence or absence of impulsive noise. More particularly, $p_i = \Pr(b=1)$ is the probability of impulsive noise occurrence. Let us furthermore denote the variance of $\boldsymbol{w}_{l_B}$ and $\boldsymbol{i}_{l_B}$ by σ_w^2 and σ_i^2, respectively, whilst representing the ratio between σ_i^2 and σ_w^2 by $\kappa = \sigma_i^2/\sigma_w^2$.

Receiver

Equipped with the DFT-based OFDM demodulator at the receiver, both the received signal and the noise are transformed to the frequency domain. Then, the resultant signal is formulated as

$$\boldsymbol{Y}_{l_B} = \sqrt{\rho}\boldsymbol{X}_{l_B} + \boldsymbol{N}_{l_B}, \tag{4.2}$$

where $\boldsymbol{Y}_{l_B}$, $\boldsymbol{X}_{l_B}$ and $\boldsymbol{N}_{l_B}$ are the complex-valued vectors with the dimension of M. Let us denote the variance of the noise in an OFDM symbol by σ_N^2. Since the DFT is a linear operation, we have $\sigma_N^2 = (1-b)\sigma_w^2 + b\sigma_i^2$. Here we assume that the binary flag b, which indicates the presence or absence of impulsive noise, can be perfectly estimated at the receiver side and σ_N^2 is then fed to the symbol detector.

4.2.2 Type-I HARQ-Assisted LDPC-Coded Scheme

In the Type-I HARQ-assisted scheme, if an LDPC codeword is correctly received, an ACK flag is fed back to the transmitter, which triggers the transmission of the next packet. However, if any of the LDPC codewords is unsuccessfully decoded, the received codeword is discarded and a NACK flag is sent back, which triggers the retransmission of the original packet. This retransmission process continues until either the packet is correctly received or the maximum number of transmissions is reached. If the LDPC codeword still remains corrupted, the packet is discarded and then an outage event is reported. This loss of the packet can be solved by ARQ in the upper radio link layer. Let us denote the maximum number of transmission rounds by T. Then the t^{th} received copy of the ${l_B}^{\text{th}}$ OFDM symbol is expressed as:

$$\boldsymbol{Y}_{l_B,t} = \sqrt{\rho}\boldsymbol{X}_{l_B} + \boldsymbol{N}_{l_B,t}, \tag{4.3}$$

where we have $t \in [1,T]$ and $l_B = [1,L_B]$.

4.2.3 Type-II HARQ-Assisted LDPC-Coded Scheme

In contrast to the Type-I HARQ-assisted scheme, the Type-II HARQ-aided arrangement saves the unsuccessfully decoded OFDM symbols and combines them with the newly received copy for joint detection and decoding. Similarly, if the packet is still detected with errors when the maximum number of transmissions is reached, an outage is reported. Note that the retransmissions take place on the basis of LDPC codewords, while the received symbol combining is carried out on the basis of OFDM symbols. Let us denote the noise variance of the $l_B{}^{\text{th}}$ OFDM symbol at the t^{th} ARQ transmission attempt by $\sigma^2_{l_B,t}$. The copies of an OFDM symbol are then multiplied by the weights of $\alpha_{l_B,t} = \sqrt{\rho}/\sigma^2_{l_B,t}$ and summed together based on the MRC principle as [189]:

$$\begin{aligned}\boldsymbol{Y}_{l_B} &= \sum_t \alpha_{l_B,t}\boldsymbol{Y}_{l_B,t} = \sum_t \frac{\sqrt{\rho}}{\sigma^2_{l_B,t}}(\sqrt{\rho}\boldsymbol{X}_{l_B} + \boldsymbol{N}_{l_B,t}) \\ &= \sum_t \frac{\rho}{\sigma^2_{l_B,t}}\boldsymbol{X}_{l_B} + \sum_t \frac{\sqrt{\rho}}{\sigma^2_{l_B,t}}N_{l_B,t}. \end{aligned} \tag{4.4}$$

The noise variance associated with the combined $l_B{}^{\text{th}}$ OFDM symbol at the output of the MRC detector is expressed as:

$$\overline{\sigma}^2_{l_B} = \mathbb{E}\left[\left(\sum_t \frac{\sqrt{\rho}}{\sigma^2_{l_B,t}}N_{l_B,t}\right)^2\right] = \sum_t \frac{\rho}{\sigma^2_{l_B,t}}. \tag{4.5}$$

It can be readily seen from (4.4) and (4.5) that the signal-to-noise ratio (SNR) of the combined copies becomes $\gamma_{l_B} = \sum_t \gamma_{l_B,t}$, where $\gamma_{l_B,t}$ is the SNR of the t^{th} copy of the $l_B{}^{\text{th}}$ OFDM symbol. Here we denote the frequency-domain sample on the m^{th} subcarrier of the OFDM symbol $\boldsymbol{X}_{l_B}$ by $X_{l_B,m}$, which is assumed to be independent of all other samples for soft demodulation, yielding

$$p(Y_{l_B,m}|X_{l_B,m}) = \frac{1}{\pi\sum_t \frac{\rho}{\sigma^2_{l_B,t}}} \times \exp\left(-\frac{Y_{l_B,m} - \left(\sum_t \frac{\rho}{\sigma^2_{l_B,t}}\right)X_{l_B,m}}{\sum_t \frac{\rho}{\sigma^2_{l_B,t}}}\right). \tag{4.6}$$

Then the *a posteriori* LLRs gleaned from the MRC detector are calculated as:

$$L_p(d(k)) = \ln\frac{\sum_{\forall X_{l_B,m}\in\boldsymbol{\mathcal{X}}_{d_k=1}} p(Y_{l_B,m}|X_{l_B,m})p(X_{l_B,m})}{\sum_{\forall X_{l_B,m}\in\boldsymbol{\mathcal{X}}_{d_k=0}} p(Y_{l_B,m}|X_{l_B,m})p(X_{l_B,m})},$$

where $\boldsymbol{\mathcal{X}}_{d_k=1}$ and $\boldsymbol{\mathcal{X}}_{d_k=0}$ denote the BPSK subsets, when the specific bit $\boldsymbol{d}_k$ is fixed to 1 and 0, respectively.

4.3 Outage Probability Analysis

In order to characterize the reliability of our HARQ-assisted LDPC-coded systems in impulsive noise environments, in this section we analyze their outage probability, namely the probability that a packet is unsuccessfully decoded within the maximum affordable number of transmissions. Specifically, we briefly review the concept of DE and waterfall-SNR analysis. Then, we appropriately adapt DE and extend the waterfall-SNR analysis concept for impulsive noise environments. Furthermore, we propose a specific algorithm for determining the outage probability versus the SNR for the pair of HARQ transmission schemes considered. Finally, our analytical and experimental results are presented.

4.3.1 Block Error Rate of Finite-Length LDPC Codes

The development of DE [181, 190] and of waterfall-SNR analysis [182] facilitates the block error rate (BLER) analysis of finite-length LDPC codes. More explicitly, DE can be used for determining the SNR threshold to be satisfied for achieving correct decoding, by evaluating the PDF of the LLRs during the decoding iterations between variable and check nodes. Based on the result of DE, the waterfall-SNR analysis is capable of providing a BLER approximation for finite-length LDPC codes. In the rest, we will briefly introduce the original DE and waterfall-SNR philosophy in the absence of impulsive noise and then present numerical results for characterizing the associated accuracy.

Density Evolution

In AWGN channels associated with a noise variance of σ^2, the LLRs output by a soft detector typically obey the classic Gaussian distribution having the mean of $2/\sigma^2$ and the variance of $4/\sigma^2$. Hence, the initial PDF of the LLRs forwarded to the variable node of the LDPC decoder can be expressed as:

$$f_v^{(0)}(LLR) = \mathcal{N}\Big(\frac{2}{\sigma^2}, \frac{4}{\sigma^2}\Big), \tag{4.7}$$

where $f_v^{(0)}(LLR)$ denotes the PDF of the input LLRs forwarded to the variable nodes (VN) of the LDPC decoder, when the iteration index is $l = 0$. Let us denote the PDF of the LLRs forwarded to a check node (CN) of the LDPC decoder at the l-th iteration by $f_u^{(l)}(LLR)$. The density evolution observed at the check and variable nodes is iteratively updated, respectively, as follows [191]:

$$f_u^{(l)}(LLR) = \Lambda^{-1}\left[\sum_{i=1}^{d_c-1} \mu_i\Big(\Lambda\big[f_v^{(l-1)}(LLR)\big]^{\otimes(i-1)}\Big)\right], \tag{4.8}$$

$$f_v^{(l)}(LLR) = f_v^{(0)}(LLR) \otimes \sum_{i=1}^{d_v-1} \lambda_i \Big(f_u^{(l)}(LLR) \Big)^{\otimes(i-1)}, \tag{4.9}$$

where d_v and d_c denote the number of neighbors of a variable node and a check node, respectively. Furthermore, λ_i and μ_i are the fractions of edges belonging to the degree-i variable and check nodes, respectively, while $\Lambda[\cdot]$ and $\Lambda^{-1}[\cdot]$ represent the changes of density due to the transformations of $g(\cdot)$ and $g^{-1}(\cdot)$, respectively, where $g(\cdot) = [\text{sign}(\cdot), \ln\coth([\cdot/2])]$. Moreover, $\otimes$ represents convolution. Assuming that the all-zero codeword ($x = +1$) is transmitted, the error probability after l iterations denoted by $P_b^{(l)}$ can be expressed as [181]:

$$P_b^{(l)} = \int_{-\infty}^{0} f_v^l(x) \mathrm{d}x. \tag{4.10}$$

With the aid of (4.7), (4.8), (4.9) and (4.10), we may search all possible values of σ^2 for obtaining the threshold value, when $P_b^{(l)}$ converges to zero as the number of iterations tends to infinity. Let us denote the threshold value by σ_{th}^2, yielding:

$$\sigma_{\text{th}}^2 = \sup\left\{\sigma^2 : \lim_{l\to\infty} P_b^l(\sigma^2) = 0\right\}. \tag{4.11}$$

Here the threshold σ_{th}^2 obtained from (4.11) represents the waterfall-SNR value for infinite-length LDPC codes. However, the waterfall-SNR is higher for the finite-length LDPC codes. Based on the result of DE, let us now discuss the BLER analysis of finite-length LDPC codes.

Waterfall Performance Analysis

For an LDPC codeword having the length of L and the threshold noise variance of σ_{th}^2, the average number of correctable bit errors can be approximated by $E_{\text{th}} = L \times Q(1/\sigma_{\text{th}})$ for a binary input AWGN channel [182], where $Q(\cdot)$ is the Gaussian Q-function. In this case, the BLER can be obtained by comparing E_{th} to the PDF of the actual number of bit errors, denoted by E_{obs}. More explicitly, given a binary-input AWGN channel having a noise variance of σ^2, its BER can be calculated as $P_b = Q(1/\sigma)$, while the PDF of E_{obs} associated with an LDPC codeword length of L can be formulated in a binomial form as:

$$f_{E_{\text{obs}}} = \binom{L}{E_{\text{obs}}} P_b^{E_{\text{obs}}} (1-P_b)^{L-E_{\text{obs}}}. \tag{4.12}$$

Given a specific value of L of our interest, the binomial form of (4.12) can be accurately approximated by the Gaussian distribution, i.e. we have $\mathcal{N}\left[LP_b, LP_b(1-P_b)\right]$. Accord-

ingly, the BLER denoted by P_B associated with L is readily expressed as:

$$P_B(L) = Q\left(\frac{1}{\sqrt{LP_b(1-P_b)}}\left(E_{\text{th}} - LP_b\right)\right). \tag{4.13}$$

Numerical Results

Table 4.1: Parameter configuration of LDPC codes

Description	Value or algorithm
Number of neighbors of a variable node	$d_v = 3$
Number of neighbors of a check node	$d_c = 6$
Number of decoding iterations	50
Decoding algorithm	Sum-product algorithm

Fig. 4.3 presents the BLER of finite-length LDPC codes in the context of BPSK-modulated systems communicating over AWGN channels. Specifically, the $1/2$-rate (3,6)-regular LDPC codes configured by Table 4.1 is used as an example. Three observations can be inferred from the figure. Firstly, the finite-length performance analysis provides a very close match to the simulations. Specifically, the SNR gap between the theoretical analysis and simulation results is within 0.1dB when $L = 2048$, and it becomes even more accurate when L reaches 6144 or higher values. Secondly, the finite-length performance analysis usually provides an under-estimated BLER prediction for LDPC codes, because of the difference between the accurate binomial form of (4.12) and the approximate Gaussian distribution invoked in (4.13). Thirdly, as expected, the BLER performance is improved upon increasing the codeword length. This also demonstrates the importance of finite-length LDPC code analysis.

4.3.2 Outage Probability Analysis in the Face of Impulsive Noise

Again, the occurrence of impulsive noise changes the distribution of the LLR input to the LDPC decoder, which profoundly influences the BLER of the LDPC codes. In this subsection, we modify the DE and the waterfall-SNR analysis, in order to facilitate the analysis in an impulsive noise environment. In order to present the outage probability caused by impulsive noise, we propose a specific algorithm for calculating the outage of LDPC-coded OFDM systems and then extend it to the Type-I and Type-II HARQ schemes.

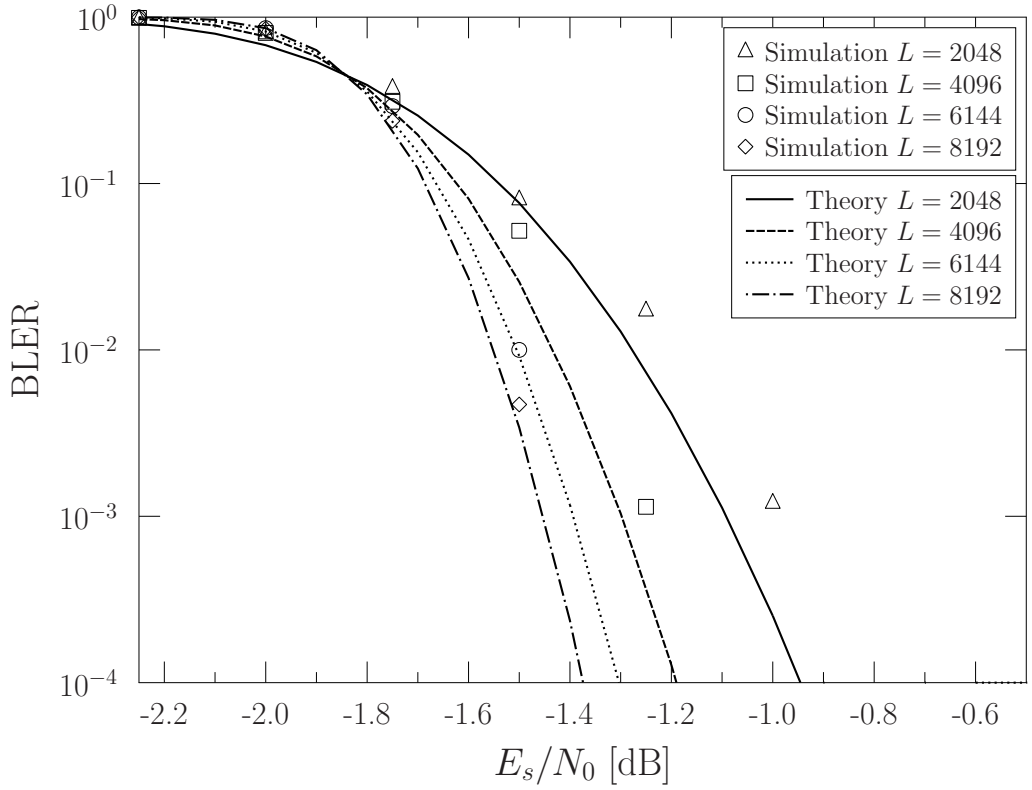

Figure 4.3: BLER of finite-length LDPC codes under various codeword lengths in AWGN channel. The $1/2$-rate (3,6)-regular LDPC codes configured by Table 4.1 is opted for example while BPSK is adopted as the mapping scheme. The theoretical results are calculated according to (4.13).

BLER of Coded OFDM Systems Inflicting IN

Since the channel-induced erroneous transmissions have to be symmetric for accurate DE [190], we have to prove that the channel noise is indeed symmetric in our system, which is seen as follows:

$$\begin{aligned} P(y|x=1) &= \frac{1-p_i}{\sqrt{2\pi\sigma_w^2}} \exp\left(-\frac{(y-1)^2}{2\sigma_w^2}\right) + \frac{p_i}{\sqrt{2\pi\sigma_i^2}} \exp\left(-\frac{(y-1)^2}{2\sigma_i^2}\right) \\ &= \frac{1-p_i}{\sqrt{2\pi\sigma_w^2}} \exp\left(-\frac{(-y+1)^2}{2\sigma_w^2}\right) + \frac{p_i}{\sqrt{2\pi\sigma_i^2}} \exp\left(-\frac{(-y+1)^2}{2\sigma_i^2}\right) \\ &= P(-y|x=-1). \end{aligned} \tag{4.14}$$

Since an LDPC codeword conveys L_B OFDM symbols, the impulsive noise corrupting an LDPC codeword may contaminate several OFDM symbols. The distribution of the initial LLRs depends on the number of impulsive-noise-infested OFDM symbols in an LDPC codeword. More explicitly, if the number of contaminated OFDM symbols is low in a long LDPC codeword, then the average initial LLRs become high and hence the LDPC codeword has a high probability of being correctly decoded. Let us denote the number of

error-infested OFDM symbols in an LDPC codeword by L_I, where we have $L_I \in [0, L_B]$. Then, the initial PDF of the LLRs gleaned from the detector and characterized in (4.7) can be reformulated as a superposition, which is a function of L_I, formulated as:

$$f_v^{(o)}(L_I) = (L_B - L_I)\mathcal{N}\Big(\frac{2}{\sigma_w^2}, \frac{4}{\sigma_w^2}\Big) + L_I\mathcal{N}\Big(\frac{2}{\sigma_i^2}, \frac{4}{\sigma_i^2}\Big). \tag{4.15}$$

The PDF of the LLRs is iteratively updated with the aid of (4.8) and (4.9). Then, the noise threshold of the channel below which error-free decoding becomes possible can be obtained with the aid of (4.10) and $\sigma_{\text{th}}^2 = \sup\{\sigma_w^2 : \lim_{l\to\infty} P_b^l(\sigma_w^2) = 0\}$. To elaborate a little further, we use the background noise to represent the channel's noise threshold, while we represent the relationship between the background and impulsive noise using $\kappa = \sigma_i^2/\sigma_w^2$.

Given the knowledge of the above noise threshold, we now extend the waterfall-SNR analysis to our impulsive noise environment. As observed in Fig. 4.3, the gap between two curves becomes smaller upon increasing the LDPC codeword length. Therefore, we use the relationship between E_{th} and E_{obs} in the OFDM symbols not infested by impulsive noise to approximate the overall BLER within an LDPC codeword containing L_B OFDM symbols, because the number of uncontaminated OFDM symbols is usually higher than the number of the symbols corrupted. For an LDPC codeword spanning L_B OFDM symbols having M subcarriers, when L_I symbols are corrupted by IN, the PDF of E_{obs} can be expressed in a similar form to (4.12) upon replacing L by $M(L_B - L_I)$, yielding

$$f_{E_{\text{obs}}}(L_I) = \binom{M(L_B - L_I)}{E_{\text{obs}}} \big(P_b\big)^{E_{\text{obs}}} \big(1 - P_b\big)^{L - E_{\text{obs}}}, \tag{4.16}$$

which can be approximated by the Gaussian distribution and then the BLER associated with L_I can be formulated as:

$$P_B(L_I) \approx Q\Bigg(\frac{1}{\sqrt{M(L_B - L_I)P_b(1 - P_b)}}\big(E_{\text{th}} - M(L_B - L_I)P_b\big)\Bigg), \tag{4.17}$$

where we have $E_{\text{th}} = M(L_B - L_I)Q(1/\sigma_{\text{th}})$.

In order to combine the analytical results associated with different values of L_I, we propose a convenient algorithm. Before explicitly outlining the algorithm, we have to make an observation. As detailed in Chapter 3 and [192], bit error floors exist in impulsive noise environments, which are determined by the noise impulse occurrence frequency. This in turn determines the number of imperfectly detected OFDM symbols per LDPC codeword, hence directly linking them to the outage probability. In other words, the outage probability is discretized into the following values $P_B(0), P_B(1), \cdots, P_B(L_B)$. More explicitly, the probability that L_I OFDM symbols are contaminated within an LDPC code-

word constituted by a total of L_B OFDM symbols, is given by the binomial expression of $p(L_I) = \binom{L_B}{L_I} p_i^{L_I}(1-p_i)^{L_B-L_I}$, where p_i represents the occurrence probability of impulsive noise. Let us use $P_{\text{OF}}(L_I)$ to denote the specific BLER at which an outage floor occurs, which is determined by the SNR value. If the SNR encountered is lower than that required for correctly decoding an LDPC codeword conveying L_I error-infested OFDM symbols, an outage event is declared. The corresponding outage probability of $P_{\text{OF}}(L_I)$ can be expressed as:

$$P_{\text{OF}}(L_I) = \begin{cases} 1, & \text{if } L_I = 0, \\ 1 - \sum_{L=0}^{L_I-1} p(L), & \text{if } 1 \leq L_I \leq L_B. \end{cases} \tag{4.18}$$

Let us now briefly summarize the BLEP calculation in the face of impulsive noise.

1. The channel threshold is obtained with the aid of (4.15), (4.8), (4.9), (4.10) and (4.11).
2. We calculate $P_B(L_I)$ upon increasing the SNR with the aid of (4.17).
3. We compare $P_B(L_I)$ to $P_{\text{OF}}(L_I+1)$. If $P_B(L_I) < P_{\text{OF}}(L_I+1)$, we set $P_B = P_{\text{OF}}(L_I+1)$ until the SNR value reaches its threshold value required for correctly decoding the LDPC codewords having L_I+1 error-infested OFDM symbols.
4. We set $L_I = L_I + 1$ and then go to the second step.

This calculation can be formulated using the pseudo-code shown in Algorithm 1.

Type-I HARQ-Assisted LDPC-Coded OFDM Scheme

Similar to the above LDPC coded systems, its HARQ-assisted counterpart also exhibits outage probability floors, which cannot be avoided even upon employing an infinite number of transmission attempts. To elaborate, when the first transmission attempt of a packet is unsuccessful due to the occurrence of impulsive noise, the following attempts may also encounter impulsive noise occurrences, (the probability of such events is dependent on p_i), which results in an outage. Let us denote by $P_{\text{OF,I}}(L_I)$ the specific BLER at which an outage floor occurs after unsuccessfully decoding an LDPC codeword having L_I error-infested OFDM symbols in Type-I HARQ schemes. Then, given a maximum number of transmission attempts T, $P_{\text{OF,I}}(L_I)$ can be expressed as:

$$P_{\text{OF,I}}(L_I) = \begin{cases} 1, & \text{if } L_I = 0 \\ \left(1 - \sum_{L=0}^{L_I-1} p(L)\right)^T, & \text{if } 1 \leq L_I \leq L_B. \end{cases} \tag{4.19}$$

Algorithm 1 P_{out} calculation in impulsive noise environment

Require: L_B, M, κ, p_i, $\text{SNR}_{\text{start}}$, SNR_{end}
1: $p = zeros(1, L_B + 1)$ {Initialization}
2: $P_{\text{OF}} = zeros(1, L_B + 2)$ {Initialization}
3: **for** $L_I = 0 : L_B$ **do**
4: Obtain $\sigma^2_{\text{th}}(L_I)$ by (4.15), (4.8), (4.9), (4.10) and (4.11); {Density evolution}
5: $p(L_I) = \binom{L_B}{L_I} p_i^{L_I}(1-p_i)^{L_B - L_I}$; {Outage floor calculation}
6: **if** $L_I = 0$ **then**
7: $P_{\text{OF}}(L_I) = 1$;
8: **else**
9: $P_{\text{OF}}(L_I) = 1 - \sum_{L=0}^{L_I-1} p(L)$;
10: **end if**
11: **end for**
12: $L_I = 0$; {Outage probability calculation}
13: **for** $\text{SNR} = \text{SNR}_{\text{start}} : \text{SNR}_{\text{end}}$ **do**
14: Obtain $P_B(L_I)$ through (4.17);
15: **if** $P_B(L_I) > P_{\text{OF}}(L_I)$ **then**
16: $P_B(\text{SNR}) = P_{\text{OF}}(L_I)$;
17: **else if** $P_B(L_I) < P_{\text{OF}}(L_I + 1)$ **then**
18: $P_B(\text{SNR}) = P_{\text{OF}}(L_I + 1)$;
19: $L_I = L_I + 1$;
20: **else**
21: $P_B(\text{SNR}) = P_B(L_I)$;
22: **end if**
23: **end for**

Assuming that the impulsive noise occurrence events of the consecutive transmissions are independent of each other, the outage probability for the Type-I HARQ-assisted scheme denoted is given by:

$$P_{\text{out,I}}(L_I) = \left[P_B(L_I)\right]^T, \tag{4.20}$$

where $P_B(L_I)$ can be calculated with the aid of DE and the finite-length analysis of (4.17). Then, the analytical outage probability can be calculated using Algorithm 1 upon replacing P_B and P_{OF} by $P_{\text{out,I}}$ in (4.19) and by $P_{\text{OF,I}}$ in (4.20), respectively.

Type-II HARQ-Assisted LDPC-Coded OFDM Scheme

In Type-II HARQ-assisted schemes, all the copies of a packet are combined for joint demodulation and decoding, so that the resultant SNR of an OFDM symbol becomes the sum of the SNRs of the corresponding OFDM symbols in the copies received. The resultant PDF of the LLRs of the combined packet may vary, as a function of the number of OFDM symbols contaminated by impulsive noise in the copies. For example, given an LDPC codeword spanning L_B OFDM symbols, there are T^{L_B+1} legitimate possibilities for the LLRs' PDF observed following the detection of the packets combined after

T transmissions. Note however that some of the T^{L_B+1} possibilities yield the same LLR distribution. Let us hence denote the total number of different LLR distributions by J. The outage probability of the scheme is then determined as follows:

1. We categorize all the combinations according to the resultant LLRs' PDF denoted by f_j, $j = \{1, \cdots, J\}$, and then obtain the noise thresholds to be satisfied σ_j^*, $j = \{1, \cdots, J\}$, for correct LDPC decoding under the different LLR PDFs, with the aid of the DE technique.

2. We sort the required noise thresholds $\boldsymbol{\sigma}_j^*$ to create $\hat{\boldsymbol{\sigma}}_j^*$ so that we arrive at $\hat{\sigma}_{j+1}^* < \hat{\sigma}_j^*$, where $j \in [1, J-1]$ and then calculate the corresponding occurrence probabilities denoted by $P(\hat{\sigma}_j^*)$, where $j = \{1, \cdots, J\}$.

3. The components denoted by $P_{\text{out,II}}(\hat{\sigma}_j^*)$ can be obtained in a form similar to (4.17).

4. The outage floor denoted by $P_{\text{OF,II}}(j)$ is obtained as $P_{\text{OF,II}}(j) = 1 - \sum_{k=0}^{j-1} P(\hat{\sigma}_k^*)$.

5. Finally, the outage probability floors can also be calculated by Algorithm 1 upon replacing P_{OF} and P_B by $P_{\text{OF,II}}$ and $P_{\text{out,II}}$, respectively.

4.3.3 Numerical Results

In this subsection, we compare the outage probability of our Type-I and Type-II HARQ-assisted OFDM systems protected by $1/2$-rate $(3, 6)$ regular LDPC codes configured in Table 4.1 and operating in impulsive noise environments, using our proposed analytical formulas and our simulation results. For simplicity, an LDPC codeword is configured to span over $L_B = 2$ OFDM symbols, each of which has 2048 subcarriers. BPSK modulation is used. Note that E_s/N_0 refers to the signal-to-background noise ratio experienced by each symbol and it is not normalized to the total number of transmission attempts.

The performance attained under various conditions is portrayed in Fig. 4.4, Fig. 4.5 and Fig. 4.6. Here we summarize our general observations. Firstly, the analytical curves are confirmed by the simulation results. Secondly, as anticipated, the outage probability curves obey a stair-case shape. Thirdly, the outage probability curves of Type-II HARQ-assisted systems exhibit more steps than those of the Type-I HARQ-assisted systems, because the received packets have a larger number of legitimate combinations due to the packet combining operation in the Type-II HARQ-assisted systems. For example, when $L_B = 2$, the components are categorized into three types, i.e. $I = 0$, $I = 1$, and $I = 2$, for the Type-I HARQ-assisted scheme, while we have 10 possible components for the Type-II HARQ-assisted scheme. In the following, we will elaborate on the specific system configuration for each figure and discuss the numerical results individually.

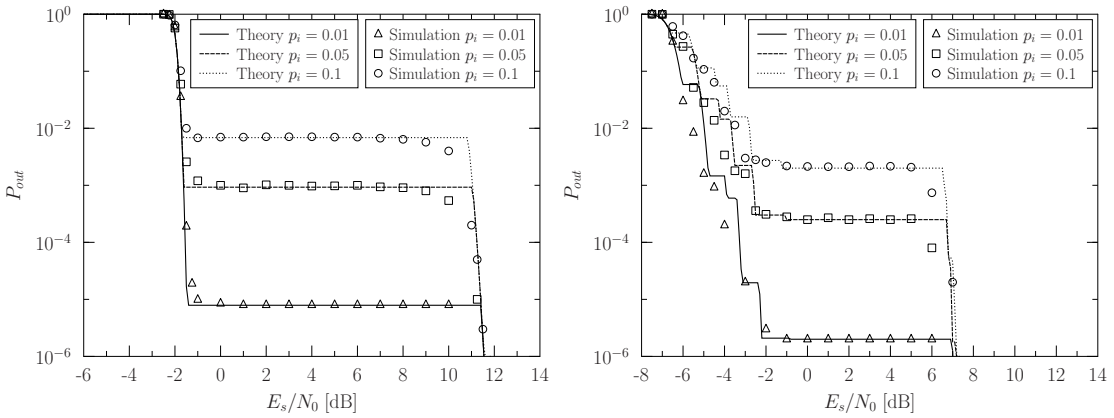

(a) Type-I HARQ.

(b) Type-II HARQ.

Figure 4.4: Outage probability performance comparison of Type-I and Type-II HARQ systems under various values of impulsive noise occurrence probability, p_i. The code is $1/2$-rate (3,6)-regular LDPC code configured by Table 4.1 and the modulation scheme is BPSK. The maximum number of transmission times T is set as 3. For the impulsive noise, $\kappa = 20$dB. The theoretical results are calculated according to Algorithm 1.

Fig. 4.4 shows the performance of Type-I and Type-II HARQ systems for impulsive noise occurrence probabilities of $p_i = 0.01, 0.05$ and 0.1. The maximum number of transmissions is set to 3. For the impulsive noise, we have $\kappa = 20$dB. Our observations are as follows. Firstly, a lower p_i implies that the outage probability floors occur at higher E_s/N_0 values, which is because a lower p_i implies that a lower number of OFDM symbols per LDPC codeword is likely to be infested by impulsive noise and hence its outage floor occurs at a lower P_{out}. In our Type-I HARQ-assisted scheme associated with $T = 3$, for example, the probability of an LDPC code being corrupted by impulsive noise is 7.88×10^{-6} and 6.86×10^{-3} for $p_i = 0.01$ and $p_i = 0.1$, respectively. Secondly, as expected, our Type-II HARQ-assisted systems outperforms the Type-I HARQ-assisted systems. More explicitly, the former requires 4.77dB lower E_s/N_0 to achieve $P_{\text{out}} = 10^{-6}$, compared to the Type-I HARQ, because the Type-II HARQ is capable of combining upto 3 packets for joint decoding.

Fig. 4.5 shows the performance of our Type-I and Type-II HARQ systems for impulsive-to-background noise ratios of $\kappa = 10$, 20 and 30 dB. The maximum number of transmissions is set to 3. For the impulsive noise, we have $p_i = 0.05$. It can be inferred from the figures that we need a higher E_s/N_0 for overcoming the outage probability floors upon increasing κ. This is because we need a higher E_s/N_0 for correctly decoding the received LDPC codeword at the same number of error-infested OFDM symbols, when κ is higher.

Fig. 4.6 shows the performance of Type-I and Type-II HARQ systems for the maximum number of transmissions given by $T = 1, 2$ and 3. As for the impulsive noise, we set $p_i = 0.05$ and $\kappa = 20$dB. It can be directly inferred from the figures that we need a lower E_s/N_0 to attain a specific outage probability upon increasing T. For the case of

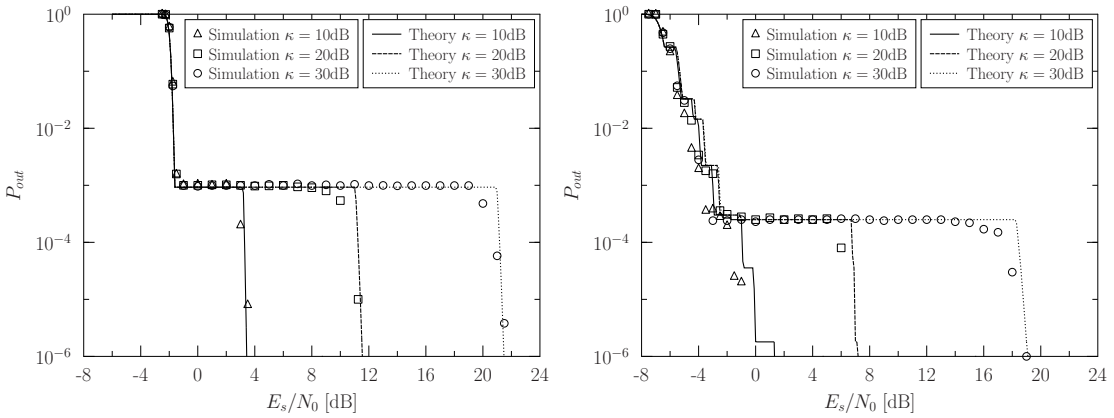

(a) Type-I HARQ. (b) Type-II HARQ.

Figure 4.5: Outage probability performance comparison of Type-I and Type-II HARQ systems under various values of ratio of background noise power to impulsive noise power, κ. The code is $1/2$-rate (3,6)-regular LDPC code configured by Table 4.1 and the modulation scheme is BPSK. The maximum number of transmission times T is set as 3. For the impulsive noise, $p_i = 0.05$. The theoretical results are calculated according to Algorithm 1.

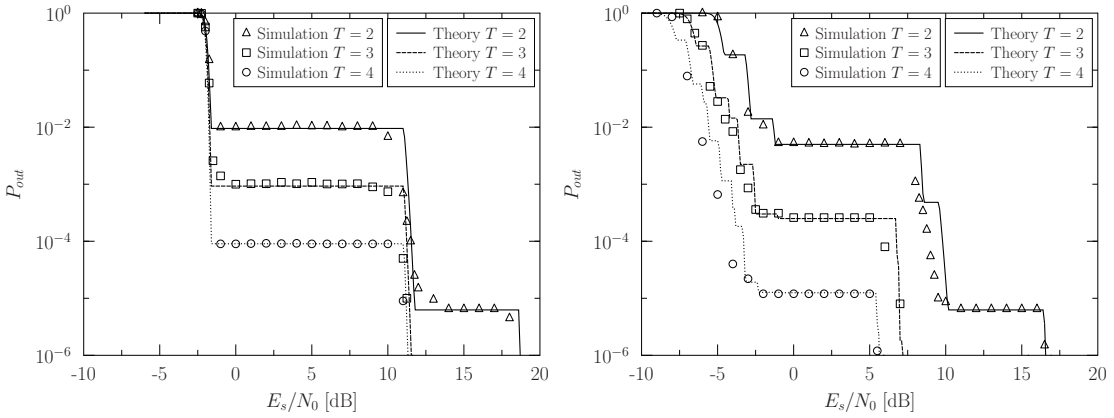

(a) Type-I HARQ. (b) Type-II HARQ.

Figure 4.6: Outage probability performance comparison of Type-I and Type-II HARQ systems under various values of maximum number transmission times, T. The code is $1/2$-rate (3,6)-regular LDPC code configured by Table 4.1 and the modulation scheme is BPSK. For the impulsive noise, $p_i = 0.05$ and $\kappa = 20$dB. The theoretical results are calculated according to Algorithm 1.

the Type-I HARQ, this is because the impulsive noise bursts are more likely to be avoided upon using more transmission attempts. Having a higher T reduces the probability that an LDPC codeword remains infested by impulsive noise and hence the outage probability floors occur at lower outage probability. Again, in Type-II HARQ, several transmissions are combined for joint decoding, hence the overall received E_s/N_0 becomes higher, which results in a higher probability of correct decoding and hence the outage probability is reduced.

4.4 The Number of Packet Transmission Attempts and Goodput

Some applications, such as, lip-synchronized video streaming, are sensitive to delays. The average number of ARQ transmissions is one of the factors affecting the delay. In a related context, goodput is defined as the number of successfully delivered bits per unit time, which reflects the transmission efficiency of the system. In this section, we characterize the average number of packet transmissions and the attainable goodput of the HARQ-assisted schemes, both analytically and by our numerical results.

4.4.1 Mathematical Analysis

Number of Transmission Attempts

Let us denote the average number of packet transmissions by $\mathbb{E}[t]$, which is expressed as [193]:

$$\mathbb{E}[t] = 1 + \sum_{t=1}^{T-1} P^{t}_{\text{out,I/II}}, \tag{4.21}$$

where $P^{t}_{\text{out,I/II}}$ represents the outage probability of Type-I and Type-II HARQ after t transmissions, respectively.

Goodput

Upon denoting the goodput by $\hat{R}$, we calculated it as the long-term average ratio of the number of successfully delivered bits over the total number of bits required [194, 195]. The initial transmission rate for a packet is denoted by $R_{\text{I},1}$ and $R_{\text{II},1}$ for the Type-I and Type-II HARQ schemes, respectively. When $(t-1)$ extra transmission attempts are used, the transmission rate becomes $R_{\text{I/II},t} = R_{\text{I/II},1}/t$. In this case, the long-term average transmission rate becomes $R_{\text{I/II}} = R_{\text{I/II},1}/\mathbb{E}[t]$ and the goodput is expressed as:

$$\hat{R}_{\text{I/II}} = \frac{R_{\text{I/II},1}(1 - P^{T}_{\text{out,I/II}})}{\mathbb{E}[t]}, \tag{4.22}$$

where $P^{T}_{\text{out,I/II}}$ is the outage probability of the Type-I and Type-II HARQ, when the number of the transmission attempts is T.

4.4.2 Numerical Results

The average number of transmission attempts and the goodput are compared between the Type-I and Type-II HARQ-assisted systems, coded by $1/2$-rate $(3, 6)$ regular LDPC codes in our impulsive noise environment. Similar to the setting in Section 4.3.3, an LDPC codeword spans over $L_B = 2$ OFDM symbols, each of which has 2048 subcarriers. BPSK modulation is used and $T = 3$ is set for the maximum number of transmissions. As for the impulsive noise, we set $\kappa = 20$dB and $p_i = 0.05$.

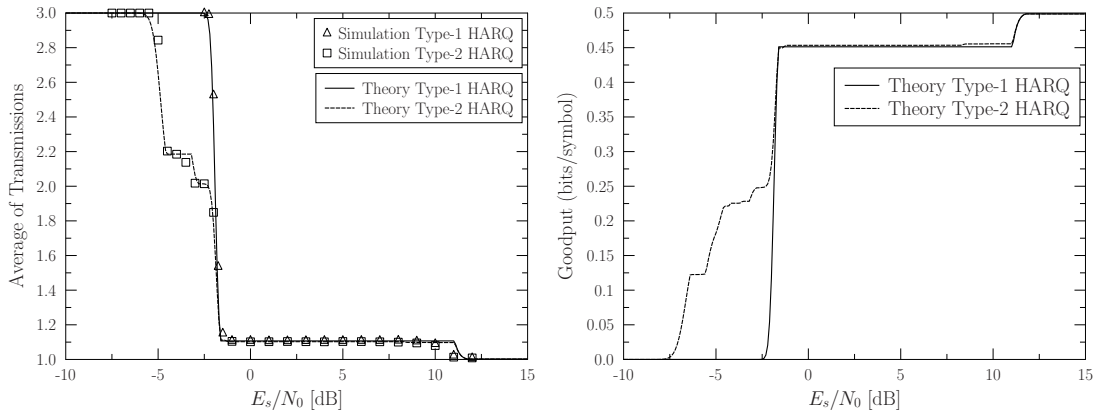

(a) Average number of transmissions.

(b) Goodput.

Figure 4.7: The average number of transmissions and goodput comparison between Type-I and Type-II HARQ systems. The code is $1/2$-rate (3,6)-regular LDPC code configured by Table 4.1 and the modulation scheme is BPSK. T is set as 3. For the impulsive noise, $p_i = 0.05$ and $\kappa = 20$dB. The theoretical results are calculated according to (4.21) and (4.22), for average number of transmissions and goodput, respectively.

Fig. 4.7a depicts our comparison between the Type-I and Type-II HARQ-assisted systems in terms of the average number of transmissions. Several observations can be made. Firstly, as expected, the Type-II HARQ outperforms the Type-I HARQ, again because the Type-II HARQ combines the consecutively received copies so that the resultant SNR becomes higher than that of any of the single packets. The other reason is that even if each transmission attempt suffers from impulsive noise, the index of the error-infested symbol may not be the same, hence the combined codeword may become correctly decoded. As for the range $1 \leq T \leq 2$, the two types of HARQ have almost identical performance. This is because when the first trial is erroneously decoded, the second transmission will be triggered regardless on which type of HARQ is used. Secondly, the average number of transmission attempts is consistent with the corresponding outage probability performance.

Fig. 4.7b presents our comparison between the Type-I and Type-II HARQ-assisted systems in terms of their goodput. Our observations are as follows. Firstly, the Type-II HARQ outperforms the Type-I HARQ in terms of its goodput, especially when $\hat{R} < 0.25$.

Secondly, the goodput has an approximately linear relationship with $\mathbb{E}[t]$ in Fig. 4.7a, because our region of interest in terms of P_{out} in (4.22) is close to 0.

4.5 Chapter Summary

Observing the numerical results, we may conclude that the proposed analysis provides a close match to simulations both of the LDPC-coded OFDM systems considered and HARQ-assisted systems considered. Moreover, as anticipated, the outage probability curves obey a stair-case shape in impulsive noise environments. The number of stairs is dependent on the impulsive noise's occurrence probability and power. Furthermore, the Type-II HARQ scheme outperforms the Type-I HARQ scheme in the system considered, in terms of the outage probability, the average number of transmission attempts and the goodput, as a benefit of exploiting the consecutively received copies.

In a nutshell, we analyzed HARQ-assisted OFDM systems contaminated by impulsive noise in a finite-length LDPC regime, both with the aid of our modified density evolution and waterfall-SNR analysis. The performance was characterized in terms of the outage probability, the average number of transmissions and the effective throughput. The simulation results confirm the accuracy of our analysis and quantify the efficiency of our HARQ-assisted schemes in hostile impulsive noise environments.

Chapter 5

Joint Impulsive Noise Estimation and Data Detection Conceived for LDPC-Coded DMT-Based DSL Systems

The LLRs of bits have to be calculated by taking into account the impulsive noise statistics in symbol detection. As for the stationary noise environment, the noise statistics may be readily estimated using pilots during the training stage. However, this process becomes challenging in the presence of impulsive noise, because the occurrence of impulsive noise will substantially affect the PDF of the noise. To overcome this problem, in this chapter we propose a joint impulsive noise estimation and data detection algorithm. Both our analytical and simulation results demonstrate that the proposed scheme is capable of achieving a near-capacity performance.

5.1 Introduction

In a DSL transmission link, the information bits are protected using channel coding and then mapped to the modulated symbols at the transmitter side. At the receiver side, the LLRs of the received symbols used for iterative decoding are obtained by exploiting both the channel knowledge estimated during the training stage and the noise statistics. The noise statistics may be readily obtained, when only background noise is encountered by the transmission link, because the process is static. However, the situation is radically different, when impulsive noise occurs. To emphasize it again, when a DMT symbol is contaminated by impulsive noise, the PDF of the noise becomes radically different from the one obtained for background noise. To address this issue, it is of paramount importance to conceive an algorithm for jointly estimating the noise statistics and detecting the symbols.

The joint estimation and detection problem of impulsive noise environments has drawn a substantial research attention in the literature [106, 108–110]. Explicitly, Fukami *et al.* [106] designed a noncoherent frequency shift keying (FSK) detector for the Middleton's Class A channel. Furthermore, both optimum and near-optimum detectors were designed for Middleton's Class A noise and general performance bounds were derived in [107]. In their contribution, Nassar *et al.* [108] proposed a low-complexity expectation-maximization (EM) based detector for the Middleton's Class A channel. The above three investigations were conceived for mitigating the discontinuous Middleton's Class A noise. As for the bursty impulsive noise, the memory of the channel has to be taken into account. Specifically, Fertonani *et al.* [109] proposed a noise-mitigating symbol detector for the channel contaminated by Markov-Gaussian impulsive noise, by appropriately modifying the maximum *a posteriori* (MAP) criterion, which was able to attain the optimum performance. Similarly, Ndo *et al.* [110] extended the optimum MAP detector of [109] to the Markov-Middleton impulsive noise model.

However, much of the existing literature [106,108–110] assumes that the noise exhibits white spectrum, which is not the case in practice. Hence, in this chapter we propose a joint two-stage impulsive noise estimation and data detection scheme, for improving the accuracy of impulsive noise estimation in advanced LDPC-coded DMT-based DSL systems. The main contributions of this chapter are listed below.

- Firstly, we propose semi-blind impulsive noise estimation as the first-stage of our estimation method, which is capable of estimating both the arrival instant of noise impulses and the power of impulsive noise at an adequate accuracy without using cyclic redundancy check. We will demonstrate that the proposed method eliminates the potential spectral efficiency degradation imposed by ARQ retransmissions.

- Secondly, in order to improve the accuracy of the impulsive noise estimation, we propose an iterative decision-directed method for LDPC-coded DMT-based DSL systems as the second-stage estimation for high-order modulation constellations. We will demonstrate that a beneficial iteration gain is achieved. Our estimation technique is then integrated into the detection and decoding process, for the sake of mitigating both the complexity and the delay imposed.

- Furthermore, in order to quantify the estimation accuracy and select the appropriate samples for impulsive noise estimation, we mathematically analyze the mean square error (MSE) of our two-stage algorithm and confirm its accuracy by simulations. Our results are also compared to the theoretical Cramer-Rao Lower Bound (CRLB).

- We optimize the number of iterations both within the LDPC decoder as well as between the soft-demapper and the decoder, with the aid of *extrinsic* information transfer (EXIT) charts [15].

- Finally, our simulation results demonstrate that the proposed scheme is capable of achieving a near-capacity performance for LDPC-coded DMT-based DSL systems in the presence of impulsive noise. For example, the SNR-difference of the BER curve of our proposed schemes and the idealistic scenarios of perfectly knowing both the arrival instant and the instantaneous power of the impulsive noise is less 0.2dBboth for 16QAM and 4096QAM.

The rest of the paper is organized as follows. In Section 5.2, we introduce both the transmission system and noise model considered. The proposed joint impulsive noise estimation and data detection scheme is detailed in Section 5.3. In Section 5.4, a pair of design examples of the novel scheme are characterized both with the aid of EXIT charts and BER evaluations. Finally, this chapter is summarized in Section 5.5.

5.2 System and Noise Model

In this section, we describe the coded DMT transceiver and the noise model.

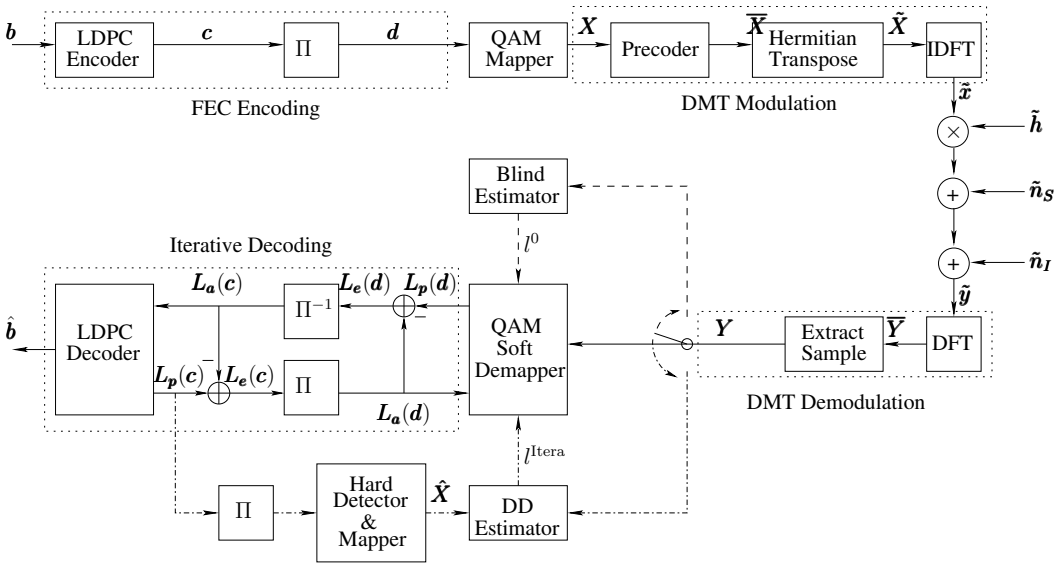

Figure 5.1: The structure of our joint impulsive noise estimation and data detection scheme conceived for LDPC coded DMT-based DSL systems. "Blind" and "DD" refer to semi-blind and decision-directed, respectively.

5.2.1 Coded DMT Transceiver

We consider a discrete multitone (DMT) system having N tones, as illustrated in Fig. 5.1. The sequence of information bits is denoted by $\boldsymbol{b} \in \{0,1\}$, which are channel-encoded, hence resulting in the bits denoted by $\boldsymbol{c} \in \{0,1\}$. For Q-ary QAM having the alphabet $\boldsymbol{\mathcal{X}}$, the interleaved bits denoted by $\boldsymbol{d} \in \{0,1\}$ are grouped into a set of BPS $= \log_2 Q$

bits and then mapped with index $X^q \in \boldsymbol{\mathcal{X}}$ to Q-ary symbols denoted by $\boldsymbol{X}$, where q is the decimal value of the binary set of the BPS number of bits. In order to ensure having a real-valued output after IDFT, $\boldsymbol{X}$ is Hermitian transposed to $\overline{\boldsymbol{X}}$, subject to the following constraint [196]:

$$\begin{cases} \overline{X}_0 = \overline{X}_{N/2} = 0 \\ \overline{X}_n = \overline{X}^*_{N-n}, \quad \text{for } n = 1, \ldots, N/2-1, N/2+1, \ldots, N \end{cases}. \tag{5.1}$$

Since the DSL channel is slowly time-variant, channel information can be estimated periodically and then compared to opt the results without the influence of impulsive noise. Therefore, it is reasonable to assume that the channel impulse response (IR) is perfectly known at the transmitter and $\overline{\boldsymbol{X}}$ is pre-equalized by the precoder, hence resulting in $\tilde{\boldsymbol{X}}$. Our Transmit Precoder (TPC) design is detailed later in this section. After the IDFT stage of Fig. 5.1, the time-domain signal denoted by $\tilde{\boldsymbol{x}} = [\tilde{x}_0, \tilde{x}_1, \ldots, \tilde{x}_{N-1}]^T$ is expressed as

$$\tilde{\boldsymbol{x}} = \boldsymbol{\mathcal{F}}^H \tilde{\boldsymbol{X}}, \tag{5.2}$$

where $\boldsymbol{\mathcal{F}}$ is the normalized discrete Fourier transform matrix, yielding $\boldsymbol{\mathcal{F}}\boldsymbol{\mathcal{F}}^H = \boldsymbol{\mathcal{F}}^H\boldsymbol{\mathcal{F}} = \boldsymbol{I_N}$, where the elements of $\boldsymbol{\mathcal{F}}$ are defined as $\mathcal{F}_{i,k} = [1/\sqrt{N}\exp(j2\pi ik/N)]$.

The DMT symbols pass through the channel denoted by $\tilde{\boldsymbol{h}}$ and they are contaminated by the stationary noise denoted by $\tilde{\boldsymbol{n}}_{\boldsymbol{S}}$ and by impulsive noise denoted by $\tilde{\boldsymbol{n}}_{\boldsymbol{I}}$. Assuming that synchronization is perfectly established, the received symbols denoted by $\tilde{\boldsymbol{y}}$ are expressed as

$$\tilde{\boldsymbol{y}} = \sqrt{\rho}\tilde{\boldsymbol{h}}\tilde{\boldsymbol{x}} + \tilde{\boldsymbol{n}}_{\boldsymbol{S}} + \tilde{\boldsymbol{n}}_{\boldsymbol{I}}, \tag{5.3}$$

where $\tilde{\boldsymbol{y}}$ is an N-element vector, $\tilde{\boldsymbol{h}}$ is an $(N \times N)$-element matrix and ρ is the received signal power per symbol.

At the receiver of Fig. 5.1, $\overline{\boldsymbol{Y}}$ can be recovered with the aid of the DFT as follows:

$$\begin{aligned} \overline{\boldsymbol{Y}} &= \boldsymbol{\mathcal{F}}\tilde{\boldsymbol{y}} = \boldsymbol{\mathcal{F}}(\sqrt{\rho}\tilde{\boldsymbol{h}}\tilde{\boldsymbol{x}} + \tilde{\boldsymbol{n}}_{\boldsymbol{S}} + \tilde{\boldsymbol{n}}_{\boldsymbol{I}}) \\ &= \boldsymbol{\mathcal{F}}(\sqrt{\rho}\tilde{\boldsymbol{h}}\boldsymbol{\mathcal{F}}^H\tilde{\boldsymbol{X}} + \tilde{\boldsymbol{n}}_{\boldsymbol{S}} + \tilde{\boldsymbol{n}}_{\boldsymbol{I}}) \\ &= \sqrt{\rho}\boldsymbol{\mathcal{F}}\boldsymbol{\mathcal{F}}^H\tilde{\boldsymbol{H}}\boldsymbol{\mathcal{F}}\boldsymbol{\mathcal{F}}^H\tilde{\boldsymbol{X}} + \boldsymbol{\mathcal{F}}\tilde{\boldsymbol{n}}_{\boldsymbol{S}} + \boldsymbol{\mathcal{F}}\tilde{\boldsymbol{n}}_{\boldsymbol{I}} \\ &= \sqrt{\rho}\tilde{\boldsymbol{H}}\tilde{\boldsymbol{X}} + \tilde{\boldsymbol{N}}_{\boldsymbol{S}} + \tilde{\boldsymbol{N}}_{\boldsymbol{I}}, \end{aligned} \tag{5.4}$$

where $\tilde{\boldsymbol{h}} = \boldsymbol{\mathcal{F}}^H\tilde{\boldsymbol{H}}\boldsymbol{\mathcal{F}}$ and $\tilde{\boldsymbol{H}}$ is a diagonal matrix having the diagonal element of $[\tilde{H}_0, \tilde{H}_1, \cdots, \tilde{H}_{N-1}]$. As mentioned above, $\tilde{\boldsymbol{X}}$ is pre-equalized for each tone $n \in [0, N-1]$ as

$$\tilde{X}_n = \frac{\tilde{H}^*_n}{|\tilde{H}_n|^2}\overline{X}_n. \tag{5.5}$$

Then, (5.4) becomes

$$\overline{\boldsymbol{Y}} = \sqrt{\rho}\overline{\boldsymbol{X}} + \tilde{\boldsymbol{N}}_{\boldsymbol{S}} + \tilde{\boldsymbol{N}}_{\boldsymbol{I}}. \tag{5.6}$$

After extracting the samples from $\overline{\boldsymbol{Y}}$, we have

$$\boldsymbol{Y} = \sqrt{\rho}\boldsymbol{X} + \boldsymbol{N}_{\boldsymbol{S}} + \boldsymbol{N}_{\boldsymbol{I}}, \tag{5.7}$$

where $\boldsymbol{Y}$ is a $\frac{N-2}{2}$-element vector, while $\boldsymbol{N}_{\boldsymbol{S}}$ and $\boldsymbol{N}_{\boldsymbol{I}}$ are the stationary noise and impulsive noise in the frequency domain, respectively. Then $\boldsymbol{Y}$ is processed in further stages, as discussed in Section III.

5.2.2 Noise Model

The noise process includes both stationary and impulsive noise, which are characterized both in the time-domain and the frequency-domain in this subsection.

Stationary Noise

As discussed in [147], the power of the stationary noise is flat over all frequencies and its amplitude is assumed to be Gaussian-distributed. Its probability density function (PDF) in the time domain can be expressed as

$$\tilde{\boldsymbol{n}}_{\boldsymbol{S}}[k] \sim \mathcal{N}(0, \sigma_S^2), \text{ for all } k, \tag{5.8}$$

where we denote the time-domain index by k and $\mathcal{N}(\mu, \sigma^2)$ represents the real-valued Gaussian distribution with the mean of μ and the variance of σ^2. The real-valued noise is transformed to the complex-valued variable after DFT and its PDF in the frequency domain is given by

$$\tilde{\boldsymbol{N}}_{\boldsymbol{S}}[n] \sim \mathcal{CN}(0, \sigma_S^2), \text{ for all } n, \tag{5.9}$$

where we denote the frequency-domain index by n and $\mathcal{CN}(\mu, \sigma^2)$ represents the complex-valued Gaussian distribution with a mean of μ and the variance of the real and imaginary parts given by $0.5\sigma^2$.

Impulsive Noise

The impulsive noise (IN) in DSL is usually characterized in terms of four aspects: amplitude, duration, IAT and spectral characteristics. The main model used for the amplitude is the Weibull distribution [147] [41]. By contrast, the commonly used distribution for

the duration is the twin-term log-normal approach of [147] [41] [9]. The IAT is usually modelled using the exponential [147], the Poisson [9] and the Markov Renewable Process (MRP) [41]. The auto-correlation function (ACF) is modelled as a negative logarithmic function [147] or as an exponentially decaying cosine function [41]. Therefore, it can be inferred that the impulsive noise in DSL is a coloured Weibull-distributed variable. When considering the DFT-based demodulation at the receiver, the behaviour of the coloured Weibull-distributed variable after DFT has to be discussed.

Here let us denote a correlated Weibull-distributed variable by $w[k]$, which is processed by DFT having a size of N. Then, we have

$$W[n] = \mathrm{DFT}\big[w[k]\big] = \frac{1}{\sqrt{N}} \sum_{n=0}^{N-1} w[k] \cdot e^{-j\frac{2\pi kn}{N}}. \tag{5.10}$$

The following convergence has been formally proved in [170]

$$\Big[\Re\big(W[n]\big), \Im\big(W[n]\big)\Big] \Rightarrow \Big[G[n], G[n]\Big], \tag{5.11}$$

where $G[n]$ is an independent identically distributed (i.i.d.) normal random variable with zero-mean and a variance of $S[n]/2$, while $S[n]$ is the spectral density associated with the autocorrelation of the process. The convergence formulated in (5.11) can be approached with a sufficiently large DFT size, which is readily satisfied by the DMT size of G.fast [174] having $N = 2048$ or 4096. As a result, the IN amplitude distribution in the frequency domain can be approximated by a Gaussian distribution. Then, the PDF of $\tilde{\boldsymbol{N}}_{\boldsymbol{I}}$ is given by

$$P\big(\tilde{\boldsymbol{N}}_{\boldsymbol{I}}[n]\big) = \sum_{\ell} p(\ell) \cdot \mathcal{CN}\big[0, \sigma^2_{I,n}(\ell)\big], \tag{5.12}$$

where ℓ is the number of samples in a DMT symbol influenced by the impulsive noise in the time domain, while $p(\ell)$ (whose expression is shown in Section B.3) is the probability that the number of samples in a DMT symbol influenced by IN in the time domain happens to be ℓ. Furthermore, let us denote the IN variance at the tone index n by $\sigma^2_{\mathrm{IN},n}$, when the whole OFDM symbol is influenced by IN in the time domain and then $\sigma^2_{I,n}(\ell)$ is a fraction of $\sigma^2_{\mathrm{IN},n}$, yielding

$$\sigma^2_{I,n}(\ell) = \frac{\ell}{N} \sigma^2_{\mathrm{IN},n}. \tag{5.13}$$

In this paper, the exponentially decaying cosine function of [41] is adopted to represent the ACF of IN:

$$R(t) = cos(2\pi\alpha t) \exp\big(-\beta|t|\big). \tag{5.14}$$

Let us denote the power spectral density of impulsive noise by $S(f) = \mathcal{FT}\big[R(t)\big]$, where $\mathcal{FT}$ represents the continuous Fourier transform. Then the IN variance can be expressed as

$$\begin{aligned}\sigma^2_{\mathrm{IN},n} &= \frac{1}{Z}\int_{n\Delta f}^{(n+1)\Delta f} S(f)\,\mathrm{d}f \\ &= \frac{1}{2\pi Z}\Bigg\{\tan^{-1}\Big(\frac{2\pi\big[(n+1)\Delta f+\alpha\big]}{\beta}\Big) - \tan^{-1}\Big(\frac{2\pi\big[n\Delta f+\alpha\big]}{\beta}\Big) \\ &\quad + \tan^{-1}\Big(\frac{2\pi\big[(n+1)\Delta f-\alpha\big]}{\beta}\Big) - \tan^{-1}\Big(\frac{2\pi\big[n\Delta f-\alpha\big]}{\beta}\Big)\Bigg\}, \end{aligned} \tag{5.15}$$

where Δf is the bandwidth of each tone in the DMT, while Z is the impedance. The spectrum of both impulsive noise and stationary noise is shown in Fig 5.2.

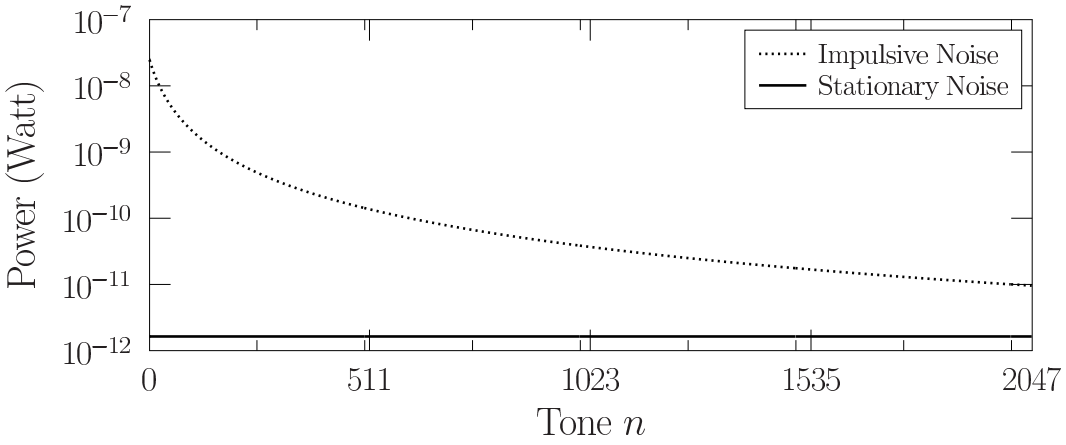

Figure 5.2: Spectrum of impulsive noise and stationary noise in DSL, for the bandwidth of 106 MHz and tone spacing of 51.75 kHz. The impulsive noise is plotted according to (5.15). For the stationary noise, the power spectral density is set to -135 dBm/Hz.

Temporal Characteristics

The duration of IN can be modelled by the two-term log-normal form [41],

$$f_{\mathrm{D}}(t) = B\frac{1}{\sqrt{2\pi}v_1 t}\exp\Big(-\frac{\ln^2(t/t_1)}{2v_1^2}\Big) + (1-B)\frac{1}{\sqrt{2\pi}v_2 t}\exp\Big(-\frac{\ln^2(t/t_2)}{2v_2^2}\Big), \tag{5.16}$$

and the IAT of IN can be modelled by the following two-state MRP [41],

$$f_{\mathrm{IAT}}(t) = \begin{cases} \frac{1}{1-\exp(-\lambda t_s)}\lambda\exp(-\lambda t), & \text{if } t < t_s \\ \theta t_s^{\theta}/t^{\theta+1}, & \text{if } t \geq t_s, \end{cases} \tag{5.17}$$

where the state-transitions occur according to the matrix $\boldsymbol{P}$. The parameters of the noise model, such as $\alpha, \beta, t_1, t_2, v_1, v_2, \lambda, \theta, B$ and $\boldsymbol{P}$ vary according to the geographic location

and the time of day according to [41] and to the realistic measurement-based document [150] by British Telecom (BT).

Based on the above temporal model, $p(\ell)$ is given as (5.18) in [192]. The expression of $p(\ell)$ is complex and long and hence readers are recommended to read the original reference [192] for more details. The cumulative density function (CDF) of ℓ is plotted in Fig 5.3.

$$p(\ell) = \begin{cases} \frac{\mathcal{E}[D_{S_0,k}]}{\mathcal{E}[D_{S_0,k}]+\mathcal{E}[D_{S_1,k}]}, & \text{if } \ell = 0 \\ \mathcal{D}_1(\ell, B, v_1, t_1) + \mathcal{D}_1(\ell, 1-B, v_2, t_2), & \text{if } \ell = 1, 2, \cdots, N-1 \\ \mathcal{D}_2(B, v_1, t_1) + \mathcal{D}_2(1-B, v_2, t_2), & \text{if } \ell = N \end{cases} \tag{5.18}$$

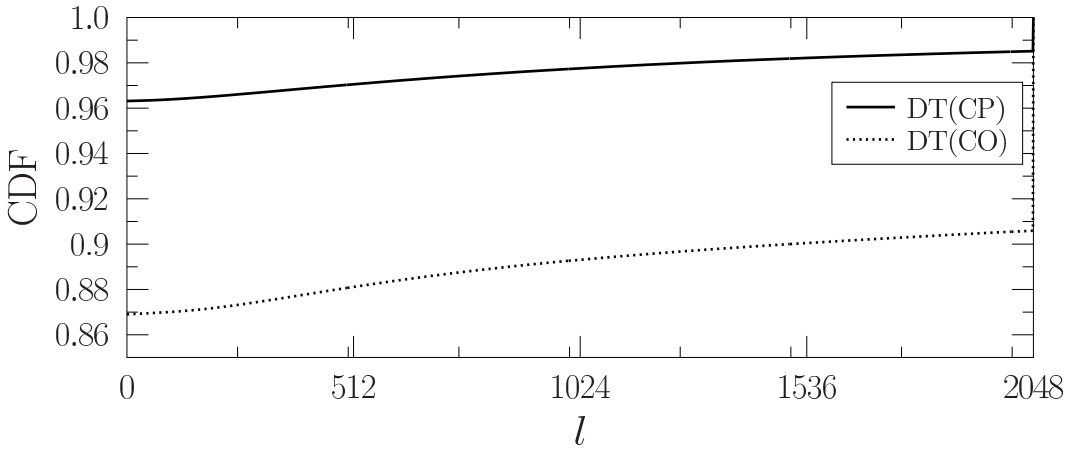

Figure 5.3: Cumulative density function of ℓ at the Deutsche Telekom (DT) central offices (CO) and DT customer premises (CP) when $T_{\text{DMT}} = 20.83\mu s$. DT central office (CO) is parametrized as $B = 0.25$, $t_1 = 8\mu$s, $t_2 = 125\mu$s, $v_1 = 0.75$, $v_2 = 1.0$, $\lambda = 0.16\text{s}^{-1}$, $\theta = 1.5$ and $t_s = 1$ms. DT(CP) is parametrized as $B = 1$, $t_1 = 18\mu$s, $v_1 = 1.15$, $\lambda = 0.16\text{s}^{-1}$, $\theta = 1.5$ and $t_s = 1$ms.

5.3 Impulsive Noise Estimation and Data Detection

In this section, we present the two-stage impulsive noise estimation and data detection, followed by an elaboration of iterative estimation and detection.

5.3.1 Impulsive Noise Estimation

The power spectrum of impulsive noise depends α and β in (5.15), which were found to be Gaussian distributed variables with a small variance [41] [150]. In this paper, we assume that the mean values of α and β are known. Furthermore, with the aid of (5.13),

assuming that the power level of stationary noise is known at the receiver, the impulsive noise estimation can be simplified to estimate ℓ, namely the number of samples influenced in the time domain representation of a DMT symbol. The structure of our proposed joint impulsive noise estimation and data detection scheme is shown in Fig. 5.1. At the receiver side, the extracted samples $\boldsymbol{Y}$ are firstly forwarded to the proposed blind estimator, which estimates ℓ as it will be detailed in Section III-A.1. With knowledge of both $\sigma^2_{\mathrm{IN},n}$ and estimated ℓ, the instantaneous impulsive noise variance level can be obtained according to (5.13). Given the estimate of the instantaneous noise variance, the QAM soft demapper becomes capable of producing more reliable LLRs for the channel decoder. For the bit-to-symbol mapping schemes of high-order modulation, where substantial iteration gains can be achieved, a further decision-directed (DD) estimator is proposed for improving the estimation accuracy. The interleaved *a posteriori* LLRs gleaned from the channel decoder are passed to the hard detector and the results then enter the proposed DD estimator as one of its inputs. Its second input is given by the extracted samples $\boldsymbol{Y}$. The DD estimator outputs the estimated value of ℓ for the QAM soft demapper, as detailed in Section III-A.2. Again, utilizing the estimated results and $\sigma^2_{\mathrm{IN},n}$, the QAM soft demapper produces the soft LLRs for further iterations, where the DD estimation is activated, until an error-free status or a pre-set outer iteration limit is achieved. The proposed blind-DD estimators are detailed as follows.

Proposed Semi-Blind Method

According to (5.7), the received symbol of tone n is expressed as

$$Y_n = \sqrt{\rho} X_n + N_{S,n} + N_{I,n}. \tag{5.19}$$

Then, we have

$$\begin{aligned} Y_n^* Y_n = \rho X_n^* X_n + N_{S,n}^* N_{S,n} + N_{I,n}^* N_{I,n} + 2\Re(N_{I,n}^* N_{S,n}) \\ + 2\sqrt{\rho}\Re(X_n^* N_{S,n}) + 2\sqrt{\rho}\Re(X_n^* N_{I,n}), \end{aligned} \tag{5.20}$$

and

$$\begin{aligned} \boldsymbol{Y}_{sel}^H \boldsymbol{Y}_{sel} = \rho \sum X_n^* X_n + \sum N_{S,n}^* N_{S,n} + \sum N_{I,n}^* N_{I,n} \\ + 2\sqrt{\rho} \sum \Re(X_n^* N_{S,n}) + 2\sqrt{\rho} \sum \Re(X_n^* N_{I,n}) \\ + 2 \sum \Re(N_{I,n}^* N_{S,n}), \end{aligned} \tag{5.21}$$

where $\boldsymbol{Y}_{sel}$ is the received vector associated with the elements selected for estimation and the selection of $\boldsymbol{Y}_{sel}$ is discussed later in Section III-A.5. Taking the expectation of (5.21),

we have

$$\mathbb{E}[\boldsymbol{Y}_{sel}^H \boldsymbol{Y}_{sel}] = \rho K + K\sigma_S^2 + \frac{\ell}{N}\sum \sigma_{I,n}^2, \tag{5.22}$$

where K is the number of elements in $\boldsymbol{Y}_{sel}$. The estimated value $\hat{\ell}$ can be obtained as:

$$\begin{aligned}\hat{\ell} &= \frac{\mathbb{E}[\boldsymbol{Y}_{sel}^H \boldsymbol{Y}_{sel}] - \rho K - \sigma_S^2 K}{\frac{1}{N}\sum \sigma_{I,n}^2} \\ &\approx \frac{\boldsymbol{Y}_{sel}^H \boldsymbol{Y}_{sel} - \rho K - \sigma_S^2 K}{\frac{1}{N}\sum \sigma_{I,n}^2} \\ &= \frac{\boldsymbol{Y}_{sel}^H \boldsymbol{Y}_{sel}}{\Omega} - \frac{\Psi}{\Omega},\end{aligned} \tag{5.23}$$

where we define $\Psi = \rho K + \sigma_S^2 K$ and $\Omega = \frac{1}{N}\sum \sigma_{I,n}^2$.

Proposed Decision-Directed Method

(5.19) can be reformulated as

$$N_{S,n} + N_{I,n} = Y_n - \sqrt{\rho} X_n. \tag{5.24}$$

Taking the square of both sides, we have

$$|N_{S,n} + N_{I,n}|^2 = |Y_n - \sqrt{\rho} X_n|^2. \tag{5.25}$$

Here we denote the samples estimated on the basis of the previous decision by $\hat{X}_n = X_n + \epsilon_n$, where ϵ_n is the error between the transmitted sample X_n and the estimated sample $\hat{X}_n$ on tone n. Taking the expectation of both sides of (5.25), we have

$$\begin{aligned}\sigma_S^2 + \frac{\ell_n}{N}\sigma_{I,n}^2 &= \mathbb{E}\{|Y_n - \sqrt{\rho} X_n|^2\} \\ &= \mathbb{E}\{|Y_n - \sqrt{\rho}(\hat{X}_n - \epsilon_n)|^2\} \\ &\approx \mathbb{E}\{|Y_n - \sqrt{\rho}\hat{X}_n|^2\} \\ &\approx |Y_n - \sqrt{\rho}\hat{X}_n|^2,\end{aligned} \tag{5.26}$$

where we denote the instantaneous estimate of ℓ at tone n by $\hat{\ell}_n$. The approximation in the third line of (5.26) is reasonable because the semi-blind estimation method results in a small value ϵ_n. Then we have

$$\hat{\ell}_n = \frac{N\left(|Y_n - \sqrt{\rho}\hat{X}_n|^2 - K\sigma_S^2\right)}{\sigma_{I,n}^2}. \tag{5.27}$$

Since ℓ may be deemed to be identical over all tones in a DMT symbol, the number of error-infested samples in a DMT symbol can be expressed as

$$\hat{\ell} = \frac{1}{K} \sum_{n=M}^{M+K-1} \frac{N\left(|Y_n - \sqrt{\rho}\hat{X}_n|^2 - K\sigma_S^2\right)}{\sigma_{I,n}^2}, \tag{5.28}$$

where M and K represent the initial tone index and the number of tones involved for variance estimation, respectively.

Numerical Results

In this subsection, we will investigate the performance of the proposed scheme.

Lemma 1. *The MSE is one of the most popular parameters used for evaluating the estimation accuracy. According to Appendix A, the MSE of the blind estimation methods may be expressed as*

$$\begin{aligned} MSE(\hat{\ell}) &= \mathbb{E}\{(\ell - \hat{\ell})^2\} \\ &= \frac{\sum \sigma_{I,n}^4}{N^2\Omega^2}\ell^2 + \frac{2(\rho + \sigma_S^2)}{\Omega}\ell + \frac{K\sigma_S^4}{\Omega^2}. \end{aligned} \tag{5.29}$$

Lemma 2. *It should be noted that the results of the proposed estimation method are unbiased. According to Appendix B, the Cramer-Rao Lower Bound (CRLB) is expressed as*

$$CRLB(\hat{\ell}) = \frac{1}{\sum_{n=M}^{M+K-1} \frac{(\sigma_{I,n}^2)^2}{(\ell\sigma_{I,n}^2 + N\sigma_S^2)^2}}. \tag{5.30}$$

The normalized MSE and CRLB are defined as follows:

$$\overline{\mathrm{MSE}}(\hat{\ell}) = \frac{\mathrm{MSE}(\hat{\ell})}{\ell}, \tag{5.31}$$

$$\overline{\mathrm{CRLB}}(\hat{\ell}) = \frac{\mathrm{CRLB}(\hat{\ell})}{\ell}. \tag{5.32}$$

Fig. 5.4 shows the normalized MSE of the blind estimation method at various SNR levels defined as ρ / N_S, when employing 16QAM and 4096QAM. Since it takes an extremely long time to evaluate the overall MSE for all possible ℓ values, we opted for the scenarios, where $\ell = 1000$ and $\ell = 2048$, respectively, while the impulsive noise occurrence probability is 0.1. Our observations are as follows. Firstly, the proposed blind estimation method has the same performance regardless of the QAM order, because the expectation of $Y_n^* Y_n$ in (5.23) is 1 for any QAM order and the results are expected to be identical for a

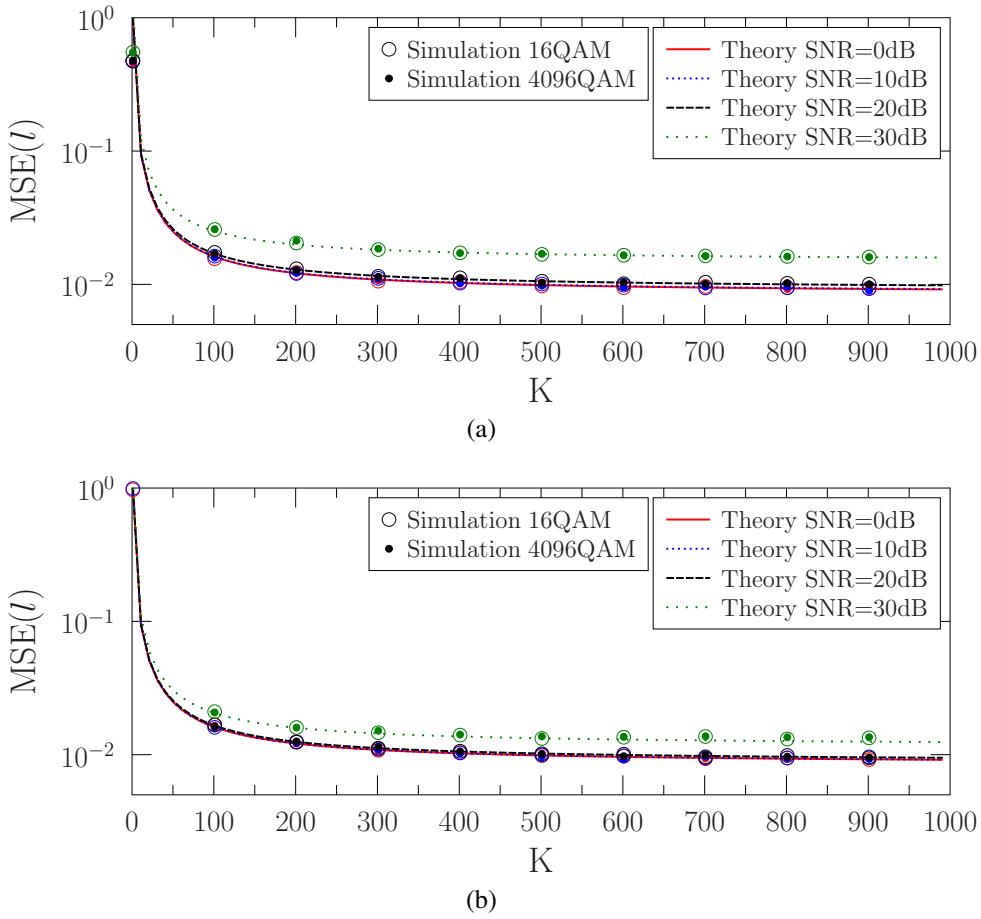

Figure 5.4: The MSE of the blind estimation method when the probability of impulsive noise occurrence is 0.1. (a): $\ell = 1000$; (b): $\ell = 2048$. The lines representing the theory calculated according to (5.29).

sufficiently large number of samples. Secondly, the MSE value does not decrease significantly for $K > 300$, which is explained as follows. It can be inferred from (5.29) that the MSE is partially dependant on the power of impulsive noise, while the power of impulsive noise becomes weaker, when the tone index increases, especially when $K > 300$ as shown in Fig 5.2. Based on this observation, the samples with indeces spanning from 1 to 300 are selected as $\boldsymbol{Y}_{sel}$ for blind estimation. Thirdly, any increase in the SNR degrades the estimation performance and the normalized MSE associated with $\ell = 2048$ is lower than that of $\ell = 1000$, which can be explained as follows. The estimation process is similar to the maximum-likelihood detection, where the detection accuracy is dependant on the power ratio between the desired variable and the undesired variable. The increase of SNR decreases the ratio of impulsive noise power over the transmitted signal power. Similarly, the impulsive noise has a higher power for $\ell = 2048$ than for $\ell = 1000$. These observations can also be directly inferred from (5.29).

Fig. 5.5 presents CRLB and the achievable normalized MSE of the proposed methods, when employing 4096QAM. Again, the impulsive noise occurrence probability is set to 0.1. The label 'Blind' refers to the blind estimation method and 'Blind+DD' refers to the

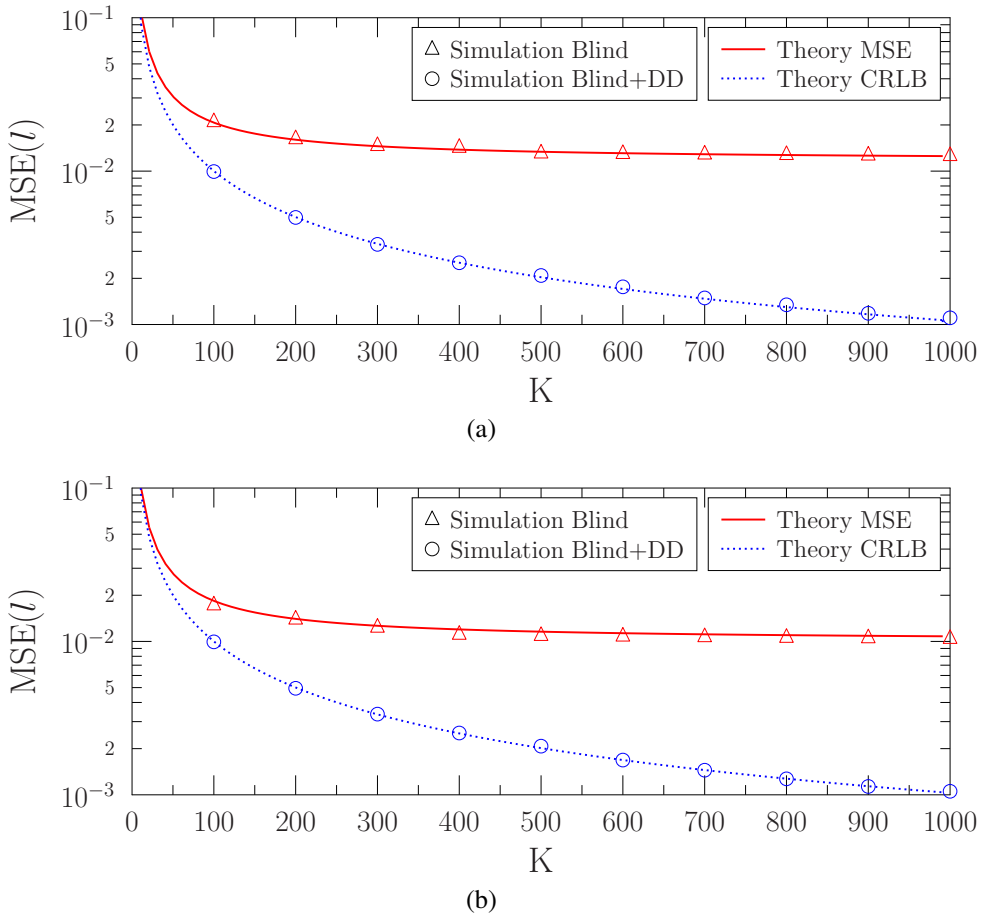

Figure 5.5: The CRLB and the MSE of the proposed estimation method at SNR = 27dB in 4096QAM. The probability of impulsive noise occurrence is 0.1 (a): $\ell = 1000$; (b): $\ell = 2048$. 'Blind' refers to the blind estimation method and 'Blind+DD' refers to the blind estimation method associated with 3 more iterations in the DD estimation method. The indeces of the samples used for blind estimation span from 1 to 300. The 'Theory MSE' and 'Theory CRLB' were calculated according to (5.31) and (5.32), respectively.

blind estimation method associated with 3 further iterations of the DD estimation method. Note that 4096QAM is considered according to the maximum number of bits (as 12) defined in [174]. Low-order QAM, such as 16QAM, is not considered for comparison with the CRLB, because as shown in Fig. 5.6, the EXIT chart of 16QAM is almost horizontal, which means that its iterations gain is negligible. Hence 16QAM cannot benefit from the proposed DD estimation. Our observations ares discussed as follows. Firstly, the proposed 'Blind+DD' algorithm outperforms the 'Blind' method and it is capable of achieving the CRLB. Secondly, the normalized MSE of the 'Blind+DD' method becomes lower when we increase the number of samples used for estimation in a single DMT symbol, because the accuracy of the estimation can be improved upon increasing the number of selected samples. Therefore, we opt for 1000 samples for the DD estimation method. Thirdly, the CRLB is not dependent on the value of ℓ, which can also be observed from (5.30).

5.3.2 Data Detection

The corresponding data detection of the receiver is also shown in Fig. 5.1, which consists of the QAM soft demapper and LDPC decoder. More explicitly, the associated *a priori* information and *extrinsic* information are interleaved and exchanged between the QAM soft demapper and the LDPC decoder L_{itera} times, while the information gleaned from the QAM soft demapper is first deinterleaved and then exchanged L_{LPDC} times within the LDPC decoder. The final hard decision is carried out by the LDPC decoder in order to produce the estimated $\hat{\boldsymbol{b}}$ of the transmitted bits $\boldsymbol{b}$.

For the ease of explanation, the information exchanged between the components during data detection, in terms of the LLRs, as shown in Fig. 5.1, is defined as follows:

- $\boldsymbol{L_a}(\boldsymbol{d})$, $\boldsymbol{L_p}(\boldsymbol{d})$, $\boldsymbol{L_e}(\boldsymbol{d})$: the *a priori*, *a posteriori* and *extrinsic* LLRs, respectively, associated with the QAM soft demapper.
- $\boldsymbol{L_a}(\boldsymbol{c})$, $\boldsymbol{L_p}(\boldsymbol{c})$, $\boldsymbol{L_e}(\boldsymbol{c})$: the *a priori*, *a posteriori* and *extrinsic* LLRs, respectively, associated with the LDPC decoder.

For Q-ary QAM associated with the alphabet $\boldsymbol{\mathcal{X}}$ as detailed in Section II-A, the *a posteriori* LLRs of the received signal can be calculated by the log-Maximum A Posterior (Log-MAP) algorithm [197] with the aid of the estimated $\hat{\iota}$, as:

$$\begin{aligned}\boldsymbol{L_p}(\boldsymbol{d}(i)) &= \log\left(\frac{\sum_{\forall X^q \in \boldsymbol{\mathcal{X}}_{\boldsymbol{d}(i)=1}} p(X^q|Y_n)}{\sum_{\forall X^q \in \boldsymbol{\mathcal{X}}_{\boldsymbol{d}(i)=0}} p(X^q|Y_n)}\right) \\ &= \log\left(\frac{\sum_{\forall X^q \in \boldsymbol{\mathcal{X}}_{\boldsymbol{d}(i)=1}} p(Y_n|X^q)p(X^q)}{\sum_{\forall X^q \in \boldsymbol{\mathcal{X}}_{\boldsymbol{d}(i)=0}} p(Y_n|X^q)p(X^q)}\right),\end{aligned} \tag{5.33}$$

where $\boldsymbol{\mathcal{X}}_{\boldsymbol{d}(i)=1}$ and $\boldsymbol{\mathcal{X}}_{\boldsymbol{d}(i)=0}$ denote the Q-ary QAM subsets, when the specific bit $\boldsymbol{d}(i)$ is fixed to 1 and 0, respectively. Then $p(Y_n|X^q)$ can be calculated as

$$p(Y_n|X^q) = \frac{1}{\pi(\sigma_S^2 + \frac{\hat{\iota}}{N}\sigma_{I,n}^2)} \exp\Big(-\frac{|Y_n - \sqrt{\rho}X^q|^2}{\sigma_S^2 + \frac{\hat{\iota}}{N}\sigma_{I,n}^2}\Big). \tag{5.34}$$

During the first inner iteration, we have the *a priori* probability of $p(X^q) = \frac{1}{Q}$ upon assuming that the transmitted symbols are with equal probability. When the soft-demapper receives the *a priori* LLRs $\boldsymbol{L_a}(\boldsymbol{d})$ from the channel decoder of Fig. 5.1, $p(X^q)$ can be calculated as

$$p(X^q) = \prod_{i=1}^{\text{BPS}} \frac{\exp\left[\boldsymbol{d}^q(i)\boldsymbol{L_a}(\boldsymbol{d})\right]}{1 + \exp\left[\boldsymbol{L_a}(\boldsymbol{d}(i))\right]}, \tag{5.35}$$

where $\{\boldsymbol{d}^q\}_{i=1}^{\text{BPS}}$ refers to the bits mapped to the specific constellation point of $X^q \in \boldsymbol{\mathcal{X}}$.

The *extrinsic* LLRs $\boldsymbol{L_e}(\boldsymbol{d}) = \boldsymbol{L_p}(\boldsymbol{d}) - \boldsymbol{L_a}(\boldsymbol{d})$ gleaned from the QAM soft demapper

are deinterleaved and fed in form of the *a priori* LLRs $\boldsymbol{L_a(c)}$ into the LDPC decoder of Fig. 5.1. Then the updated *extrinsic* LLRs $\boldsymbol{L_e(c)}$ are fed back and interleaved again as the *a priori* LLRs to the QAM soft demapper of Fig. 5.1 for the next iteration. After the convergence of the iterations both within the LDPC decoder and between the QAM soft-demapper and the LDPC decoder or after the predefined iteration limits specified by L_{itera} and L_{LDPC} are met, the LDPC decoder will finally carry out a hard-decision yielding $\hat{\boldsymbol{b}}$.

5.4 EXIT Chart and BER Performance Evaluation

Let us now investigate the achievable performance of our joint impulsive noise estimation and data detection schemes shown in Fig. 5.1. A $1/2$-rate 61380-bit LDPC code and the min-sum decoding algorithm having the maximum number of decoding iterations given by 25 and 100 were adopted for the channel code. The samples spanning from 1 to 300 were used for the blind estimator and the samples spanning from 1 to 1000 were used for the DD estimator. The SNR of the system is set to ρ/σ_S^2, which represents the received signal power normalized by the stationary noise of each tone. The achievable performance is assessed through two examples in terms of two metrics: the achievable BER and the EXIT charts, as follows.

5.4.1 Example 1

A DMT-based system associated with $N = 2048$ using 16QAM under the impulsive noise model of DT central office (CO) was simulated. An interleaver length of 900 DMT symbols was used.

Fig. 5.6 plots the EXIT chart of the LDPC decoder and of the soft demapper for different types of impulsive noise variance knowledge, namely for perfect knowledge, for the knowledge extracted from the proposed blind estimator and no knowledge. The selected samples used for blind estimation are those spanning from 1 to 300. The impulsive noise model is parametrized by DT(CO) as shown in Fig 5.3. Our observations are listed as follows. Firstly, the EXIT curve of the soft demapper gleaning its knowledge from the blind estimator is above that of the scenario operating without estimation and it is quite close to the case with perfect knowledge. Hence, as expected the blind estimation method is capable of providing a more reliable LLR for the soft demapper. Secondly, the EXIT curve of the 16QAM soft-demapper is almost horizontal, while the *extrinsic* LLR of 4096QAM soft demapper increases visibly upon the increasing the *apriori* LLRs. This is because 16QAM has no iteration gains, while 4096QAM benefits from increasing the number of the iterations between the soft demapper and the channel decoder. Thirdly, as shown in Fig. 5.6b, there is still a gap in the EXIT curve of the QAM soft demapper having per-

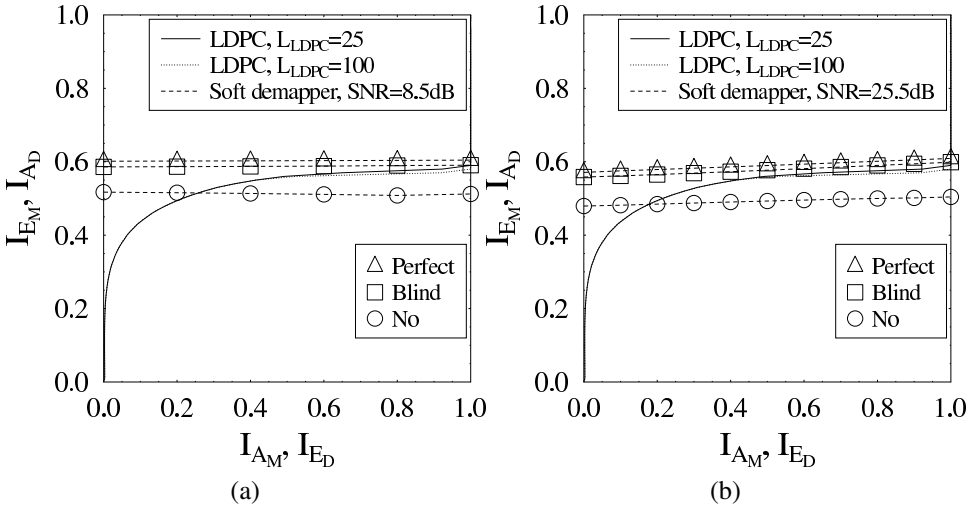

Figure 5.6: EXIT chart of the QAM demapper Fig. 5.1 with different impulsive noise variance knowledge: Perfect (perfect estimation), Blind (blind estimation) and No (no estimation). The impulsive noise is configured according to the statistical model of DT central office (CO). The modulation schemes are (a) 16QAM; (b): 4096QAM. The indeces of the samples used for blind estimation span from 1 to 300. L_{LDPC} refers to the number of iterations within the LDPC decoder.

fect knowledge and that relying on the blind estimation. Hence, the DD estimator can be incorporated into the iterative loop of high-order QAM schemes during further iterations. Fourthly, increasing the number of inner iterations within the LDPC decoder from 25 to 100 improves its EXIT-chart performance albeit the improvement is not very significant.

As shown in Fig. 5.6a, the EXIT curve of the 16QAM soft-demapper is almost horizontal, which means that the iteration gain of 16QAM is negligible. Therefore, it is desired to opt for a higher number L_{LDPC} of inner iterations and lower number L_{itera} of outer iterations. The BER performance of the proposed joint impulsive noise estimation and data detection scheme is shown in Fig. 5.7, in comparison to that of the perfect variance knowledge and of no knowledge of the impulsive noise variance. Our observations are discussed as follows. Firstly, the error floor is formed for the system without impulsive noise estimation, which is explained as follows. The channel state information and noise variance level as well as the received signal are fed into the QAM soft-demapper at the receiver of Fig. 5.1. If we rely on using the stationary noise variance level to detect the samples suffering from impulsive noise, unreliable LLRs will be calculated, which may result in error bursts. Secondly, our proposed joint impulsive noise estimation and data detection aided 16QAM has a similar BER performance to that associated with perfect knowledge of the impulsive noise variance and exhibits a significant improvement over that operating without IN variance estimation. Thirdly, the E_b/N_0 gap between our proposed scheme and the maximum achievable limit is as low as 1.7 dB, hence our scheme is capable of attaining a near-capacity performance.

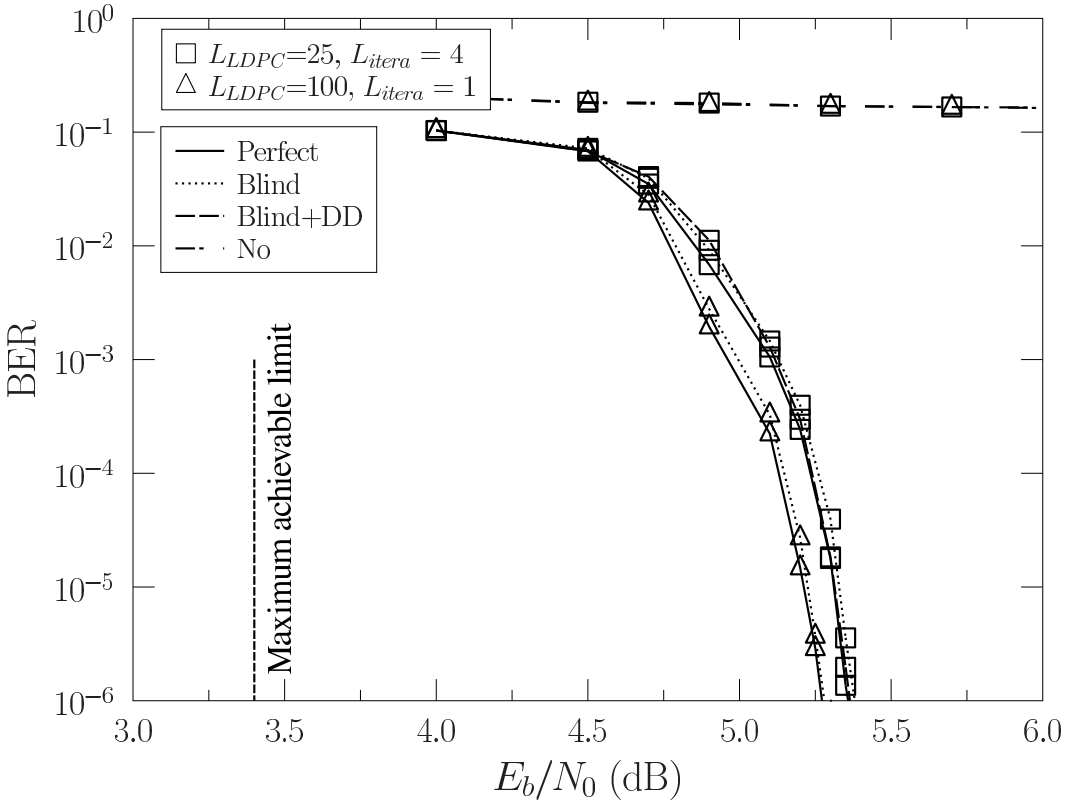

Figure 5.7: BER performance of 16QAM for various impulsive noise variance knowledge. The impulsive noise is modelled according to the parameters specified by DT(CO). The interleaver length is 900 DMT symbols. The lines correspond to the different types of impulsive noise variance knowledge: 'Perfect' (perfect knowledge), 'Blind' (Blind estimation without DD estimation, 'Blind+DD' (blind estimation and 3 more DD estimation) and 'No' (no knowledge).

5.4.2 Example 2

The system setup is identical to that of Example 1, except that 4096QAM was employed. As discussed above, 4096QAM has a significant iteration gain and hence it is desired to use a higher number L_{itera} of outer iterations and a lower number L_{LDPC} of the inner iterations. We can select the optimal number of outer iterations with the aid of Fig. 5.8. On one hand, it can be observed that our proposed scheme achieves a better BER performance, when we increase the number L_{itera} of outer iterations. On the other hand, the improvement becomes smaller, when L_{itera} increases. To elaborate a little further, the SNR gap between 'Blind+3DD' and 'Blind+4DD' is small, but 'Blind+4DD' requires a further outer iteration. Considering the trade off between the complexity and the BER performance, the system 'Blind+3DD' is deemed to be the most attractive, hence it is selected for our further investigations.

Fig. 5.9 plots our EXIT chart analysis, where the soft-demapper is fed by our proposed estimation method, or alternatively, it relies on perfect impulsive noise variance knowledge, respectively. Since the EXIT curve of the soft-demapper associated with the DD

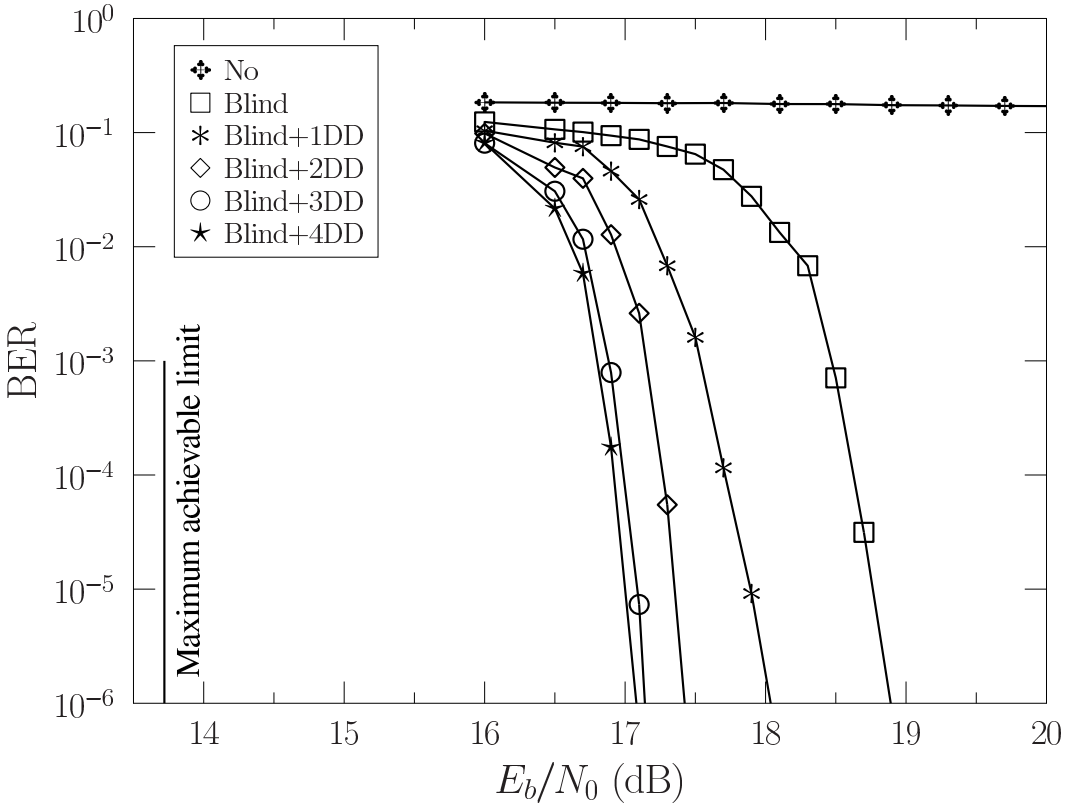

Figure 5.8: BER performance of 4096QAM for various impulsive noise variance estimation methods. The impulsive noise is modelled according to the parameters specified by DT(CO). The interleaver length is 900 DMT symbols. The symbols represent the different types of impulsive noise estimations: 'No' (no estimation), 'Blind' (blind estimation), 'Blind+jDD' (blind estimation with j more iterations DD estimation). The outer iterations for each case can be calculated as $L_{itera} = j + 1$.

estimator cannot be plotted, only the EXIT curve of perfect knowledge is plotted. It can be inferred that an open tunnel emerges at SNR $=$ 25 dB. The two stair-case shaped decoding trajectories were recorded for the soft-demapper fed with the exact impulsive noise variance information, or by that estimated using our proposed algorithm. The point of convergence around $(1.0, 0.6)$ is reached by both types of variance estimation schemes relying on $L_{\text{itera}} = 4$ iterations, which means that the proposed scheme is capable of approaching the optimal ML detection performance recorded for perfect variance knowledge at the same number of iterations.

Fig. 5.10 shows the BER performance of different combinations of our proposed joint impulsive noise estimation and data detection scheme under the DT(CO) impulsive noise model, in comparison to both the perfect knowledge and no knowledge scenarios. Our observations are listed as follows. Firstly, the E_b/N_0 gap between the schemes fed with our 'Blind+DD' estimation results and with perfect impulsive noise variance knowledge is less 0.1dB, when we have $L_{\text{itera}} = 4$ and $L_{\text{LDPC}} = 25$. Secondly, it requires 1.2 dB lower SNR for the 'Blind+DD' method to attain BER $= 10^{-6}$ than for the 'Blind' method, which

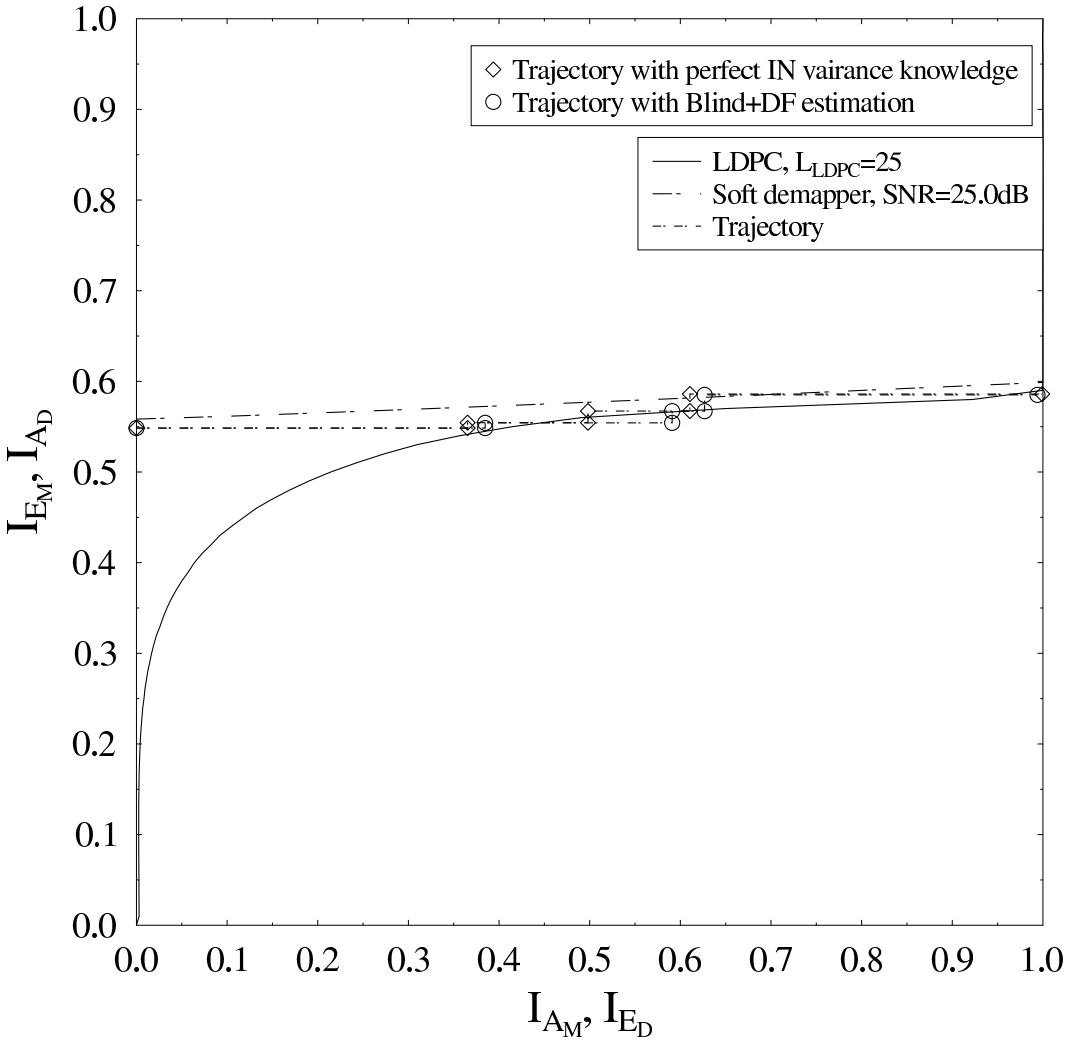

Figure 5.9: EXIT chart of 4096QAM for perfect impulsive noise variance knowledge. The impulsive noise is modelled according to the parameter specified by DT(CO). The interleaver length is 900 DMT symbols. 'Blind+DD' refers to blind estimation with 3 additional iterative DD estimations.

means that our proposed DD estimator beneficially improves the performance. Thirdly, the E_b/N_0 gap between our proposed scheme and the maximum achievable limit is 3.4 dB at BER $= 10^{-6}$. Therefore we conclude that our proposed joint estimation and decoding relying on the 'Blind+DD' scheme is capable of achieving a near-capacity performance.

5.4.3 Effect of Interleaver Length

Since using the interleaver length of 900 DMT symbols is not plausible for some application scenarios, we investigate the effect of the interleaver length by simulations. The system setup is identical to the case of Example 1 and Example 2, except for employing an interleaver length of 90 DMT symbols, as seen in Fig. 5.11 and Fig. 5.12 for 16QAM and 4096QAM, respectively. The different schemes have the same trends as in the above examples. Comparing them to the corresponding performance in Fig. 5.7 an Fig. 5.10, it

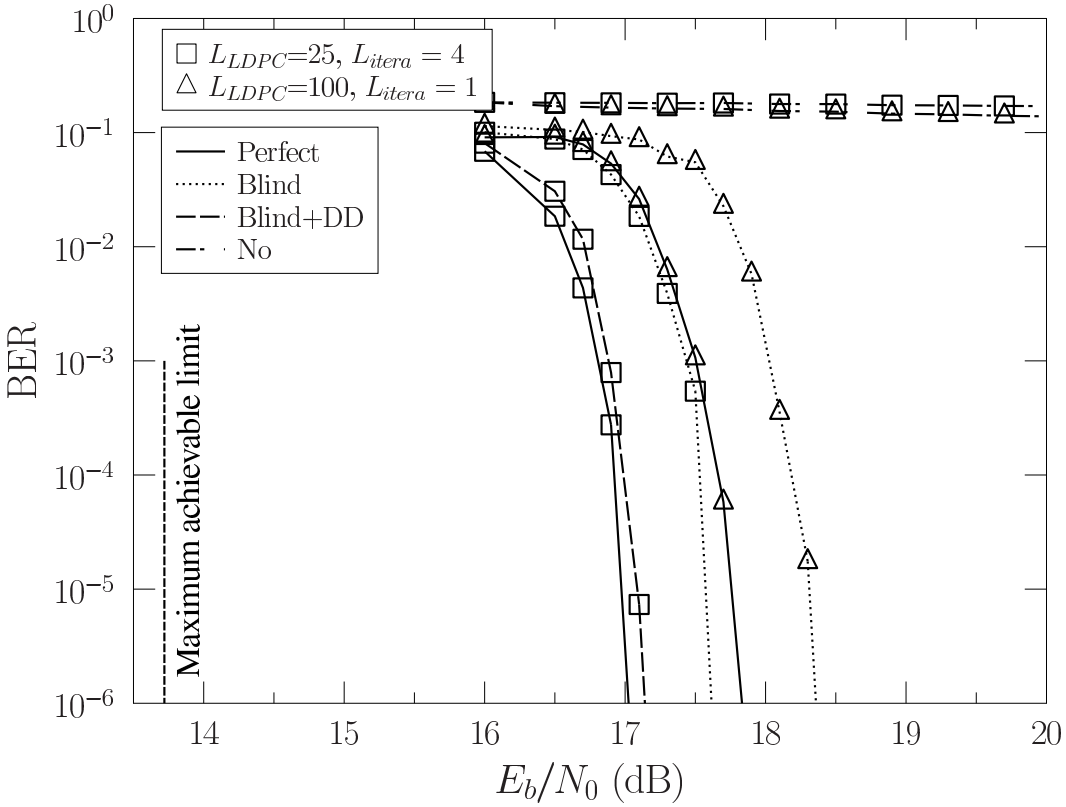

Figure 5.10: BER performance of 4096QAM for various impulsive noise variance provision methods. The impulsive noise is modelled according to the parameters specified by DT(CO). The lines in the figure correspond to different types of impulsive noise variance knowledge: 'Perfect' (perfect knowledge), 'Blind' (Blind estimation without DD estimation, 'Blind+DD' (blind estimation and 3 more DD estimation) and 'No' (no knowledge).

can be inferred that the system associated with an interleaver length of 90 DMT symbols requires about 1.3 dB and 2 dB higher E_b/N_0 to achieve the point of BER $= 10^{-6}$, which is explained as follows. Even if the reliable LLRs of the samples suffering from impulsive noise can be calculated by our proposed estimation algorithm, the LLRs still remain relatively small and the corresponding bits have to be recovered with the aid of the neighbouring LLRs. The system having a shorter interleaver length sometimes fails to spread these LLRs uniformly, hence the channel decoder cannot recover all the transmitted bits. However, compared to the BER performance recorded without impulsive noise estimation, our proposed method is still capable of significantly improving the system performance.

5.5 Chapter Summary

Observing the numerical results, we may conclude that the proposed two-stage impulsive noise estimation algorithm is capable of achieving the lower bound of the solution to the unbiased estimation problem. This in turn effectively improve the robustness of our data

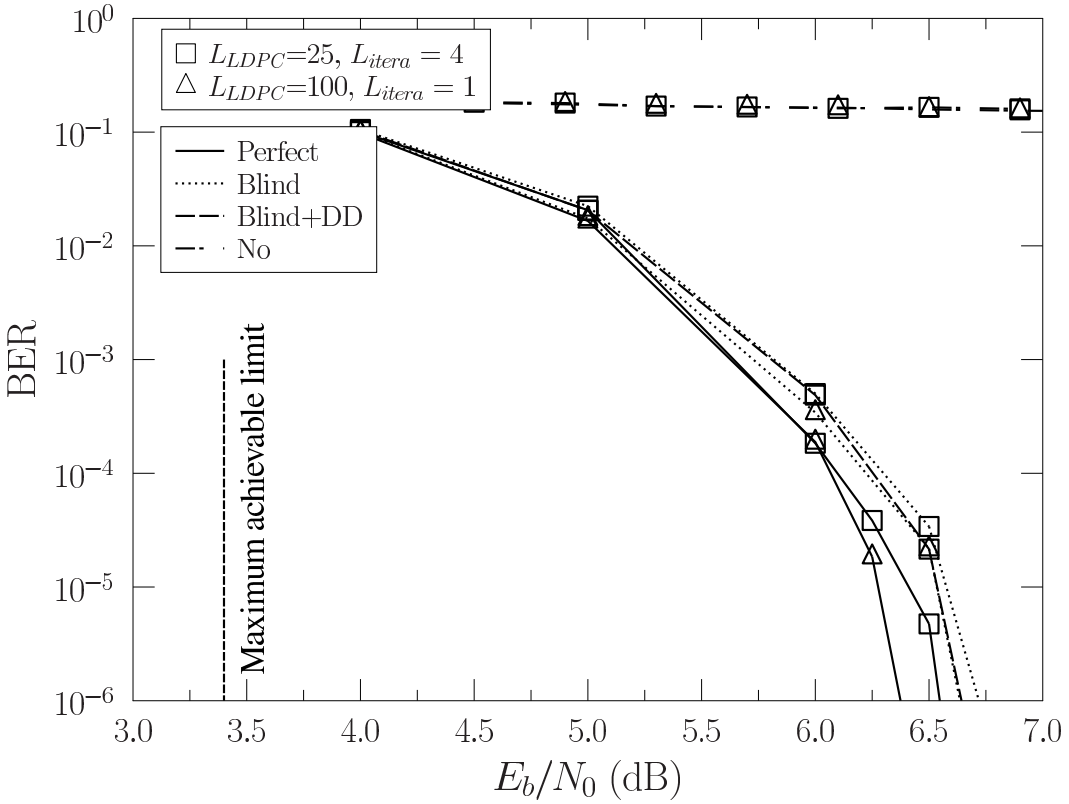

Figure 5.11: BER performance of 16QAM for various impulsive noise variance estimation methods. The impulsive noise is modelled according to the parameters specified by DT(CO). The interleaver length is 90 DMT symbols. The lines in the figure correspond to the different types of impulsive noise variance knowledge: 'Perfect' (perfect knowledge), 'Blind' (Blind estimation without DD estimation, 'Blind+DD' (blind estimation and 3 more DD estimation) and 'No' (no knowledge).

detection. Moreover, the iterative process between the impulsive noise estimation and the data detection substantially improves the system's BER performance, especially when a high-order modulation scheme is invoked. Finally, the system's BER performance is also dependent on the length of interleaver, since an interleaver of a long length is likely to spread the unreliable LLRs uniformly, which can be readily corrected by exploiting the LLRs in vicinity.

In a nutshell, the major challenge in coded DSL systems operating in the presence of impulsive noise has been the acquisition of the reliable LLRs from the samples suffering from impulsive noise. We have proposed a two-stage impulsive noise estimation algorithm for determining the arrival instant and the variance of impulsive noise, so that reliable LLRs of the samples inflicting impulsive noise can be calculated. The MSE and CRLB results characterize the accuracy of the blind estimation method and of our DD estimation method. Based on the results, we also select the appropriate samples for two different estimation methods in our system considered. We have also optimized the joint estimation and data detection scheme conceived for our LDPC coded DMT-based DSL

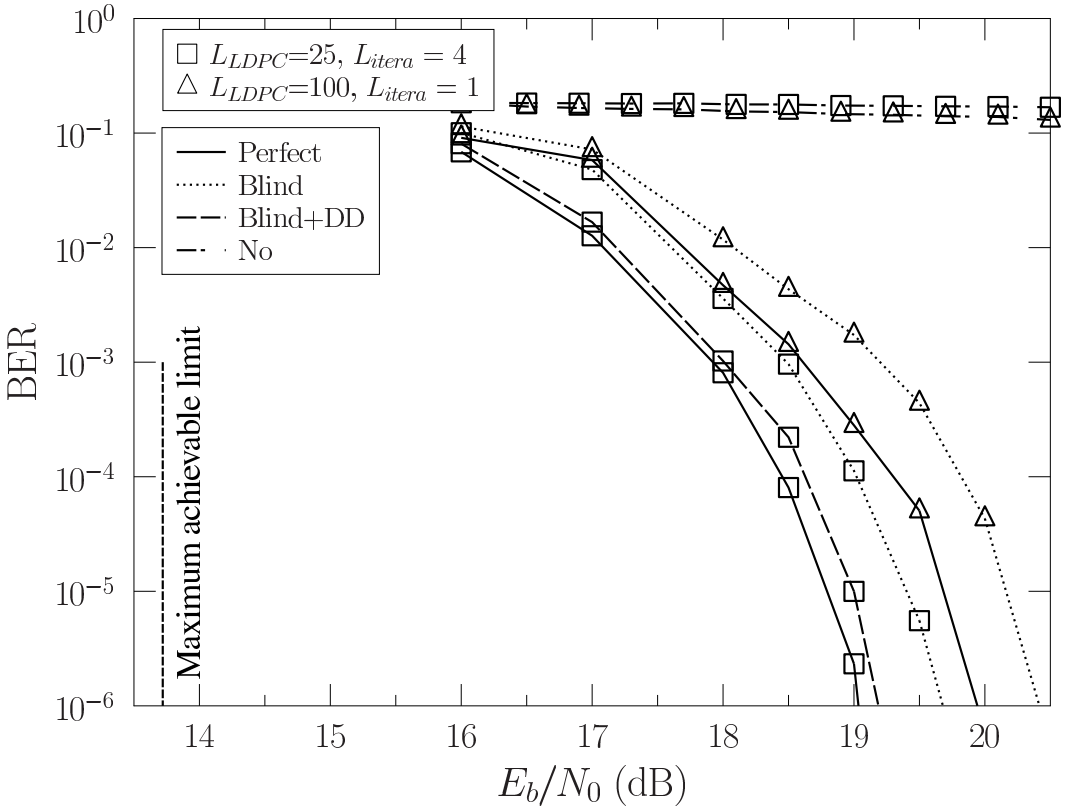

Figure 5.12: BER performance of 4096QAM for various impulsive noise variance estimation methods. The impulsive noise is modelled according to the parameters specified by DT(CO). The interleaver length is 90 DMT symbols. The lines in the figure correspond to the different types of impulsive noise variance knowledge: 'Perfect' (perfect knowledge), 'Blind' (Blind estimation without DD estimation, 'Blind+DF' (blind estimation and 3 more DD estimation) and 'No' (no knowledge).

systems two different estimation methods in our system considered, with the aid of EXIT chart. Our extensive simulation results have confirmed that the proposed scheme is capable of providing accurate impulsive noise variance estimation, and exhibiting a near-capacity performance associated with the idealized perfect impulsive noise variance knowledge at a low number of iterations.

Derivation of the MSE

Here let us introduce the short-hand of $\Omega = \frac{1}{N}\sum \sigma_{I,n}^2$ and $\Psi = \rho K + \sigma_S^2 K$. Then MSE of the estimated value $\hat{\ell}$ is expressed as

$$\begin{aligned}
\mathrm{MSE}_{\hat{\ell}} &= \mathbb{E}\{(\ell - \hat{\ell})^2\} \\
&= \mathbb{E}\left\{\left(\ell - \frac{\boldsymbol{Y}_{sel}^H \boldsymbol{Y}_{sel}}{\Omega} + \frac{\Psi}{\Omega}\right)^2\right\} \\
&= \mathbb{E}\left\{\left(\ell + \frac{\Psi}{\Omega}\right)^2\right\} - 2\mathbb{E}\left\{\left(\ell + \frac{\Psi}{\Omega}\right)\frac{\boldsymbol{Y}_{sel}^H \boldsymbol{Y}_{sel}}{\Omega}\right\} + \mathbb{E}\left\{\left(\frac{\boldsymbol{Y}_{sel}^H \boldsymbol{Y}_{sel}}{\Omega}\right)^2\right\}. \quad (5.36)
\end{aligned}$$

Let us denote the first, second and third term of (5.36) by T_1, T_2 and T_3, respectively. Then T_2 becomes

$$\begin{aligned}
&2\mathbb{E}_{(\ell,\rho,\sigma_S,\sigma_I,\boldsymbol{X})}\left\{\left(\ell + \frac{\Psi}{\Omega}\right)\frac{\boldsymbol{Y}_{sel}^H \boldsymbol{Y}_{sel}}{\Omega}\right\} \\
&= 2\mathbb{E}_{(\ell,\rho,\sigma_S,\sigma_I)}\left\{\left(\ell + \frac{\Psi}{\Omega}\right)\mathbb{E}_{\boldsymbol{X}}\left\{\frac{\boldsymbol{Y}_{sel}^H \boldsymbol{Y}_{sel}}{\Omega}\right\}\right\} \\
&= 2\mathbb{E}\left\{\left(\ell + \frac{\Psi}{\Omega}\right)^2\right\}\Big\}. \quad (5.37)
\end{aligned}$$

Furthermore, T_3 can be expanded as

$$\begin{aligned}
&\mathbb{E}\left\{\left(\frac{\boldsymbol{Y}_{sel}^H \boldsymbol{Y}_{sel}}{\Omega}\right)^2\right\} \\
&= \frac{1}{\Omega^2}\mathbb{E}\Big\{\Big(\rho\sum X_n^* X_n\Big)^2 + 2\Big(\rho\sum X_n^* X_n\Big) \times \Big(N_{S,n}^* N_{S,n} + N_{I,n}^* N_{I,n} + 2\Re(N_{I,n}^* N_{S,n}) \\
&\quad + 2\sqrt{\rho}\Re(X_n^* N_{S,n}) + 2\sqrt{\rho}\Re(X_n^* N_{I,n})\Big) + \Big(N_{S,n}^* N_{S,n} + N_{I,n}^* N_{I,n} + 2\Re(N_{I,n}^* N_{S,n}) \\
&\quad + 2\sqrt{\rho}\Re(X_n^* N_{S,n}) + 2\sqrt{\rho}\Re(X_n^* N_{I,n})\Big)^2\Big\} \\
&= \frac{\rho^2 K^2 + 2\rho K^2\sigma_S^2 + 2\rho K\Omega\mathbb{E}[\ell]}{\Omega^2} + \frac{1}{\Omega^2}\mathbb{E}\Big\{\Big(N_{S,n}^* N_{S,n} + N_{I,n}^* N_{I,n} \\
&\quad + 2\Re(N_{I,n}^* N_{S,n}) + 2\sqrt{\rho}\Re(X_n^* N_{S,n}) + 2\sqrt{\rho}\Re(X_n^* N_{I,n})\Big)^2\Big\}. \quad (5.38)
\end{aligned}$$

The second term of (5.38), denoted by T_{32} can then be expanded as

$$\begin{aligned}
T_{32} &= \frac{1}{\Omega^2}\Big\{\mathbb{E}\Big\{\Big(\sum N_{S,n}^* N_{S,n}\Big)^2\Big\} + \mathbb{E}\Big\{\Big(\sum N_{I,n}^* N_{I,n}\Big)^2\Big\} + \mathbb{E}\Big\{2\Big(\sum N_{S,n}^* N_{S,n}\Big)\Big(\sum N_{I,n}^* N_{I,n}\Big)\Big\} \\
&\quad + \mathbb{E}\Big\{4\rho\Big[\sum \Re(X_n^* N_{S,n})\Big]^2\Big\} + \mathbb{E}\Big\{4\rho\Big[\sum \Re(X_n^* N_{I,n})\Big]^2\Big\} + \mathbb{E}\Big\{4\Big[\sum \Re(N_{S,n}^* N_{I,n})\Big]\Big\}\Big\} \\
&= \frac{1}{\Omega^2}\Big\{\mathrm{MSE}_1 + \mathrm{MSE}_2 + \mathrm{MSE}_3 + \mathrm{MSE}_4 + \mathrm{MSE}_5 + \mathrm{MSE}_6\Big\}. \quad (5.39)
\end{aligned}$$

To expound further, MSE_1 can be simplified as

$$\begin{aligned}\mathrm{MSE}_1 &= \mathbb{E}\Big[\sum |N_{S,n}|^4\Big] + \mathbb{E}\Big[\sum |N_{S,n}|^2 \sum_{n\neq m} |N_{S,m}|^2\Big] \\ &= 2K\sigma_S^2 + (K^2-K)\sigma_S^2 \\ &= (K^2+K)\sigma_S^2. \end{aligned} \tag{5.40}$$

Similarly, MSE_2 can be simplified as

$$\begin{aligned}\mathrm{MSE}_2 &= \mathbb{E}\Big[\sum |N_{I,n}|^4\Big] + \mathbb{E}\Big[\sum |N_{I,n}|^2 \sum_{n\neq m} |N_{I,m}|^2\Big] \\ &= \frac{2\mathbb{E}[\ell^2]}{N}\sum \sigma_{I,n}^4 + \frac{\mathbb{E}[\ell^2]}{N^2}\sum_{n=M}^{M+K-1} \sigma_{I,n}^2 (\sum_{n\neq m} \sigma_{I,j}^2) \\ &= \frac{\ell^2}{N}\sum \sigma_{I,n}^4 + \Omega^2\ell^2. \end{aligned} \tag{5.41}$$

While MSE_3 can be simplified to

$$\mathrm{MSE}_3 = 2K\sigma_S^2\Omega\ell. \tag{5.42}$$

Substituting $\Re(X_n^* N_{S,n}) = \Re(X_n^*)\Re(N_{S,n}) + \Im(X_n^*)\Im(N_{S,n})$ into MSE_4, we have

$$\begin{aligned}\mathrm{MSE}_4 &= 4\rho\mathbb{E}\Big\{\sum(\Re(X_n^*))^2(\Re(N_{S,n}))^2\Big\} + 4\rho\mathbb{E}\Big\{\sum(\Im(X_n^*))^2(\Im(N_{S,n}))^2\Big\} \\ &= \sum\frac{1}{2}\frac{\sigma_S^2}{2} + \sum\frac{1}{2}\frac{\sigma_S^2}{2} \\ &= 2\rho K\sigma_S^2. \end{aligned} \tag{5.43}$$

Similarly, substituting $\Re(X_n^* N_{I,n}) = \Re(X_n^*)\Re(N_{I,n}) + \Im(X_n^*)\Im(N_{I,n})$ into MSE_4, we have

$$\begin{aligned}\mathrm{MSE}_5 &= 4\rho\mathbb{E}\Big\{\sum(\Re(X_n^*))^2(\Re(N_{I,n}))^2\Big\} + 4\rho\mathbb{E}\Big\{\sum(\Im(X_n^*))^2(\Im(N_{I,n}))^2\Big\} \\ &= 2\rho\Omega\ell. \end{aligned} \tag{5.44}$$

Similarly,

$$\mathrm{MSE}_6 = 2\sigma_S^2\Omega\ell. \tag{5.45}$$

In this way, it is easy to get T_{32} from all the MSE_i contributions. Summing up T_1, T_2 and T_3, we arrive at the MSE of the estimated $\hat{\ell}$ as

$$\mathrm{MSE}(\hat{\ell}) = \frac{\sum\sigma_{I,n}^4}{N^2\Omega^2}\ell^2 + \frac{2(\rho+\sigma_S^2)}{\Omega}\ell + \frac{K\sigma_S^4}{\Omega^2}. \tag{5.46}$$

Since the stationary noise power is much lower than that of the impulsive noise, the third term is negligible. The first term dominates $\mathrm{MSE}_{\hat{\ell}}$, when ρ is relatively small. The second term has a significant impact on the $\mathrm{MSE}_{\hat{\ell}}$, when ρ is increasing. Therefore, the proposed estimation method works well in the relatively low SNR range.

Derivation of the CRLB

For the tone having an index n in the DMT symbol, the received signal is expressed as

$$\begin{aligned} Y_n &= \sqrt{\rho}X_n + N_{I,n} + N_{S,n} \\ &= \sqrt{\rho}X_n + \sqrt{\frac{\ell}{N}} \cdot \sigma_{I,n} \cdot W_{I,n} + \sigma_S \cdot W_{S,n}, \end{aligned} \tag{5.47}$$

where $W_{I,n}$ and $W_{S,n}$ are zero-mean unit-variance Gaussian variables. Then it is easy to obtain

$$Y_n - \sqrt{\rho}X_n = \sqrt{\frac{\ell}{N}}\sigma_{I,n}W_{I,n} + \sigma_S \cdot W_{S,n}. \tag{5.48}$$

Then $Y_n - \sqrt{\rho}X_n$ is Gaussian with zero mean and an $(K \times K)$-element covariance matrix. Let us denote the covariance of the left side as $\mathbf{C}(\ell)$, whose $[i,j]$th element is

$$\begin{aligned} [\mathbf{C}(\ell)]_{ij} &= \mathbb{E}\left[\left(\sqrt{\frac{\ell}{N}}\sigma_{I,i}W_{I,i} + \sigma_S \cdot W_{S,i} \right) \left(\sqrt{\frac{\ell}{N}}\sigma_{I,j}W_{I,j} + \sigma_S \cdot W_{S,j} \right)^* \right] \\ &= \frac{\ell}{N}\sigma_{I,i}^2\delta_{ij} + \sigma_S^2\delta_{ij}. \end{aligned} \tag{5.49}$$

Therefore,

$$\mathbf{C}(\ell) = \mathrm{diag}\left\{ \frac{\ell\sigma_{I,M}^2}{N} + \sigma_S^2, \frac{\ell\sigma_{I,M+1}^2}{N} + \sigma_S^2, \cdots, \frac{\ell\sigma_{I,M+K-1}^2}{N} + \sigma_S^2 \right\}, \tag{5.50}$$

where $\mathrm{diag}\{\boldsymbol{a}\}$ refers to the diagonal matrix with elements in $\boldsymbol{a}$ on its diagonal. We have

$$\mathbf{C}^{-1}(\ell) = \mathrm{diag}\left\{ \frac{1}{\frac{\ell}{N}\sigma_{I,M}^2 + \sigma_S^2}, \frac{1}{\frac{\ell}{N}\sigma_{I,M+1}^2 + \sigma_S^2}, \cdots, \frac{1}{\frac{\ell}{N}\sigma_{I,M+K-1}^2 + \sigma_S^2} \right\}. \tag{5.51}$$

Furthermore, since

$$\frac{\partial \mathbf{C}(\ell)}{\partial \ell} = \mathrm{diag}\left\{ \frac{1}{N}\sigma_{I,M}^2, \frac{1}{N}\sigma_{I,M+1}^2, \cdots, \frac{1}{N}\sigma_{I,M+K-1}^2 \right\}. \tag{5.52}$$

we have

$$\begin{aligned}&\mathbf{C}^{-1}(\ell)\frac{\partial \mathbf{C}(\ell)}{\partial \ell}\\ &= \text{diag}\Big\{\frac{\sigma_{I,M}^2}{\ell\sigma_{I,M}^2+N\sigma_S^2}, \frac{\sigma_{I,M+1}^2}{\ell\sigma_{I,M+1}^2+N\sigma_S^2}, \cdots, \frac{\sigma_{I,M+K-1}^2}{\ell\sigma_{I,M+K-1}^2+N\sigma_S^2}\Big\}. \end{aligned} \tag{5.53}$$

According to [198], the Fisher information matrix is expressed as

$$\begin{aligned}\boldsymbol{I}(\ell) &= \text{tr}\Big[\Big(\mathbf{C}^{-1}(\ell)\frac{\partial \mathbf{C}(\ell)}{\partial \ell}\Big)^2\Big]\\ &= \sum_{n=M}^{M+K-1}\frac{(\sigma_{I,n}^2)^2}{(\ell\sigma_{I,n}^2+N\sigma_S^2)^2}. \end{aligned} \tag{5.54}$$

Therefore, the CRLB becomes:

$$\begin{aligned}\text{CRLB}(\hat{\ell}) &= \frac{1}{\boldsymbol{I}(\ell)}\\ &= \frac{1}{\sum_{n=M}^{M+K-1}\frac{(\sigma_{I,n}^2)^2}{(\ell\sigma_{I,n}^2+N\sigma_S^2)^2}}. \end{aligned} \tag{5.55}$$

Chapter 6

Conclusions and Future Research

In Section 6.1, we summarize the main findings of our investigations, while a range of ideas concerning future research is presented in Section. 6.2.

6.1 Summary and Conclusions

In this thesis, we have provided the performance analysis of DSL techniques and investigated their impairment mitigation solutions in the face of impulsive noise. In particular, we have analyzed the performance both of uncoded as well as coded systems and then proposed a joint impulsive noise estimation and symbol detection algorithm, as detailed below.

Chapter 1: In Section 1.1 and Section 1.2, we detailed our motivation and introduced the family of DSL solutions relying both on twisted pairs. Our discussions have shown that DSL constitutes a compelling technique for supporting home area networks, as a benefit of its cost-efficiency and high-quality data transmission service. In Section 1.3, we briefly outlined the detrimental influence of impulsive noise imposed on DSL and demonstrated the necessity of performance analysis and impairment mitigation in the face of impulsive noise. Our studies have shown that the impulsive noise severely degrades the DSL system's throughput and reliability. Hence a quantitative investigation of these deleterious effects is warranted with a view to conceive efficient mitigation techniques. In Section 1.4, the state-of-the-art of DSL techniques was reviewed in the context of mitigation both at transmitter and at the receiver.

Chapter 2: We outlined the parameters characterizing both the background and the impulsive noise in Section 2.2, including the impulse duration and IAT as well as PSD. In Section 2.3, we presented the existing empirical noise models used in DSL.

Our investigations have shown that the amplitude of impulsive noise obeys a non-Gaussian distribution and the duration of impulses is typically long enough for contaminating several consecutive OFDM symbols. Hence impulse noise imposes substantial detrimental effects on the classic receivers that were originally designed for stationary noise processes. In this context, a range of empirical models have been conceived for accurately reflecting the nature of impulsive noise. However, they are often modeled by its mathematically intractable functions which do not lend themselves to convenient performance analysis and system design. To overcome this impediment, a range of simplified mathematical models have been proposed, which were reviewed in Section 2.4. Specifically, we classified them into discontinuous and bursty approaches, which are routinely used to model the noise in systems relying on interleaving or dispensing with interleaving, respectively.

Chapter 3: We analyzed the performance of DMT-based DSL systems in the face of impulsive noise. In Section 3.1, we discussed the relevant existing work. Our discussions have shown that the performance of DSL systems can be readily analyzed using an empirical noise model in the context of DMT-based systems. In Section 3.2, we described the DMT signaling and the noise model that we considered. Since the BER performance is directly dependent on the number of samples that are contaminated by impulsive noise, we analyzed the statistics of noise samples both in the time domain and in the frequency domain in Section 3.3, with the aid of the hidden-semi Markov model. Bearing in mind that the impulsive noise is colored in the frequency domain, we further investigated the feasibility of using the conventional Q-function in Section 3.4. Our investigations have shown that the distribution of the received noise obeys Gaussian distribution after the DFT-based demodulation, which is a consequence of the central limit theorem. Then, the closed-form BER formula is readily obtained for Q-ary QAM. The simulation results presented in Section 3.5 verified our analysis. Moreover, it can be inferred that the DSL system inflicting impulsive noise requires almost 55 dB higher SNR to attain the same BER performance as that in the absence of impulsive noise. In this way, we have quantitatively demonstrated the necessity of impulsive noise mitigation.

Chapter 4: We analyzed the performance of two types of HARQ schemes in LDPC-coded OFDM-based systems in a finite block-length regime. In Section 4.1, we introduced the related existing work. The system model and the pair of HARQ schemes are described in Section 4.2. In Section 4.3, we analyzed the outage probability of the systems equipped with no HARQ as well as Type-I and Type-II HARQ. This was carried out by modifying the density evolution that was originally designed for stationary noise processes and then integrating it with our waterfall-SNR analysis. Our simulation results verified the accuracy of the analysis and have shown that

as expected, the Type-II HARQ scheme outperforms the Type-I HARQ scheme. In Section 4.4, we further analyzed the performance in terms of both the expected number of retransmissions and the goodput of these HARQ schemes. Our studies have shown that the of Type-II scheme has no advantage over the Type-I scheme when the maximum number of retransmisions is set as 1, but becomes significantly better, when we increase the retransmission limit.

Chapter 5: We firstly discussed the existing work on the joint design of impulsive noise estimation and data detection in Section 5.1. In Section 5.2, we described both the transceiver and the noise model, which are in line with the recent DSL standard and empirical modeling. We then presented our two-stage impulsive noise estimation and data detection scheme in Section 5.3. Specifically, the initial data detection is based on blind impulsive noise estimation. Then the detected bits are re-modulated and fed back to the decision-directed impulsive noise estimation. This iterative process continues until we arrive at an error-free state or exhaust the maximum number of iterations. Our analytical and simulation results confirm that the proposed estimation method is capable of approaching the Cramer-Rao lower bound. In Section 5.4, we optimized the number of iterations involved by the joint estimation and detection process with the aid of the EXIT chart. Our simulation results have demonstrated that the proposed scheme is capable of achieving the same performance as in the idealistic scenario of perfectly knowing both the arrival time and the instantaneous power of noise impulses.

6.2 Future Research

In this section, we elaborate on a range of future research opportunities in the area of impulsive noise mitigation in DSL both in terms of noise modeling for invoking parametric mitigation, as well as in the context of hybrid mitigation techniques and machine-learning-aided impulsive noise mitigation.

6.2.1 Noise Modeling for Parametric Mitigation

Having statistical knowledge concerning the impulsive noise is a prerequisite for parametric mitigation techniques. Therefore, the characteristics of impulsive noise have to be further investigated in the new environment for supporting next-generation DSL services in the smart home. Firstly, as shown in Fig. 1.1, the optical network terminal will be deployed closer to the CPE at home, moving it from the conventional fiber-to-the-distribution-point (FTTdp) to the FTTF, which may modify the noise's amplitude as well as the duration and the IAT distributions at the ONT. Secondly, the smart home network of the future is

expected to support diverse appliances and sensors, whose switch-on/off operations potentially increase the impulsive noise imposed on the CPE. Thirdly, in order to enhance the throughput, we could aim for extending the operational spectrum upto 500 MHz. However, the system would suffer from increased impulsive noise. Nonetheless, there have been some trials already [199]. Fourthly, the existing single-input single-output (SISO) transmission is expected to be replaced by advanced multiple-input multiple-output (MIMO) techniques, which impose spatial correlation on the impulsive noise. To elaborate, the existing SISO transmission is realized by a differential mode, relying on a single twisted pair. This actually constitutes a waste of resources, because in the final drop from the frontage to the home, often two twisted pairs are available owing to the historical installment of full-duplex telephone lines. In fact, these two pairs can be bonded together, hence resulting in an additional physical link. Moreover, the advent of the so-called phantom mode enables us to create a "virtual" data stream, by mapping data using the difference between the two common mode signals on both twisted pairs. Since both pairs are physically adjacent to each other, the impulsive noise is correlated spatially due to the coupling effect. In this case, the impulsive noise of MIMO transmission becomes correlated both in the time-, frequency- and spatial-domain, which is worthy of further analysis.

6.2.2 Advanced System Analysis and Design

In contrast to the conventional Quality-of-Service (QoS) that is typically measured using packet loss rates or average throughput, the novel concept of Quality-of-Experience (QoE) entails an assessment of human expectations, feelings, perceptions, etc. and plays a crucial role in the design of the DSL-aided smart home [200].

Given that DSL channels exhibit strongly frequency-dependent characteristics as discussed in Chapter 3, adaptive bit-loading [201] can be invoked with the aid of the classic water-filling algorithms [202] for transmitting different number bits over each subcarrier. As a benefit, the system throughput can be maximized. Alternatively, spreading techniques [165] can be employed either in the time domain or in the frequency domain, which are capable of facilitating the employment of a single modulation scheme. Furthermore, the packet size of the HARQ scheme analyzed in Chapter 4, the packet size has to be carefully designed for minimizing the probability that consecutive transmission attempts of a packet are contaminated by impulsive noise. Additionally, as mentioned in Chapter 3, the amplitude of impulsive noise obeys an α-stable like distribution []. Fortunately, there have been a number of existing contributions on dealing with systems operating in α-stable environments using adaptive filters [103], which may be beneficially incorporated into DSL systems.

6.2.3 Hybrid Impulsive Noise Mitigation

Given that the impulsive noise emerging from diverse sources may exhibit different behaviors in terms of its amplitude, duration, IAT and spectrum, there is no universally applicable mitigation technique that can eliminate all these noise components. To address this issue, hybrid mitigation schemes can be conceived. For example, CS-based impulsive noise detection can also be integrated into erasure based decoding for the sake of identifying the specific impaired symbols. Moreover, the unreliable soft information representing the symbols impaired by high-magnitude impulses may also lead to unsuccessful decoding, which can be alleviated by incorporating nonlinear pre-processing that is capable of restricting the magnitude of the received signals.

6.2.4 Machine-Learning Aided Noise Mitigation

The signal processing techniques applied in communication systems have solid statistical and information theoretical foundations, which are often accompanied by tractable mathematical models, which tend to obey linear, stationary and Gaussian statistics. By contrast, the occurrence of impulsive noise in DSL introduces non-stationary and intractable factors. Hence, a machine-learning (ML) based communication system that does not require a tractable mathematical model may be capable of improving the attainable performance. On one hand, ML-based methods can be utilized for augmenting parts of the existing algorithms. For example, the generation of impulsive noise in the home is often related to the human behavior of switching on/off home appliances and other electronic devices. In this context, ML-based algorithms can be used for investigating the human behavior and accordingly predicting the arrival of impulses. In this way, both the spectral efficiency and the processing delay may potentially be improved, if the impulsive noise mitigation can be triggered during the specific instances, when impulses are indeed predicted to occur. On the other hand, inspired by the concept of the "autoencoder" [203], we may directly apply ML to the physical layer, by completely replacing the existing communication system. To elaborate, the chain of multiple independent blocks (channel codec, modem, etc.) can be replaced by a single deep learning based black box. Beneficially, we may improve the performance by exploiting the joint optimization capability of such a deep learning based black box. Moreover, the statistical knowledge of both the channel and of the noise is no longer a prerequisite. Hence, the corresponding overheads can be avoided, resulting in an enhanced spectral efficiency.

Special Operations

$\sum$: the summation of all elements.

$\prod$: the product of all elements.

$\forall$: for all elements within a certain range.

$\|\cdot\|^2$: the Euclidean norm of a vector/matrix.

$(\cdot)^H$: rhe Hermitian transpose of a matrix.

$(\cdot)^T$: rhe transpose of a matrix.

$(\cdot)^*$: rhe conjugate of a complex symbol/vector/matrix.

$\arg(x)$: the angle of a complex value x.

$\mathcal{E}(\cdot)$: The expectation function.

$\mathcal{F}(\cdot)$: the Fourier transform operator

$\mathcal{F}^{-1}(\cdot)$: the inverse Fourier transform operator

$\boldsymbol{\mathcal{F}}$: normalized discrete Fourier transform matrix.

$f(x)$: the output of a function f given a input x.

$\int_a^b f(x)\,\mathrm{d}x$: the definite integral of a function $f(x)$ over the interval $[a,b]$.

$p_X(x)$: the probability density function of a random variable $X = x$

$P_X(x)$: the cumulative density function of a random variable $X = x$

$Q(x)$: the Q-function defined as $Q(x) = \int_x^\infty \exp(-u^2/2)/\sqrt{2\pi}\,\mathrm{d}u$

$\Re(x)$: the real part of a complex value x.

$\Im(x)$: the imaginary part of a complex value x.

Glossary

2B1Q:	two-Binary one-Quaternary.
αS:	Alpha-Stable.
ACF:	Auto-Correlation Function.
ACK:	Acknowledgment.
ADSL:	Asymmetric Digital Subscriber Line.
ARMA:	Auto-Regressive Moving Average.
ARQ:	Automatic Repeat reQuest.
AWGN:	Additive White Gaussian Noise.
BER:	Bit Error Rate.
BLC:	Bit-Level Combining.
BLER:	Block Error Rate.
BGM:	Bernoulli-Gaussian Model.
BPDN:	Basis Pursuit De-Noising.
CAP:	Carrierless Amplitude/Phase Modulation.
CDF:	Cumulative Density Function.
CIS:	Compressed Impairment Sensing.
CO:	Central Office.
CRLB:	Cramer-Rao Lower Bound.
CPE:	Customer Premise Equipment

DD: Decision-Directed.

DE: Density Evolution.

DL: Deep Learning

DLC: Distance-Level Combining.

DMT: Discrete Multi-tone.

DPU: Distribution Point Unit.

DSL: Digital Subscriber Line.

DSLAM: Digital Subscriber Line Access Multiplexer.

DSM: Dynamic Spectrum Management.

ECM: Expanded Constellation Mapping.

EXIT: *Extrinsic* Information Transfer.

FDCHTF: Frequency-Domain Channel Transfer Function.

FDD: Frequency Division Duplex.

FEC: Forward Error Correction.

FEQ: Frequency-domain channel EQualizer.

FEXT: Far-End Crosstalk.

FT: Fourier Transform.

FTTF: Fiber-to-the-Frontage.

FTTH: Fiber-to-the-Home.

GBG: Gated Bernoulli-Gaussian.

GMM: Gaussian Mixture Model.

HARQ: Hybrid Automatic Repeat reQuest.

HDSL: High-rate Digital Subscriber Line.

HMM: Hidden Markov Model.

HSMM: Hidden Semi-Markov model.

IAT: Inter-Arrival Time.

IDFFT: Interleaved-Double-FFT.

IDFT: Inverse Discrete Fourier Transform.

ISDN: Integrated Services Digital Network.

ISI: Inter-Symbol Interference.

JELVA: Joint Erasure Marking and list Viterbi Algorithm.

LDPC: Low Density Parity-Check.

LLR: Log-Likelihood Ratio.

LPTV: Linear Periodic Time Variant.

LT: Luby Transform.

MCA: Middleton Class A.

MCM: Multi-Carrier Modulation.

MIMO: Multiple-Input Multiple-Output.

ML: Machine-Learning.

MMSE: Minimum Mean Square Error.

MRC: Maximum-Ratio Combining.

MSE: Mean Square Error.

NACK: Non-ACKnowledgement.

NEXT: Near-End Crosstalk.

OFDM: Orthogonal Frequency Division Multiplexing.

ONT: Optical Network Terminal.

PAPR: Peak-to-Average Power Ratio.

PA-SAMP: Priori Aided-Sparsity Adaptive Matching Pursuit.

PDF: Probability Density Function.

PMC: Partitioned Markov Chain.

PMF: Probability Mass Function.

PSD: Power Spectral Density.

QAM: Quadrature Amplitude Modulation.

RS: Reed-Solomon codes.

SISO: Single-Input Single-Output.

SNR: Signal-to-Noise Ratio.

SSM: Static Spectrum Management.

TDI: Time-Domain Interleaver.

TCM: Trellis Coded Modulation.

TDD: Time Division Duplex.

TDI-OT: Time-Domain Interleaver with additional Orthogonal Transform.

THP: Tomlinson-Harashima Precoding.

VDSL: Very high-speed Digital Subscriber Line.

ZFP: Zero-Forcing Precoding.

ZMNL: Zero Memory Non-Linearity

Bibliography

[1] R. Ferrus, O. Sallent, J. Perez-Romero, and R. Agusti, "A solution framework to provide management services for wireless communications in the digital home," *IEEE Communications Magazine*, vol. 50, no. 11, pp. 132–141, 2012.

[2] J. Maes and C. J. Nuzman, "The past, present, and future of copper access," *Bell Labs Technical Journal*, vol. 20, pp. 1–10, 2015.

[3] W. Coomans, R. B. Moraes, K. Hooghe, A. Duque, J. Galaro, M. Timmers, A. J. van Wijngaarden, M. Guenach, and J. Maes, "XG-fast: the 5th generation broadband," *IEEE Communications Magazine*, vol. 53, no. 12, pp. 83–88, 2015.

[4] T. Bai, H. Zhang, R. Zhang, L.-L. Yang, A. F. Al Rawi, J. Zhang, and L. Hanzo, "Discrete multi-tone digital subscriber loop performance in the face of impulsive noise," *IEEE Access*, vol. 5, pp. 10478–10495, 2017.

[5] P. Ödling, T. Magesacher, S. Höst, P. O. Börjesson, M. Berg, and E. Areizaga, "The fourth generation broadband concept," *IEEE Communications Magazine*, vol. 47, no. 1, pp. 62–69, 2009.

[6] T. Starr, J. M. Cioffi, and P. J. Silverman, *Understanding digital subscriber line technology*. Prentice Hall PTR, 1999.

[7] J.-J. Werner, "The HDSL environment (high bit rate digital subscriber line)," *IEEE Journal on selected areas in communications*, vol. 9, no. 6, pp. 785–800, 1991.

[8] J. M. Cioffi, S. Jagannathan, M. Mohseni, and G. Ginis, "Cupon: the copper alternative to pon 100 Gb/s DSL networks," *IEEE Communications Magazine*, vol. 45, no. 6, pp. 132–139, 2007.

[9] W. Henkel and T. Keßler, "A wideband impulsive noise survey in the German telephone network: statistical description and modeling," *Archiv fur Elektronik und Ubertragungstechnik*, vol. 48, pp. 277–277, 1994.

[10] S. Sugimoto, K. Hayashi, and F. Mano, "Design of 2B1Q transceiver for ISDN subscriber loops," in *IEEE International Conference on Communications, World Prosperity Through Communications,*, pp. 228–232 vol.1, Jun 1989.

[11] G.-H. Im and J.-J. Werner, "Bandwidth-efficient digital transmission over unshielded twisted-pair wiring," *IEEE Journal on Selected Areas in Communications*, vol. 13, pp. 1643–1655, Dec 1995.

[12] B. Daneshrad and H. Samueli, "Performance analysis of a QAM adaptive receiver for 1.6 Mbps digital subscriber line transmission," in *IEEE International Conference on Communications, 1992.*, pp. 937–941 vol.2, Jun 1992.

[13] J. Chow, J. Tu, and J. Cioffi, "A discrete multitone transceiver system for HDSL applications," *IEEE Journal on Selected Areas in Communications*, vol. 9, pp. 895–908, Aug 1991.

[14] B. Shim and N. R. Shanbhag, "Complexity analysis of multicarrier and single-carrier systems for very high-speed digital subscriber line," *IEEE Transactions on Signal Processing*, vol. 51, pp. 282–292, Jan 2003.

[15] L. Hanzo, T. Liew, B. Yeap, R. Tee, and S. X. Ng, *Turbo coding, turbo equalisation and space-time coding: EXIT-chart-aided near-capacity designs for wireless channels*, vol. 22. John Wiley & Sons, 2011.

[16] R. Gallager, "Low-density parity-check codes," *IRE Transactions on Information Theory*, vol. 8, pp. 21–28, January 1962.

[17] K. J. Kerpez, "Forward error correction for asymmetric digital subscriber lines (ADSL)," in *Global Telecommunications Conference, 1991. GLOBECOM '91.*, pp. 1974–1978 vol.3, Dec 1991.

[18] K. J. Kerpez and K. Sistanizadeh, "High bit rate asymmetric digital communications over telephone loops," *IEEE Transactions on Communications*, vol. 43, pp. 2038–2049, Jun 1995.

[19] E. Eleftheriou, S. Olcer, and H. Sadjadpour, "Application of capacity approaching coding techniques to digital subscriber lines," *IEEE Communications Magazine*, vol. 42, pp. 88–94, Apr 2004.

[20] J. Neckebroek, M. Moeneclaey, M. Guenach, M. Timmers, and J. Maes, "Comparison of error-control schemes for high-rate communication over short DSL loops affected by impulsive noise," in *IEEE International Conference on Communications (ICC)*, pp. 4014–4019, June 2013.

[21] A. Al-Dweik, A. Hazmi, B. Sharif, and C. Tsimenidis, "Efficient interleaving technique for OFDM system over impulsive noise channels," in *21st Annual IEEE International Symposium on Personal, Indoor and Mobile Radio Communications*, pp. 167–171, Sept 2010.

[22] D. Toumpakaris, J. M. Cioffi, and D. Gardan, "Reduced-delay protection of DSL systems against nonstationary disturbances," *IEEE Transactions on Communications*, vol. 52, pp. 1927–1938, Nov 2004.

[23] S. V. Zhidkov, "Analysis and comparison of several simple impulsive noise mitigation schemes for OFDM receivers," *IEEE Transactions on Communications*, vol. 56, pp. 5–9, January 2008.

[24] R. Fantacci, A. Tani, and D. Tarchi, "Impulse noise mitigation techniques for xDSL systems in a real environment," *IEEE Transactions on Consumer Electronics*, vol. 56, pp. 2106–2114, November 2010.

[25] T. Y. Al-Naffouri, A. A. Quadeer, and G. Caire, "Impulse noise estimation and removal for OFDM systems," *IEEE Transactions on Communications*, vol. 62, pp. 976–989, March 2014.

[26] H. Zhang, L. L. Yang, and L. Hanzo, "Compressed impairment sensing-assisted and interleaved-double-FFT-aided modulation improves broadband power line communications subjected to asynchronous impulsive noise," *IEEE Access*, vol. 4, pp. 81–96, 2016.

[27] C. Leung, S. Huberman, K. Ho-Van, and T. Le-Ngoc, "Vectored DSL: potential, implementation issues and challenges," *IEEE Communications Surveys & Tutorials*, vol. 15, no. 4, pp. 1907–1923, 2013.

[28] R. Cendrillon, G. Ginis, E. V. D. Bogaert, and M. Moonen, "A near-optimal linear crosstalk canceler for upstream VDSL," *IEEE Transactions on Signal Processing*, vol. 54, pp. 3136–3146, Aug 2006.

[29] M. Tomlinson, "New automatic equaliser employing modulo arithmetic," *Electronics Letters*, vol. 7, pp. 138–139, March 1971.

[30] G. Ginis and J. M. Cioffi, "Vectored transmission for digital subscriber line systems," *IEEE Journal on Selected Areas in Communications*, vol. 20, no. 5, pp. 1085–1104, 2002.

[31] C. B. Peel, B. M. Hochwald, and A. L. Swindlehurst, "A vector-perturbation technique for near-capacity multiantenna multiuser communication-Part I: Channel inversion and regularization," *IEEE Transactions on Communications*, vol. 53, pp. 195–202, Jan 2005.

[32] B. M. Hochwald, C. B. Peel, and A. L. Swindlehurst, "A vector-perturbation technique for near-capacity multiantenna multiuser communication-Part II: Perturbation," *IEEE Transactions on Communications*, vol. 53, pp. 537–544, March 2005.

[33] R. Zhang, A. F. A. Rawi, L. D. Humphrey, and L. Hanzo, "Expanded constellation mapping for enhanced far-end-cross-talk cancellation in G.fast," *IEEE Communications Letters*, vol. 21, pp. 56–59, Jan 2017.

[34] F. Sjoberg, M. Isaksson, R. Nilsson, P. Ödling, S. K. Wilson, and P. O. Börjesson, "Zipper: A duplex method for VDSL based on DMT," *IEEE Transactions on Communications*, vol. 47, no. 8, pp. 1245–1252, 1999.

[35] S. Huberman, C. Leung, and T. Le-Ngoc, "Dynamic spectrum management (DSM) algorithms for multi-user xDSL," *IEEE Communications Surveys & Tutorials*, vol. 14, no. 1, pp. 109–130, 2012.

[36] "Spectrum management for loop transmission systems," *ANTI Standard T1.417-2001*, 2001.

[37] W. Yu, G. Ginis, and J. M. Cioffi, "Distributed multiuser power control for digital subscriber lines," *IEEE Journal on Selected Areas in Communications*, vol. 20, no. 5, pp. 1105–1115, 2002.

[38] Y. Xu, T. Le-Ngoc, and S. Panigrahi, "Global concave minimization for optimal spectrum balancing in multi-user DSL networks," *IEEE Transactions on Signal Processing*, vol. 56, pp. 2875–2885, July 2008.

[39] A. R. Forouzan, M. Moonen, J. Maes, and M. Guenach, "Joint level 2 and 3 dynamic spectrum management for downstream DSL," *IEEE Transactions on Communications*, vol. 60, no. 10, pp. 3111–3122, 2012.

[40] R. V. Sonalkar and R. R. Shively, "An efficient bit-loading algorithm for DMT applications," *IEEE Communications Letters*, vol. 4, no. 3, pp. 80–82, 2000.

[41] I. Mann, S. McLaughlin, W. Henkel, R. Kirkby, and T. Kessler, "Impulse generation with appropriate amplitude, length, inter-arrival, and spectral characteristics," *IEEE Journal on Selected Areas in Communications*, vol. 20, no. 5, pp. 901–912, 2002.

[42] I. Mann, S. McLaughlin, W. Henkel, R. Kirkby, and T. Kessler, "Impulse generation with appropriate amplitude, length, inter-arrival, and spectral characteristics," *IEEE Journal on Selected Areas in Communications*, vol. 20, pp. 901–912, Jun 2002.

[43] E. Biglieri, "Coding and modulation for a horrible channel," *IEEE Communications Magazine*, vol. 41, no. 5, pp. 92–98, 2003.

[44] S. Lin, D. J. Costello, and M. J. Miller, "Automatic-repeat-request error-control schemes," *IEEE Communications Magazine*, vol. 22, no. 12, pp. 5–17, 1984.

[45] J. Lin, M. Nassar, and B. L. Evans, "Impulsive noise mitigation in powerline communications using sparse Bayesian learning," *IEEE Journal on Selected Areas in Communications*, vol. 31, no. 7, pp. 1172–1183, 2013.

[46] S. V. Zhidkov, "Analysis and comparison of several simple impulsive noise mitigation schemes for OFDM receivers," *IEEE Transactions on Communications*, vol. 56, no. 1, 2008.

[47] J. Lin and B. L. Evans, "Cyclostationary noise mitigation in narrowband powerline communications," in *2012 Asia-Pacific Signal & Information Processing Association Annual Summit and Conference (APSIPA ASC)*, pp. 1–4, IEEE, 2012.

[48] D. Umehara, H. Yamaguchi, and Y. Morihiro, "Turbo decoding in impulsive noise environment," in *2004 IEEE Global Telecommunications Conference (GLOBECOM'04)*, vol. 1, pp. 194–198, IEEE, 2004.

[49] D. Toumpakaris, W. Yu, J. M. Cioffi, D. Gardan, and M. Ouzzif, "A simple byte-erasure method for improved impulse immunity in DSL," in *2003 IEEE International Conference on Communications*, vol. 4, pp. 2426–2430, IEEE, 2003.

[50] G. Caire, and T. Y. Al-Naffouri, and A. K. Narayanan,, "Impulse noise cancellation in OFDM: an application of compressed sensing," in *2008 IEEE International Symposium on Information Theory*, pp. 1293–1297, July 2008.

[51] M. Ardakani, F. R. Kschischang, and W. Yu, "Low-density parity-check coding for impulse noise correction on power-line channels," in *2005 International Symposium on Power Line Communications and Its Applications*, pp. 90–94, IEEE, 2005.

[52] L. Guerrieri, P. Bisaglia, G. Dell'Amico, and E. Guerrini, "Performance of the turbo coded HomePlug AV system over power-line channels," in *2007 IEEE International Symposium on Power Line Communications and Its Applications*, pp. 138–143, IEEE, 2007.

[53] R. Hormis, I. Berenguer, and X. Wang, "A simple baseband transmission scheme for power line channels," *IEEE Journal on Selected Areas in Communications*, vol. 24, no. 7, pp. 1351–1363, 2006.

[54] N. Andreadou and A. M. Tonello, "On the mitigation of impulsive noise in power-line communications with LT codes," *IEEE Transactions on Power Delivery*, vol. 28, no. 3, pp. 1483–1490, 2013.

[55] A. Hadi, K. M. Rabie, and E. Alsusa, "Polar codes based OFDM-PLC systems in the presence of middleton class-A noise," in *2016 10th International Symposium on Communication Systems, Networks and Digital Signal Processing (CSNDSP)*, pp. 1–6, IEEE, 2016.

[56] I. S. Reed and G. Solomon, "Polynomial codes over certain finite fields," *Journal of the society for industrial and applied mathematics*, vol. 8, no. 2, pp. 300–304, 1960.

[57] C. Berrou, A. Glavieux, and P. Thitimajshima, "Near shannon limit error-correcting coding and decoding: Turbo-codes (1)," in *IEEE International Conference on Communications*, vol. 2, pp. 1064–1070, IEEE, 1993.

[58] E. Arikan, "Channel polarization: A method for constructing capacity-achieving codes for symmetric binary-input memoryless channels," *IEEE Transactions on Information Theory*, vol. 55, no. 7, pp. 3051–3073, 2009.

[59] S. Benedetto and G. Montorsi, "Unveiling turbo codes: Some results on parallel concatenated coding schemes," *IEEE Transactions on Information theory*, vol. 42, no. 2, pp. 409–428, 1996.

[60] H. Imai and S. Hirakawa, "A new multilevel coding method using error-correcting codes," *IEEE Transactions on Information Theory*, vol. 23, no. 3, pp. 371–377, 1977.

[61] G. Caire, G. Taricco, and E. Biglieri, "Bit-interleaved coded modulation," *IEEE Transactions on Information Theory*, vol. 44, no. 3, pp. 927–946, 1998.

[62] A. Nasri and R. Schober, "Performance of BICM-SC and BICM-OFDM systems with diversity reception in non-Gaussian noise and interference," *IEEE Transactions on Communications*, vol. 57, no. 11, 2009.

[63] H. H. Nguyen and T. Q. Bui, "Bit-interleaved coded modulation with iterative decoding in impulsive noise," *IEEE Transactions on Power Delivery*, vol. 22, no. 1, pp. 151–160, 2007.

[64] H. H. Nguyen and T. Q. Bui, "Bit-interleaved coded OFDM with iterative decoding in impulsive noise," *IEEE Transactions on Power Delivery*, vol. 23, no. 2, pp. 640–649, 2008.

[65] P. Amirshahi, S. M. Navidpour, and M. Kavehrad, "Performance analysis of uncoded and coded OFDM broadband transmission over low voltage power-line channels with impulsive noise," *IEEE Transactions on Power Delivery*, vol. 21, no. 4, pp. 1927–1934, 2006.

[66] R. Pighi, M. Franceschini, G. Ferrari, and R. Raheli, "Fundamental performance limits of communications systems impaired by impulse noise," *IEEE Transactions on Communications*, vol. 57, no. 1, pp. 171–182, 2009.

[67] A. Al-Dweik, A. Hazmi, B. Sharif, and C. Tsimenidis, "Efficient interleaving technique for OFDM system over impulsive noise channels," in *IEEE 21st International Symposium on Personal Indoor and Mobile Radio Communications (PIMRC)*, pp. 167–171, IEEE, 2010.

[68] S. Nayyef, C. Tsimenidis, A. Al-Dweik, B. Sharif, and A. Hazmi, "Time-and frequency-domain impulsive noise spreader for OFDM systems," in *2012 IEEE 11th International Conference on Trust, Security and Privacy in Computing and Communications (TrustCom)*, pp. 1856–1861, IEEE, 2012.

[69] S. Bernard, "Digital communications fundamentals and applications," *Prentice Hall, USA*, 2001.

[70] M. Mirahmadi, A. Al-Dweik, and A. Shami, "BER reduction of OFDM based broadband communication systems over multipath channels with impulsive noise," *IEEE Transactions on Communications*, vol. 61, no. 11, pp. 4602–4615, 2013.

[71] J. Wolf, "Redundancy, the discrete fourier transform, and impulse noise cancellation," *IEEE Transactions on Communications*, vol. 31, no. 3, pp. 458–461, 1983.

[72] K. H. Afkhamie, S. Katar, L. Yonge, and R. Newman, "An overview of the upcoming HomePlug AV standard," in *2005 International Symposium on Power Line Communications and Its Applications*, pp. 400–404, IEEE, 2005.

[73] I. H. Kim, B. Varadarajan, and A. Dabak, "Performance analysis and enhancements of narrowband OFDM powerline communication systems," in *2010 First IEEE International Conference on Smart Grid Communications (SmartGridComm)*, pp. 362–367, IEEE, 2010.

[74] H. Chen, R. G. Maunder, and L. Hanzo, "Low-complexity multiple-component turbo-decoding-aided hybrid ARQ," *IEEE Transactions on Vehicular Technology*, vol. 60, no. 4, pp. 1571–1577, 2011.

[75] R. Zhang and L. Hanzo, "Superposition-coding-aided multiplexed hybrid ARQ scheme for improved end-to-end transmission efficiency," *IEEE Transactions on Vehicular Technology*, vol. 58, no. 8, pp. 4681–4686, 2009.

[76] A. U. Rehman, L.-L. Yang, and L. Hanzo, "Delay and throughput analysis of cognitive go-back-n HARQ in the face of imperfect sensing," *IEEE Access*, vol. 5, pp. 7454–7473, 2017.

[77] S. Lin, D. J. Costello Jr, and M. J. Miller, "Automatic-repeat-request error control schemes," *IEEE Communications Magazine*, 1983.

[78] D. Chase, "Code combining–a maximum-likelihood decoding approach for combining an arbitrary number of noisy packets," *IEEE Transactions on Communications*, vol. 33, no. 5, pp. 385–393, 1985.

[79] S. Sesia, G. Caire, and G. Vivier, "Incremental redundancy hybrid ARQ schemes based on low-density parity-check codes," *IEEE Transactions on Communications*, vol. 52, no. 8, pp. 1311–1321, 2004.

[80] T. Bai, C. Xu, R. Zhang, A. F. Al Rawi, and L. Hanzo, "Performance of HARQ-assisted OFDM systems contaminated by impulsive noise: Finite-length LDPC code analysis," *IEEE Access*.

[81] F. H. Juwono, Q. Guo, D. Huang, and K. P. Wong, "Deep clipping for impulsive noise mitigation in OFDM-based power-line communications," *IEEE Transactions on Power Delivery*, vol. 29, no. 3, pp. 1335–1343, 2014.

[82] V. N. Papilaya and A. H. Vinck, "Investigation on a new combined impulsive noise mitigation scheme for OFDM transmission," in *2013 17th IEEE International Symposium on Power Line Communications and Its Applications (ISPLC)*, pp. 86–91, IEEE, 2013.

[83] M. Korki, N. Hosseinzadeh, H. L. Vu, T. Moazzeni, and C. H. Foh, "Impulsive noise reduction of a narrowband power line communication using optimal nonlinearity technique," in *2011 Australasian Telecommunication Networks and Applications Conference (ATNAC)*, pp. 1–4, IEEE, 2011.

[84] G. Ndo, P. Siohan, M.-H. Hamon, and J. Horard, "Optimization of turbo decoding performance in the presence of impulsive noise using soft limitation at the receiver side," in *2008 IEEE Global Telecommunications Conference (GLOBECOM 2008)*, pp. 1–5, IEEE, 2008.

[85] G. Ndo, P. Siohan, and M.-H. Hamon, "Adaptive noise mitigation in impulsive environment: Application to power-line communications," *IEEE Transactions on Power Delivery*, vol. 25, no. 2, pp. 647–656, 2010.

[86] D.-F. Tseng, Y. S. Han, W. H. Mow, L.-C. Chang, and A. H. Vinck, "Robust clipping for OFDM transmissions over memoryless impulsive noise channels," *IEEE Communications Letters*, vol. 16, no. 7, pp. 1110–1113, 2012.

[87] E. Alsusa and K. M. Rabie, "Dynamic peak-based threshold estimation method for mitigating impulsive noise in power-line communication systems," *IEEE Transactions on Power Delivery*, vol. 28, no. 4, pp. 2201–2208, 2013.

[88] J. Armstrong, "Peak-to-average power reduction for OFDM by repeated clipping and frequency domain filtering," *Electronics Letters*, vol. 38, no. 5, pp. 246–247, 2002.

[89] F. H. Juwono, Q. Guo, D. Huang, and K. P. Wong, "Joint peak amplitude and impulsive noise clippings in OFDM-based power line communications," in *2013 19th Asia-Pacific Conference on Communications (APCC)*, pp. 567–571, IEEE, 2013.

[90] J. A. Davis and J. Jedwab, "Peak-to-mean power control in OFDM, Golay complementary sequences, and Reed-Muller codes," *IEEE Transactions on Information Theory*, vol. 45, no. 7, pp. 2397–2417, 1999.

[91] J. Tellado, "Peak-to-average power reduction for multicarrier modulation," *Ph. D. Thesis*, 1999.

[92] K. M. Rabie and E. Alsusa, "Preprocessing-based impulsive noise reduction for power-line communications," *IEEE Transactions on Power Delivery*, vol. 29, no. 4, pp. 1648–1658, 2014.

[93] K. Rabie, E. Alsusa, A. Familua, and L. Cheng, "Constant envelope OFDM transmission over impulsive noise power-line communication channels," in *2015 International Symposium on Power Line Communications and its Applications (ISPLC)*, pp. 13–18, IEEE, 2015.

[94] K. M. Rabie and E. Alsusa, "Single-carrier FDMA with blanking/clipping for mitigating impulsive noise over PLC channels," in *2014 18th IEEE International Symposium on Power Line Communications and its Applications (ISPLC)*, pp. 340–345, IEEE, 2014.

[95] C.-H. Yih, "Iterative interference cancellation for OFDM signals with blanking nonlinearity in impulsive noise channels," *IEEE Signal Processing Letters*, vol. 19, no. 3, pp. 147–150, 2012.

[96] A. Mengi and A. H. Vinck, "Successive impulsive noise suppression in OFDM," in *2010 IEEE International Symposium on Power Line Communications and Its Applications (ISPLC)*, pp. 33–37, IEEE, 2010.

[97] E. Guerrini, L. Guerrni, and D. Veronesi, "HomePlug AV system and DLC bitloading algorithm over OPERA power-line channels with impulsive noise," in *2008 IEEE International Symposium on Power Line Communications and Its Applications*, pp. 164–169, IEEE, 2008.

[98] H.-M. Oh, Y.-J. Park, S. Choi, J.-J. Lee, and K.-C. Whang, "Mitigation of performance degradation by impulsive noise in LDPC coded OFDM system," in *2006*

IEEE International Symposium on Power Line Communications and Its Applications, pp. 331–336, IEEE, 2006.

[99] M. Katayama, T. Yamazato, and H. Okada, "A mathematical model of noise in narrowband power line communication systems," *IEEE Journal on Selected areas in Communications*, vol. 24, no. 7, pp. 1267–1276, 2006.

[100] Y. G. Yoo and J. H. Cho, "Asymptotic analysis of CP-SC-FDE and UW-SC-FDE in additive cyclostationary noise," in *2008 IEEE International Conference on Communications*, pp. 1410–1414, IEEE, 2008.

[101] R. García, L. Díez, J. A. Cortés, and F. J. Cañete, "Mitigation of cyclic short-time noise in indoor power-line channels," in *2007 IEEE International Symposium on Power Line Communications and Its Applications*, pp. 396–400, IEEE, 2007.

[102] A. Llano, A. Sendin, A. Arzuaga, and S. Santos, "Quasi-synchronous noise interference cancellation techniques applied in low voltage PLC," in *2011 IEEE International Symposium on Power Line Communications and Its Applications (ISPLC)*, pp. 108–112, IEEE, 2011.

[103] S. P. Talebi, S. Werner, and D. P. Mandic, "Distributed adaptive filtering of α-stable signals," *IEEE Signal Processing Letters*, vol. 25, no. 10, pp. 1450–1454, 2018.

[104] S. Miyamoto, M. Katayama, and N. Morinaga, "Performance analysis of QAM systems under class A impulsive noise environment," *IEEE Transactions on Electromagnetic Compatibility*, vol. 37, no. 2, pp. 260–267, 1995.

[105] M. Nassar, K. Gulati, M. R. DeYoung, B. L. Evans, and K. R. Tinsley, "Mitigating near-field interference in laptop embedded wireless transceivers," *Journal of Signal Processing Systems*, vol. 63, no. 1, pp. 1–12, 2011.

[106] T. Fukami, D. Umehara, M. Kawai, and Y. Morihiro, "Noncoherent PSK optimum receiver over impulsive noise channels," in *Proc. of the 2002 IEEE International Symposium on Power Line Communications and Its Applications*, pp. 235–238, 2002.

[107] R. Haring and A. H. Vinck, "Performance bounds for optimum and suboptimum reception under Class-A impulsive noise," *IEEE Transactions on Communications*, vol. 50, no. 7, pp. 1130–1136, 2002.

[108] M. Nassar and B. L. Evans, "Low complexity EM-based decoding for OFDM systems with impulsive noise," in *2011 Conference Record of the Forty Fifth Asilomar Conference on Signals, Systems and Computers (ASILOMAR),*, pp. 1943–1947, IEEE, 2011.

[109] D. Fertonani and G. Colavolpe, "On reliable communications over channels impaired by bursty impulse noise," *IEEE Transactions on Communications*, vol. 57, no. 7, 2009.

[110] G. Ndo, F. Labeau, and M. Kassouf, "A Markov-Middleton model for bursty impulsive noise: Modeling and receiver design," *IEEE Transactions on Power Delivery*, vol. 28, no. 4, pp. 2317–2325, 2013.

[111] L. Bahl, J. Cocke, F. Jelinek, and J. Raviv, "Optimal decoding of linear codes for minimizing symbol error rate," *IEEE Transactions on Information Theory*, vol. 20, no. 2, pp. 284–287, 1974.

[112] J. Hagenauer, E. Offer, and L. Papke, "Iterative decoding of binary block and convolutional codes," *IEEE Transactions on Information Theory*, vol. 42, no. 2, pp. 429–445, 1996.

[113] H. Nakagawa, D. Umehara, S. Denno, and Y. Morihiro, "A decoding for low density parity check codes over impulsive noise channels," in *2005 International Symposium on Power Line Communications and Its Applications*, pp. 85–89, IEEE, 2005.

[114] J. Mitra and L. Lampe, "On joint estimation and decoding for channels with noise memory," *IEEE Communications Letters*, vol. 13, no. 10, 2009.

[115] J. Mitra and L. Lampe, "Convolutionally coded transmission over Markov-Gaussian channels: Analysis and decoding metrics," *IEEE Transactions on Communications*, vol. 58, no. 7, pp. 1939–1949, 2010.

[116] J. Haring and A. H. Vinck, "Iterative decoding of codes over complex numbers for impulsive noise channels," *IEEE Transactions on Information Theory*, vol. 49, no. 5, pp. 1251–1260, 2003.

[117] F. Abdelkefi, P. Duhamel, and F. Alberge, "Impulsive noise cancellation in multicarrier transmission," *IEEE Transactions on Communications*, vol. 53, no. 1, pp. 94–106, 2005.

[118] T. Bai, C. Xu, R. Zhang, A. F. Al Rawi, and L. Hanzo, "Joint impulsive noise estimation and data detection conceived for LDPC-coded DMT-based DSL systems," *IEEE Access*, vol. 5, pp. 23133–23145, 2017.

[119] K. Leung and L. Welch, "Erasure decoding in burst-error channels," *IEEE Transactions on Information Theory*, vol. 27, no. 2, pp. 160–167, 1981.

[120] M. Elgenedy, M. Sayed, M. Mokhtar, M. Abdallah, and N. Al-Dhahir, "Interference mitigation techniques for narrowband powerline smart grid communications," in

2015 IEEE International Conference on Smart Grid Communications (SmartGridComm), pp. 368–373, IEEE, 2015.

[121] T. Li, W. H. Mow, and M. H. Siu, "A joint approach to erasure marking and Viterbi decoding for impulsive noise channels," in *4th IEEE Workshop on Signal Processing Advances in Wireless Communications*, pp. 180–184, IEEE, 2003.

[122] T. Li, W. H. Mow, V. K. Lau, M. Siu, R. S. Cheng, and R. D. Murch, "Robust joint interference detection and decoding for OFDM-based cognitive radio systems with unknown interference," *IEEE Journal on Selected Areas in Communications*, vol. 25, no. 3, 2007.

[123] T. Li, W. H. Mow, and M. Siu, "Joint erasure marking and list Viterbi algorithm for decoding in unknown non-Gaussian noise," *IEEE Transactions on Wireless Communications*, vol. 7, no. 3, pp. 787–792, 2008.

[124] L. Lampe, "Bursty impulse noise detection by compressed sensing," in *2011 IEEE International Symposium on Power Line Communications and Its Applications (ISPLC),*, pp. 29–34, April 2011.

[125] G. Ren, S. Qiao, and Y. Hei, "Asynchronous impulsive noise mitigation in OFDM using adaptive threshold compressive sensing," in *2014 IEEE 15th Annual Wireless and Microwave Technology Conference (WAMICON)*, pp. 1–5, IEEE, 2014.

[126] T. Y. Al-Naffouri, A. A. Quadeer, and G. Caire, "Impulse noise estimation and removal for OFDM systems," *IEEE Transactions on Communications*, vol. 62, no. 3, pp. 976–989, 2014.

[127] S. Liu, F. Yang, W. Ding, and J. Song, "Double kill: Compressive-sensing-based narrow-band interference and impulsive noise mitigation for vehicular communications.," *IEEE Transactions on Vehicular Technology*, vol. 65, no. 7, pp. 5099–5109, 2016.

[128] M. Korki, J. Zhang, C. Zhang, and H. Zayyani, "Block-sparse impulsive noise reduction in OFDM systems–A novel iterative Bayesian approach," *IEEE Transactions on Communications*, vol. 64, no. 1, pp. 271–284, 2016.

[129] D. Toumpakaris, J. M. Cioffi, and D. Gardan, "Reduced-delay protection of DSL systems against nonstationary disturbances," *IEEE Transactions on Communications*, vol. 52, no. 11, pp. 1927–1938, 2004.

[130] M. Luby, "LT codes," in *IEEE Symp. Foundations of Computer Science*, pp. 271–280, IEEE, 2002.

[131] N. Seshadri and C.-E. Sundberg, "List Viterbi decoding algorithms with applications," *IEEE Transactions on Communications*, vol. 42, no. 234, pp. 313–323, 1994.

[132] I. S. Association *et al.*, "IEEE standard for broadband over power line networks: medium access control and physical layer specifications," *IEEE Std 1901*, vol. 2010, pp. 1–1586, 2010.

[133] HomePlug Powerline Alliance, *HomePlug AV2 White Paper*, 2013. Available at `http://www.homeplug.org/`.

[134] T. Bai, H. Zhang, J. Zhang, C. Xu, A. F. Al Rawi, and L. Hanzo, "Impulsive noise mitigation for digital subscriber lines: the state-of-the-art and research opportunities," *submitted to IEEE Communications Magazine*.

[135] T. Bai, H. Zhang, J. Wang, C. Xu, and L. Hanzo, "Thirty years of noise modeling and processing in power-line communications," *submitted to IEEE Communications Surveys & Tutorials*.

[136] H. Meng, Y. L. Guan, and S. Chen, "Modeling and analysis of noise effects on broadband power-line communications," *IEEE Transactions on Power delivery*, vol. 20, no. 2, pp. 630–637, 2005.

[137] M. Ghosh, "Analysis of the effect of impulse noise on multicarrier and single carrier QAM systems," *IEEE Transactions on Communications*, vol. 44, pp. 145–147, Feb 1996.

[138] M. Nassar, K. Gulati, Y. Mortazavi, and B. L. Evans, "Statistical modeling of asynchronous impulsive noise in powerline communication networks," in *2011 IEEE Global Telecommunications Conference (GLOBECOM 2011)*, pp. 1–6, IEEE, 2011.

[139] D. Middleton, "Statistical-physical models of electromagnetic interference," *IEEE Transactions on Electromagnetic Compatibility*, no. 3, pp. 106–127, 1977.

[140] D. Middleton, "Non-gaussian noise models in signal processing for telecommunications: new methods an results for class A and class B noise models," *IEEE Transactions on Information Theory*, vol. 45, no. 4, pp. 1129–1149, 1999.

[141] J. Wang, E. E. Kuruoglu, and T. Zhou, "Alpha-stable channel capacity," *IEEE Communications Letters*, vol. 15, no. 10, pp. 1107–1109, 2011.

[142] H. Zhang, L.-L. Yang, and L. Hanzo, "Performance analysis of orthogonal frequency division multiplexing systems in dispersive indoor power line channels inflicting asynchronous impulsive noise," *IET Communications*, vol. 10, no. 5, pp. 453–461, 2016.

[143] J. A. Cortes, L. Diez, F. J. Canete, and J. J. Sanchez-Martinez, "Analysis of the indoor broadband power-line noise scenario," *IEEE Transactions on Electromagnetic Compatibility*, vol. 52, pp. 849–858, Nov 2010.

[144] V. Degardin, M. Lienard, A. Zeddam, F. Gauthier, and P. Degauquel, "Classification and characterization of impulsive noise on indoor powerline used for data communications," *IEEE Transactions on Consumer Electronics*, vol. 48, no. 4, pp. 913–918, 2002.

[145] V. Degardin, M. Lienard, P. Degauque, E. Simon, and P. Laly, "Impulsive noise characterization of in-vehicle power line," *IEEE Transactions on Electromagnetic Compatibility*, vol. 50, no. 4, pp. 861–868, 2008.

[146] M. Zimmermann and K. Dostert, "Analysis and modeling of impulsive noise in broad-band powerline communications," *IEEE Transactions on Electromagnetic Compatibility*, vol. 44, pp. 249–258, Feb 2002.

[147] W. Henkel, T. Kessler, and H. Y. Chung, "Coded 64-CAP ADSL in an impulse-noise environment-modeling of impulse noise and first simulation results," *IEEE Journal on Selected Areas in Communications*, vol. 13, no. 9, pp. 1611–1621, 1995.

[148] B. Mandelbrot, "Self-similar error clusters in communication systems and the concept of conditional stationarity," *IEEE Transactions on Communication Technology*, vol. 13, no. 1, pp. 71–90, 1965.

[149] D. B. Levey and S. McLaughlin, "The statistical nature of impulse noise interarrival times in digital subscriber loop systems," *Signal Processing*, vol. 82, no. 3, pp. 329–351, 2002.

[150] T. Kessler, R. Kirkby, W. Henkel, and S. McLaughlin, "Text for 'realistic impulsive noise model'," *ETSI TM6 011T20*, February 2001.

[151] B. Liu and D. C. Munson Jr, "Generation of a random sequence having a jointly specified marginal distribution and autocovariance," *IEEE Transactions on Acoustics, Speech and Signal Processing*, vol. 30, no. 6, pp. 973–983, 1982.

[152] R. Tough and K. Ward, "The correlation properties of Gamma and other non-Gaussian processes generated by memoryless nonlinear transformation," *Journal of Physics D: Applied Physics*, vol. 32, no. 23, p. 3075, 1999.

[153] J. C. Silveira Santos and M. Daoud Yacoub, "Coloring non-Gaussian sequences," *IEEE Transactions on Signal Processing*, vol. 56, no. 12, pp. 5817–5822, 2008.

[154] S. M. Kay and S. L. Marple, "Spectrum analysis – a modern perspective," *Proceedings of the IEEE*, vol. 69, pp. 1380–1419, Nov 1981.

[155] M. Abramowitz and I. A. Stegun, *Handbook of mathematical functions: with formulas, graphs, and mathematical tables*, vol. 55. Courier Corporation, 1964.

[156] A. Papoulis and S. U. Pillai, "Probability, random variables, and stochastic processes," *McGraw-Hill*, 1985.

[157] S. P. Herath, N. H. Tran, and T. Le-Ngoc, "Optimal signaling scheme and capacity limit of PLC under Bernoulli-Gaussian impulsive noise," *IEEE Transactions on Power Delivery*, vol. 30, no. 1, pp. 97–105, 2015.

[158] E. N. Gilbert, "Capacity of a burst-noise channel," *Bell Labs Technical Journal*, vol. 39, no. 5, pp. 1253–1265, 1960.

[159] E. O. Elliott, "Estimates of error rates for codes on burst-noise channels," *The Bell System Technical Journal*, vol. 42, no. 5, pp. 1977–1997, 1963.

[160] T. Shongwey, A. H. Vinck, and H. C. Ferreira, "On impulse noise and its models," in *2014 18th IEEE International Symposium on Power Line Communications and its Applications (ISPLC)*, pp. 12–17, IEEE, 2014.

[161] M. Ghosh, "Analysis of the effect of impulse noise on multicarrier and single carrier QAM systems," *IEEE Transactions on Communications*, vol. 44, no. 2, pp. 145–147, 1996.

[162] Y. Chew, T. Tjhung, T. He, and C. Ko, "Estimation of BER performance over an impulse noise channel," *Electronics Letters*, vol. 35, no. 4, pp. 273–274, 1999.

[163] N. Nedev, S. McLaughlin, and D. I. Laurenson, "Estimating errors in transmission systems due to impulse noise," in *IET Proceedings Communications*, vol. 153, pp. 651–656, IET, 2006.

[164] L. Hanzo, M. Münster, B. Choi, and T. Keller, *OFDM and MC-CDMA for broadband multi-user communications, WLANs and broadcasting*. John Wiley & Sons, 2005.

[165] L.-L. Yang, *Multicarrier communications*. John Wiley & Sons, 2009.

[166] S.-Z. Yu, "Hidden semi-Markov models," *Artificial Intelligence*, vol. 174, no. 2, pp. 215–243, 2010.

[167] Y. Ephraim and N. Merhav, "Hidden Markov processes," *IEEE Transactions on Information Theory*, vol. 48, pp. 1518–1569, Jun 2002.

[168] H. Zhang, L. L. Yang, and L. Hanzo, "Performance analysis of orthogonal frequency division multiplexing systems in dispersive indoor power line channels inflicting

asynchronous impulsive noise," *IET Communications*, vol. 10, no. 5, pp. 453–461, 2016.

[169] A. J. Goldsmith and M. Effros, "The capacity region of broadcast channels with intersymbol interference and colored Gaussian noise," *IEEE Transactions on Information Theory*, vol. 47, no. 1, pp. 219–240, 2001.

[170] M. Peligrad and W. B. Wu, "Central limit theorem for Fourier transforms of stationary processes," *The Annals of Probability*, pp. 2009–2022, 2010.

[171] E. Bertin and M. Clusel, "Generalized extreme value statistics and sum of correlated variables," *Journal of Physics A: Mathematical and General*, vol. 39, no. 24, p. 7607, 2006.

[172] C. Chatfield, *The analysis of time series: an introduction*. CRC press, 2016.

[173] L.-L. Yang and L. Hanzo, "A recursive algorithm for the error probability evaluation of M-QAM," *IEEE Communications Letters*, vol. 4, no. 10, pp. 304–306, 2000.

[174] "Fast access to subscriber termials (G.fast) - physical layer specification," *Recommendation Draft ITU-T G.9701*, 2014.

[175] G. Caire and D. Tuninetti, "The throughput of hybrid-ARQ protocols for the Gaussian collision channel," *IEEE Transactions on Information Theory*, vol. 47, pp. 1971–1988, Jul 2001.

[176] J.-F. Cheng, "Coding performance of hybrid ARQ schemes," *IEEE Transactions on Communications*, vol. 54, pp. 1017–1029, June 2006.

[177] P. Wu and N. Jindal, "Performance of hybrid-ARQ in block-fading channels: A fixed outage probability analysis," *IEEE Transactions on Communications*, vol. 58, pp. 1129–1141, April 2010.

[178] S. Sesia, G. Caire, and G. Vivier, "Incremental redundancy hybrid ARQ schemes based on low-density parity-check codes," *IEEE Transactions on Communications*, vol. 52, pp. 1311–1321, Aug 2004.

[179] J. Kim, A. Ramamoorthy, and S. W. Mclaughlin, "The design of efficiently-encodable rate-compatible LDPC codes," *IEEE Transactions on Communications*, vol. 57, pp. 365–375, February 2009.

[180] D. N. Rowitch and L. B. Milstein, "On the performance of hybrid FEC/ARQ systems using rate compatible punctured turbo (RCPT) codes," *IEEE Transactions on Communications*, vol. 48, pp. 948–959, Jun 2000.

[181] T. J. Richardson and R. L. Urbanke, "The capacity of low-density parity-check codes under message-passing decoding," *IEEE Transactions on Information Theory*, vol. 47, pp. 599–618, Feb 2001.

[182] R. Yazdani and M. Ardakani, "Waterfall performance analysis of finite-length LDPC codes on symmetric channels," *IEEE Transactions on Communications*, vol. 57, pp. 3183–3187, Nov 2009.

[183] J. Lin, M. Nassar, and B. L. Evans, "Impulsive noise mitigation in powerline communications using sparse Bayesian learning," *IEEE Journal on Selected Areas in Communications*, vol. 31, pp. 1172–1183, July 2013.

[184] A. Nasri and R. Schober, "Performance of BICM-SC and BICM-OFDM systems with diversity reception in non-Gaussian noise and interference," *IEEE Transactions on Communications*, vol. 57, pp. 3316–3327, Nov 2009.

[185] D. Middleton, "Statistical-physical models of electromagnetic interference," *IEEE Transactions on Electromagnetic Compatibility*, vol. 19, pp. 106–127, Aug 1977.

[186] Y. H. Ma, P. L. So, and E. Gunawan, "Performance analysis of OFDM systems for broadband power line communications under impulsive noise and multipath effects," *IEEE Transactions on Power Delivery*, vol. 20, pp. 674–682, April 2005.

[187] R. Pighi, M. Franceschini, G. Ferrari, and R. Raheli, "Fundamental performance limits of communications systems impaired by impulse noise," *IEEE Transactions on Communications*, vol. 57, pp. 171–182, January 2009.

[188] M. Mirahmadi, A. Al-Dweik, and A. Shami, "BER reduction of OFDM based broadband communication systems over multipath channels with impulsive noise," *IEEE Transactions on Communications*, vol. 61, pp. 4602–4615, November 2013.

[189] D. G. Brennan, "Linear diversity combining techniques," *Proceedings of the IEEE*, vol. 91, pp. 331–356, Feb 2003.

[190] S.-Y. Chung, T. J. Richardson, and R. L. Urbanke, "Analysis of sum-product decoding of low-density parity-check codes using a Gaussian approximation," *IEEE Transactions on Information Theory*, vol. 47, pp. 657–670, Feb 2001.

[191] Z. Mei, M. Johnston, S. L. Goff, and L. Chen, "Performance analysis of LDPC-coded diversity combining on Rayleigh fading channels with impulsive noise," *IEEE Transactions on Communications*, vol. 65, pp. 2345–2356, June 2017.

[192] T. Bai, H. Zhang, R. Zhang, L. L. Yang, A. F. A. Rawi, J. Zhang, and L. Hanzo, "Discrete multi-tone digital subscriber loop performance in the face of impulsive noise," *IEEE Access*, vol. 5, pp. 10478–10495, 2017.

[193] H. E. Gamal, G. Caire, and M. O. Damen, "The MIMO ARQ channel: Diversity-Multiplexing-Delay tradeoff," *IEEE Transactions on Information Theory*, vol. 52, pp. 3601–3621, Aug 2006.

[194] A. Chelli, E. Zedini, M. S. Alouini, J. R. Barry, and M. Pätzold, "Performance and delay analysis of Hybrid ARQ with incremental redundancy over double Rayleigh fading channels," *IEEE Transactions on Wireless Communications*, vol. 13, pp. 6245–6258, Nov 2014.

[195] P. Wu and N. Jindal, "Coding versus ARQ in fading channels: How reliable should the PHY be?," *IEEE Transactions on Communications*, vol. 59, pp. 3363–3374, December 2011.

[196] J. S. Chow, J. C. Tu, and J. M. Cioffi, "A discrete multitone transceiver system for HDSL applications," *IEEE Journal on Selected Areas in Communications*, vol. 9, pp. 895–908, Aug 1991.

[197] L. Hanzo, O. Alamri, M. El-Hajjar, and N. Wu, *Near-capacity multi-functional MIMO systems: sphere-packing, iterative detection and cooperation*, vol. 4. John Wiley & Sons, 2009.

[198] S. M. Kay, *Fundamentals of Statistical Signal Processing: Practical Algorithm Development*, vol. 3. Pearson Education, 2013.

[199] B. Drooghaag, J. Maes, M. El Fani, and V. Moeyaert, "Exploring field noise on G.fast frequencies," in *IEEE Global Communications Conference (GLOBECOM)*, pp. 1–6, IEEE, 2017.

[200] A. Ligata, E. Perenda, and H. Gacanin, "Quality of experience inference for video services in home WiFi networks," *IEEE Communications Magazine*, vol. 56, no. 3, pp. 187–193, 2018.

[201] A. Mahmood and J.-C. Belfiore, "An efficient algorithm for optimal discrete bit-loading in multicarrier systems," *IEEE transactions on communications*, vol. 58, no. 6, 2010.

[202] L. Hanzo, S. X. Ng, W. Webb, and T. Keller, *Quadrature amplitude modulation: From basics to adaptive trellis-coded, turbo-equalised and space-time coded OFDM, CDMA and MC-CDMA systems*. IEEE Press-John Wiley, 2004.

[203] S. Dörner, S. Cammerer, J. Hoydis, and S. ten Brink, "Deep learning based communication over the air," *IEEE Journal of Selected Topics in Signal Processing*, vol. 12, no. 1, pp. 132–143, 2018.